1-1-2007

Mitigation of torsional vibration in large mill drive train system using state feedback control method

Ehsan Al-Nabi
Ryerson University

MITIGATION OF TORSIONAL VIBRATION IN LARGE MILL DRIVE TRAIN SYSTEM USING STATE FEEDBACK CONTROL METHOD

By

EHSAN AL-NABI

MS.c, Al-Mustansiria University, IRAQ, 1997

BS.c, Al-Mustansiria University, IRAQ, 1992

A thesis
presented to Ryerson University
in partial fulfillment of the
requirements for the degree of
Master of Applied Science
in the Program of
Electrical and Computer Engineering

Toronto, Ontario, Canada, 2007

Ehsan Al-nabi, MASc, Electrical and Computer Engineering,
Ryerson University, Toronto, 2007

ABSTRACT

Torsional vibration limits the speed loop response of industrial drives and servo systems, deteriorating the transient response to speed commands and load disturbances. This thesis presents a damping method for torsional vibration produced by compliant components between the motor and the load in rolling mill applications. The proposed damping algorithm can solve the limitation of the classical damping approaches due to the large values of system time delay. The proposed algorithm is based on State Feedback Control (SFC) method with a modified Linear Quadratic Gaussian (LQG) approach using a torque sensor as a feedback element. The result of modification is a low order single-input single-output compensator that mitigates the torsional vibration without affecting the speed loop. The verification of the design and the dynamic performance is accomplished by using time and frequency domain responses with real rolling mill system parameters. The performance of step commands, mitigation of torsional vibration and robustness to parameter variation is satisfied by using the proposed method. Also disturbance rejection performance is improved through load torque compensation. The experiment is performed on a 0.8 KW system with 24 Hz mechanical resonant frequency. Simulation and experimental results from the experimental system verify the proposed damping algorithm.

ACKNOWLEDGEMENTS

The work presented in the thesis was carried out at the Laboratory of Electric Drive Research and Application (LEDAR) at Ryerson University.

First of all, I would like to thank Professor Bin Wu for his continuous and paramount support and help during the period when I studied at Ryerson. The precious advices and numerous discussions triggered insightful research and enhanced my academic knowledge and scientific inspiration.

I am grateful to Professor Richard Cheung, Professor David Xu, and all the fellow students at LEDAR (Bing, Raja and Ahmad) for their support and friendly atmosphere. My appreciation also goes to Mr. Jim Koch for his help in preparing the motors, and my friend Mr. Karim Muslim for his valuable assistance.

My sincere gratitude is extended to the engineers of the Power Electronic Group of Rockwell Automation Canada for the beneficial discussions and technical meetings.

I would like to share the joy of achievements with my families, my wife Nedea and our kids Azher and Hassan. I am very grateful for my dear wife's long-time understanding and support.

TO MY PARENTS

TABLE OF CONTENTS

LIST OF TABLES

LIST OF FIGURE

LIST OF PRINCIPLE SYMBOLS

ω_M, ω_L	Motor and load speeds
T_M, T_L, T_{sh}	Motor, load, and shaft torques
J_M, J_L	Motor and load moment of inertias
K_{sh}	Shaft Stiffness
D_M, D_L, D_{sh}	Motor, load and shaft damping coefficients
θ_M, θ_L	Motor and load angles
$\Delta\theta$	Difference angle
$\Delta\omega$	Speed difference
ω_n	Mechanical resonant frequency
ω_o	Anti-resonant frequency
ξ	Mechanical damping factor
s	Laplace operator
ω_{CC}	Cut-off frequency of torque regulator
ω_{cs}	Cut-off frequency of speed regulator
τ	PI- Integration time constant
K_P	PI- proportional gain
J_T	Total moment of inertia
ΔT	Time between samples
f_s	Sampling frequency
α_r	Angle of the torque regulator pole to the positive resonant pole
$\theta_{departure}$	Departure angle of the resonant poles
$\hat{\omega}_n$	Estimated resonant frequency
$\hat{T}_{sh}$	Estimated shaft torque
T_d	Time delay

T_{ds}	Significant time delay
ω_{Lag}	Cut-off frequency of lag filter
ξ_n , ξ_o	Numerator and denominator damping factor of notch filter
K_m	State feedback gain
K_f	Kalman Filter gain
P	Solution of algebraic Ricatti Equation (ARE)
J	Quadratic performance index
Q , R	State and control action weighting matrices
v	Kalman Filter measurement noise added to the output
w	Kalman Filter process noise added to the state dynamic
T_{ref}	Reference torque
q	Design free parameter of LTR method
A_s,B_s,C_s,D_s,E_s	System matrices
A_o,B_o,C_o,D_o	System matrices with load compensation
a	d.c bias
x	System state variable
$\hat{x}$	Observer state variable
u	Control law of the State Feedback Control method

CHAPTER 1: INTRODUCTION

1.1 Introduction

To increase productivity and reduce costs, drive systems having faster dynamic performance (high speed response) are now being employed in many industrial applications such as steel rolling mills, paper machines and very precise positioning systems [1,2,3]. With the increase in speed and torque bandwidth associated with new motor and drive designs, the likelihood of mechanical torsional vibration (or torsional chatter) has increased. In rolling mill applications, the torsional vibration may affect the quality of the end products by causing significant periodic variation in product gauge and surface finish. It may also cause severe damage to the rolling mill system [4]. Therefore, efforts should be made to eliminate and reduce the mechanical torsional vibration.

To meet the requirements of rolling mills, dc drives have been used in the past. However, the limitation of the dc motor capacity, the needs of costly periodical maintenance and low overall efficiency severely restrict the application of the dc drive systems. The limitation of the dc motor capacity leads to the combination of several motors in series or parallel. Such a requirement limits the design of the plant, especially in high speed rolling mills [5].

In order to improve the limitation of dc drives, variable frequency ac drives using voltage source inverter (VSI), current source inverter (CSI) and load commutated inverter (LCI) have been employed [5,6]. Recently, these drives offer a solution to the requirement of rolling mills [7]. The price to be paid from using the ac drives is the torque ripple which increases the possibility of exciting the torsional vibration. Also, the increase in the speed response with the use of an ac drive plays a key factor for exciting the torsional vibration. These two reasons for torsional vibration will be discussed in detail in the next section.

1.2 Causes of Torsional Vibration

Many reasons can cause torsional vibrations in a drive system [3,4,6,8,9,10]. In general, the excitation of torsional vibration can be classified into mechanical and

electrical excitation. Figure1-1 shows the mechanism of mechanical excitation in rolling mill applications. In Figure1-1(a), the motor and the roll rotate at the same speed equal to the speed reference in steady state running with no vibration. Once the steel enters between the rolls of the rolling mill, the speed of the rolls will slow down first. If the shaft "spindle" is perfectly rigid, the motor speed also slows down at the same rate at the same time. No torsion occurs in this situation.

In practice, there are certain technical considerations such as using long and small diameter shaft between the motors and the rolls. Therefore, the flexibility of the shaft cannot be neglected. This flexibility retards the travel of torque along the shaft "spindle" to the motor. The motor speed, therefore, remains constant immediately after the load torque application and deviates from that of the roll. The difference in the speeds between the motor and rolls causes tension on the shaft as shown in Figure 1-1(b). Once the shaft is distorted, torsional vibration results due to the "spring property" of the shaft and last for certain time depending on the system damping. In real system, to improve the strip-thickness and strip-width accuracy, the response bandwidth of the controller becomes higher and higher even to the range near the mechanical resonant frequency. In this case, the motor speed and load speed can be very different in transient state and cause large torsional vibration that may damage the system.

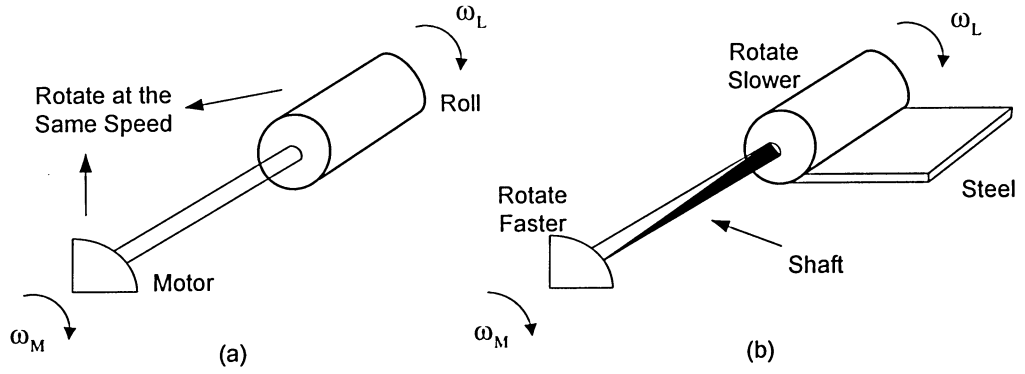

Figure 1-1 Mechanism of mechanical excitation.

The other type of excitation, often called electrical excitation, can be explained with the interference diagrams [6] shown in Figure 1-2. Figure 1-2(a) shows the interference diagram for a constant speed system with a single exciting order, which means that there is only one intersection between the operating speed and the natural resonant frequency. For this type of system, it may be sufficient to calculate

the torsional natural frequency of the system and determine the separation margin. If there is a 20 percent separation margin between the operating speed and the natural resonant frequency, then the system may be acceptable. In most practical systems, the motors are driven by variable frequency drive (VFD) with a wide operating speed range. This increases the likelihood that, at some operating speeds, a coincidence between a natural resonant frequency and the harmonic excitation frequency. This can amplify the mechanical resonance vibration and cause damage in the system.

The electrical excitation of the variable frequency drive (VFD) includes the fundamental electrical frequency, and multiples of 6,12,18,24, etc of the operating frequency. Figure 2-1(b) shows the interference diagram of a system with multiple operating speeds and a single exciting natural frequency.

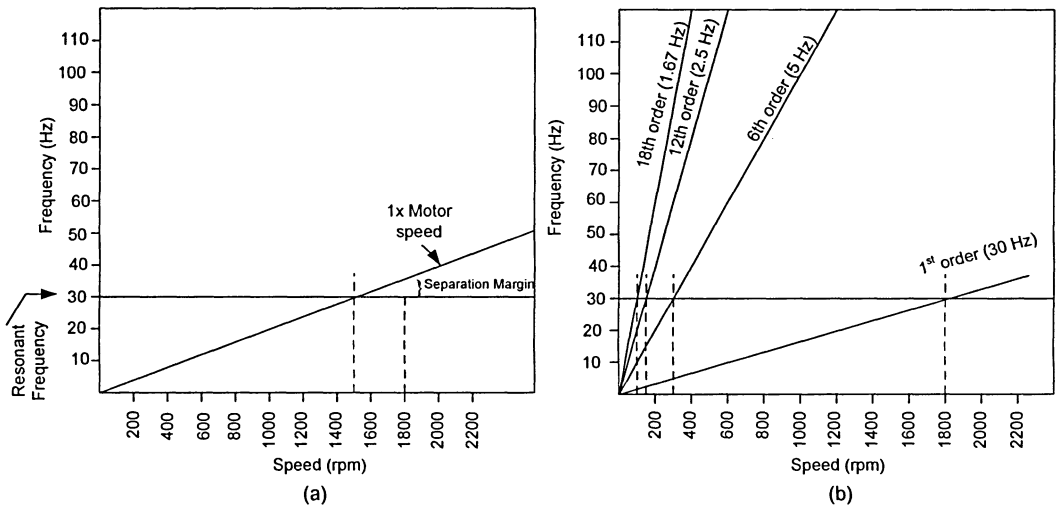

Figure 1-2 Interference diagram.

Generally speaking, a mill drive train has three types of vibration "chatter" and can be categorized according to the resonant frequency into [4]:

(1) Torsional chatter, with natural frequency ranging approximately from 5 to 20 Hz.

(2) Third octave mode chatter, with natural frequencies ranging from 125 to 240 Hz.

(3) Fifth octave mode chatter, occurring in the range of approximately 500 to 700 Hz on large production mills.

Usually, the first resonance (5-20 Hz) is the worst and can cause severe damage in the rolling mill system. This frequency is usually modeled by using an equivalent two mass model as will be discussed in the next chapter.

This thesis will focus on the analysis and modeling of a resonant elastic system for steel rolling mill drive train system. Evaluation and comparison will be performed for different torsional vibration damping methods. Finally, a proposed resonant compensator will be developed based on State Feedback Control method using torque sensor signal as a feedback element. The development stage of the resonant compensator starts with the dynamic simulation using MATLAB and its modern control tool boxes. The development proceeds to the laboratory testing using motor generator set coupled by a shaft "spindle" with a resonant frequency of 24 Hz.

1.3 Literature review

1.3.1 Model Following Control Methods

A control technique called Model Following Control (MFC) method for shaft vibration suppression was introduced by Katsuhilo Doi, et al [10]. MFC calculates the ideal speed by simulation of a two-mass mechanical model and compares the simulated ideal speed with the actual motor speed. The resultant signal from the comparison was applied to a transfer function (G) to generate the disturbance compensative current signal which was then injected into the current regulator reference to suppress the torsional vibration in the mechanical system. There is no detail about the design of the transfer function (G) used in this paper.

Another control method based on the MFC technique called Estimated Torque Controller (ETC) was presented by H. Naitoh, and K. Suzuki [11]. This software based implementation controller multiplies the difference between the ideal and the actual speed of the motor by a constant (K) to estimate the shaft torque. The estimated shaft torque was then added to the output of the speed regulator through a transfer function with gain (H). No information has been given about the design of the transfer function (H). This method has been verified through an experimental setup which contains an induction motor driven by a GTO-NPC inverter with a carrier frequency of 512 Hz. The resultant mechanical motor/load inertia used in this experiment was 6:1. The experiment results look promising since oscillations caused by the load impact were largely suppressed. In both MFC and ETC methods

robustness analysis was not discussed in particular with respect to time delay. Analysis by the author of this thesis indicated that the compensated signal of these methods can affect the speed loop with the load step change. Also, system time delay could reduce the damping effect of this method.

1.3.2 Speed Deviation Filter Base Control Method

A ripple suppression control method based on detecting the velocity fluctuation component and current amplitude control was developed by Hiroshi Nagase, et al [12]. The speed fluctuation was detected by using a filter that had a differential element. This paper shows that the current amplitude control is effective for suppressing the torque ripple at the resonant frequency. The proposed method was verified through the simulation of mechanical system with 3.4 Hz resonant frequency. It was claimed that this method was already applied to a drive system in the steel industry and yielded satisfactory results. Robustness analysis was not covered especially with respect to system time delay. Simulation by the author of this thesis for this method indicated that system time delay could limit the damping effect of this method.

1.3.3 Disturbance Observer Control Method

An observed shaft torque base compensation method was developed by Tsutomu Ohmae, et al [13]. Using motion equation, the shaft torque was estimated by measuring only motor speed and motor current (torque). The estimated shaft torque was then used to suppress the oscillation in the shaft torque by feeding it back to the current reference through a differentiator filter. It is stated that the estimated torque can be affected by the quality and the delay of the current and speed sensors. The design was tested on a laboratory d.c drive system which had a mechanical resonance frequency of 15 Hz. The experimental results look very promising. The advantage of this design is that it is simple and no prior identification for the mechanical system is needed. However, problems were found at low speed because of the low resolution of the speed decoder which can be solved by using a high resolution speed decoder. Robustness was not discussed, in particular with respect to time delay. Analysis and simulation by the author of this thesis indicated that time delay could cause stability problem.

1.3.4 Observer-Based State Feedback Controller

A robust speed controller for the suppression the torsional vibration was proposed by R. Dhoauadi, et al [14]. The robust speed controller based on a state feedback control structure with the use of speed sensor signal. The feedback compensator was designed as a state feedback controller with an observer for the reconstruction of the inaccessible system states. The loop transfer recovery (LTR) design methodology was used to design the observer so as to recover either exactly or approximately the target loop transfer function, i.e. the open loop compensator which contains estimator becomes close to the open loop ideal compensator. Two types of observer schemes were examined in the design: A Kalman Filter (full state observer) and a reduced observer. The state feedback gains were selected using the pole placement design approach. Attention has been given to the stability robustness to unmodeled dynamics, the effects of disturbances and the plant parameters variation. The simulation results of this paper looks satisfactory and within the design specification limits. In this control method, the speed regulator was included in the design of the state feedback design. This may add some difficulty in adjusting the speed response in the practical field.

1.3.5 Shaft Torque Sensor Based Control

A control scheme using torque sensor feedback was discussed by David H. Butler, et al [15]. A scale model and a large full-scale mill were both tested with the proposed control loop. Apart from the torque feedback loop, the control was a conventional two-loop speed and current regulator. The torque feedback signal serves as an auxiliary current reference substituting in the output of the speed regulator. A phase advance was used to compensate the phase lags introduced by sampling time delay. For the full-scale implementation a differentiator with the proportional gain was used in the shaft torque signal which was fed into the digital current regulator as an additional reference. The paper shows that the speed-sensor ripple and sampling delay of the digital speed regulator can be limit the damping of the system. It is obvious that the shaft torque signal is a good signal for damping if an accurate torque sensor is used. The authors of this paper mention that there are problems with torque sensors, such as noise spikes, notches, noise bursts, as well

as drift of gain and offset because of the telemetry. Permanent transmitter power supplies were installed to solve these problems.

1.4 Motivation and Objective

The increasing demand for higher quality steel strips and higher strip thickness precision in the steel industry has lead to more demanding performance requirements from rolling mill drive. However, the mechanical vibrations inherited in rolling mill drives remain a big obstacle for achieving high-performance speed control loops with higher bandwidth and higher accuracy. Therefore, the mechanical torsional vibration can be considered a major problem in rolling mill speed control drive. The other major problems in mill drives are: the uncontrolled load disturbances, the plant uncertainties (such as parameters variation) and the plant constants (such us actuator saturation).

Based on the study and analysis of different control schemes of mill drives presented in previous section, a conventional PI controller is used for speed regulation with feedforward compensation signal to damp the mechanical torsional vibration. However, these methods may not be robust to the plant variation and plant constraints. Also, they have limitation in damping due to the large time delay and they may affect the speed loop response.

Therefore, the main objective of this thesis is to develop an effective resonant compensator to suppress the undesirable mechanical torsional vibration for system with significant time delay. Furthermore, this should be achieved without affecting the speed loop response.

The other important objective is to design robust compensator against the plant parameters variation, uncertain dynamics, significant time delay in the drive, and load torque disturbance to guarantee system stability and high performance operation of the system.

In brief, the effort devoted to the resonant compensator of the rolling mill drive system is targeted to:

(1) Analyze damping algorithm based on State Feedback Control method using torque sensor as a feedback signal. The state feedback approach need not only the internal states but also the unknown input. Therefore, observer-based state feedback controller can be used to estimate the inaccessible states.

(2) Develop resonant compensator to damp the mechanical resonant pole to the desired position. This compensator should have a transparent effect to the speed loop response and robust to parameters variation, especially the drive time delay; and

(3) Simplify the structure of the developed algorithm by reducing its order and minimizing the number of tuning parameters of the compensator.

1.5 Thesis Organization

The thesis is organized into 5 chapters.

Following the introduction in Chapter 1, Chapter 2 deals with a mathematical model of drive train systems. The mathematical model can be used to understand the interaction between the mechanical system and the system regulators. Also, this model can be used to investigate the behavior of load speed, motor speed, and shaft torque during speed reference steps and load disturbances. Using the mathematical model of the system, the effect of the system parameter on damping is covered in detail. Also, different torsional vibration mitigation methods are discussed in this chapter to obtain good insight for the developed damping method. Classical control tools, such as Bode plots and root locus, and computer time simulation are used to understand the characteristics of the resonant mechanical system.

Chapter 3 emphasizes the modeling of the developed resonant compensator using the state feedback control method. The Linear Quadratic Gaussian with Linear Transfer Recovery (LQG/LTR) algorithm is discussed. Robustness of the compensator against different system uncertainty is covered in detail to examine the system stability margin. The performance of the developed algorithm is verified by extensive classical control tools and computer time domain simulation.

The experimental verification is given in Chapter 4. The experimental setup includes two dc motors connected together through a long shaft to simulate rolling mill system with 24 Hz resonant frequency. A DSP2812 controller is used to implement the proposed control algorithm. Torque responses and speed responses results are examined and discussed in association with the simulation. Finally, chapter 5 presents the conclusions for the work performed.

CHAPTER 2: DRIVE TRAIN MODEL AND TORSIONAL VIBRATION MITIGATION METHODS

2.1 Introduction

The process of rolling mills may contain several stands in one process. Each stand is fed by one or two motors in twin-drive configuration. The motors could be dc or ac motors coupled with the rolls by shafts and gear box.

It is very advantageous if a model of drive train with a closed loop control is available with sufficient accuracy. First, it helps to understand the mechanical system and its interaction with the speed and torque regulators. Secondly it is possible to investigate the behavior of the load speed, motor speed and shaft torque during speed step changes and load disturbances. Also, the developed model can be used to determine the robustness and sensitivity of system parameters to different disturbances such as motor torque ripple.

This chapter focuses on the modeling of drive train system, investigation of effect of system parameters on damping, and survey of different mitigation methods of torsional vibration.

2.2 Mathematical Model of the Drive

A typical electrical drive system is composed of a power converter fed motor coupled to a mechanical system, a microprocessor based system controller, and sensors used as feedback signals. Figure 2-1 shows the entire drive train model used in developing the proposed resonant damping algorithm. Apart from the resonant compensator block, the drive system is a standard industrial drive train system with two major control loops.

The inner control loop performs a motor torque regulation and consists of the power converter, electromagnetic part of the motor, current sensor, and the current or torque controller. This control loop is usually designed to provide sufficiently fast torque control, so it can be approximated by an equivalent first-order term with a certain time delay. Provided that the inner control loop is insured, the driven machine could be AC or DC motor, with no difference in the outer control loop.

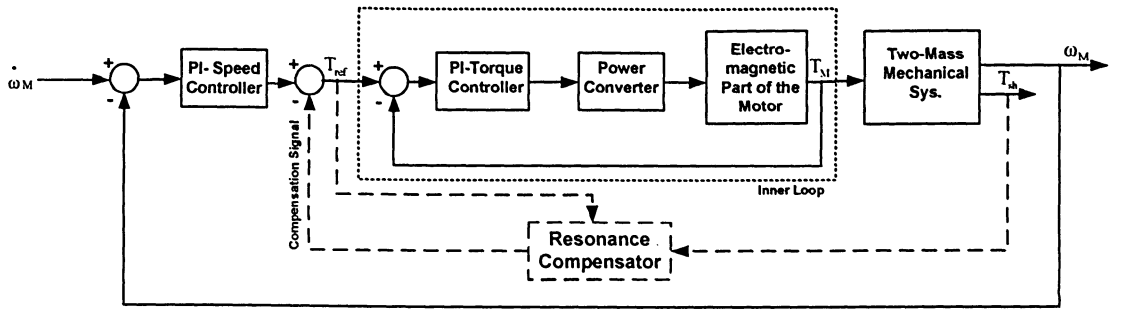

Figure 2-1 Entire drive train model.

The outer speed loop consists of the mechanical system, speed sensor and the speed controller. This loop provides speed control according to the reference value. The mechanical part of the drive is modeled as a two-mass mechanical model due to the characteristics of the shaft between motors and the rolls. Figure 2-2 shows the approximate model used in the system analysis. This model includes three parts: two-mass mechanical model, torque regulator model, and speed regulator.

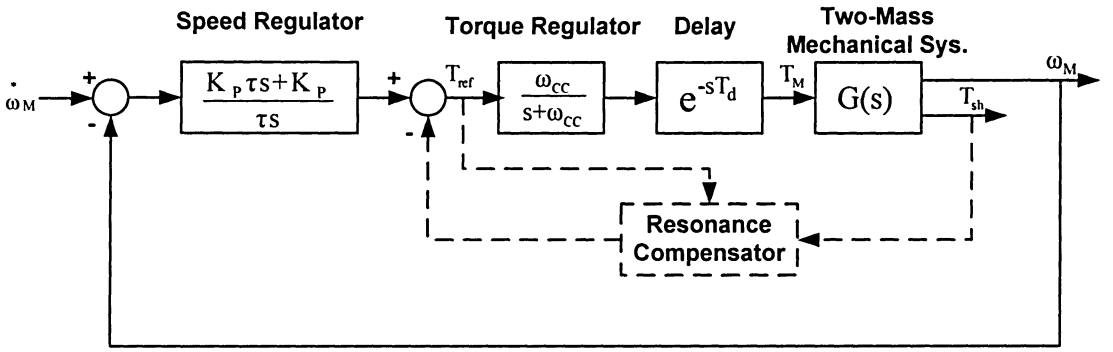

Figure 2-2 Approximation model of the entire drive train system.

2.2.1 Two-mass Mechanical System

The practical mechanical system of a mill drive is a complex multi-mass system and has a number of resonant frequencies depending on the configuration of shaft, gears, etc. As mentioned in Chapter 1, the lowest resonant frequency is usually the worst and is modeled with the equivalent two-mass model shown in Figure 2-3. In the two-mass model, the separate motors are lumped into a single unit as are the rolls. These two lumped inertias are connected together by the shaft as shown in Figure 2-3(a).

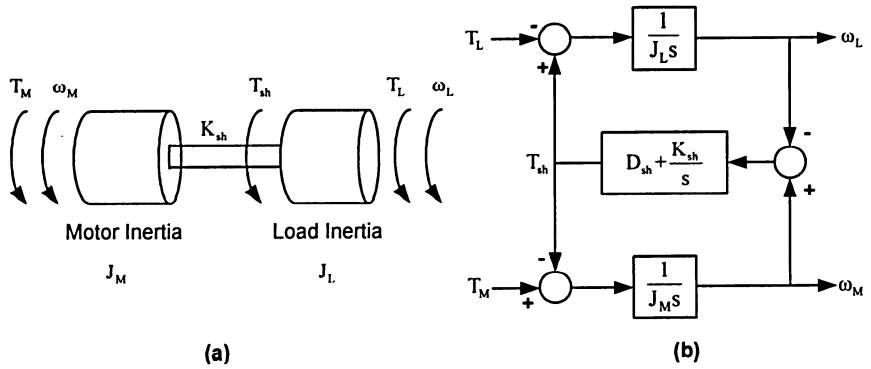

Figure 2-3 Two mass model of the mechanical system.

The two-mass system shown in Figure 2-3(b) can be modeled as follows [16]:

$$\left.\begin{aligned} J_M\dot{\omega}_M &= -D_M\omega_M - T_{sh} + T_M \\ J_L\dot{\omega}_L &= -D_L\omega_L + T_{sh} - T_L \\ \Delta\omega &= \omega_M - \omega_L \end{aligned}\right\} \tag{2-1}$$

$$\left.\begin{aligned} \dot{\theta}_M &= \omega_M \\ \dot{\theta}_L &= \omega_L \\ \Delta\dot{\theta} &= \omega_M - \omega_L \end{aligned}\right\} \tag{2-2}$$

$$\left.\begin{aligned} T_{sh} &= K_{sh}(\theta_M - \theta_L) + D_{sh}(\omega_M - \omega_L) \\ &= K_{sh}\Delta\theta + D_{sh}\Delta\omega \end{aligned}\right\} \tag{2-3}$$

where

T_M, T_L, T_{sh} are the motor, load, and shaft torques [N.m]
J_M, J_L are the motor and load moment of inertias [kgm^2]
K_{sh} is the shaft Stiffness [Nm/rad]
D_M, D_L, D_{sh} are the motor, load and shaft damping coefficients [Nm/(rad/sec)]
ω_M, ω_L is the motor and load speeds [rad/sec]
θ_M, θ_L are the motor and load angles [rad]
$\Delta\theta$ is the difference angle [rad]
$\Delta\omega$ is the speed difference [rad/sec]

Substituting Equation (2-3) into Equation (2-1) results:

$$\left.\begin{aligned}\dot{\omega}_M &= -\frac{K_{sh}}{J_M}\Delta\theta - \frac{D_{sh}}{J_M}\omega_M + \frac{D_{sh}}{J_M}\omega_L + \frac{T_M}{J_M}\\ \dot{\omega}_L &= \frac{K_{sh}}{J_L}\Delta\theta + \frac{D_{sh}}{J_L}\omega_M - \frac{D_{sh}}{J_L}\omega_L - \frac{T_L}{J_L}\\ \Delta\dot{\theta} &= \omega_M - \omega_L\end{aligned}\right\} \qquad (2\text{-}4)$$

The state space representation of the system in Equation (2-4) can be arranged as follows:

$$\left.\begin{aligned}\dot{x} &= Ax + BT_M + ET_L\\ T_{sh} &= C_1 x\\ \omega_M &= C_2 x\end{aligned}\right\} \qquad (2\text{-}5)$$

where

$$x=[\omega_M \quad \omega_L \quad \Delta\theta]^T \; ; \; A=\begin{bmatrix} -\frac{D_{sh}}{J_M} & \frac{D_{sh}}{J_M} & -\frac{K_{sh}}{J_M} \\ \frac{D_{sh}}{J_L} & -\frac{D_{sh}}{J_L} & \frac{K_{sh}}{J_L} \\ 1 & -1 & 0 \end{bmatrix} \; ; \; B=\begin{bmatrix} \frac{1}{J_M} & 0 & 0 \end{bmatrix}^T$$

$$E=\begin{bmatrix} 0 & -\frac{1}{J_L} & 0 \end{bmatrix}^T \; ; \; C_1=[D_{sh} \quad -D_{sh} \quad K_{sh}] \; ; \; C_2=[1 \quad 0 \quad 0]$$

The following transfer functions can be derived from the two-mass model:

$$\frac{\omega_M}{T_M} = \frac{s^2 + D_{sh}/J_L + \omega_o^2}{J_M s(s^2 + 2\xi\omega_o s + \omega_n^2)} \qquad (2\text{-}6)$$

$$\frac{\omega_L}{T_M} = \frac{D_{sh}/J_L + \omega_o^2}{J_M s(s^2 + 2\xi\omega_o s + \omega_n^2)} \qquad (2\text{-}7)$$

$$\frac{T_{sh}}{T_M} = \frac{D_{sh} + K_{sh}}{J_M(s^2 + 2\xi\omega_o s + \omega_o^2)} \qquad (2\text{-}8)$$

where

$\omega_n = \sqrt{\frac{K_{sh}(J_M + J_L)}{J_M J_L}}$ is the mechanical resonant frequency ;

$\omega_o = \sqrt{\frac{K_{sh}}{J_L}}$ is the anti-resonant frequency; and

$\xi = \frac{D_{sh}}{2}\sqrt{\frac{J_M + J_L}{K_{sh} J_M J_L}}$ is the damping factor.

The transfer functions of (2-6), (2-7), and (2-8) have two dominant poles called resonant poles that cause the mechanical system to become marginally stable. Figure 2-4 shows the magnitude Bode plots of the ω_M/T_M, ω_L/T_M, and T_{sh}/T_M transfer functions of the two-mass mechanical system. From Figure 2-4, two dramatic changes are noticed at the magnitudes of the Bode plots, one at the resonant frequency and the other at ant-resonant frequency. These dramatic changes appear because of the effects of mechanical poles and zeros respectively.

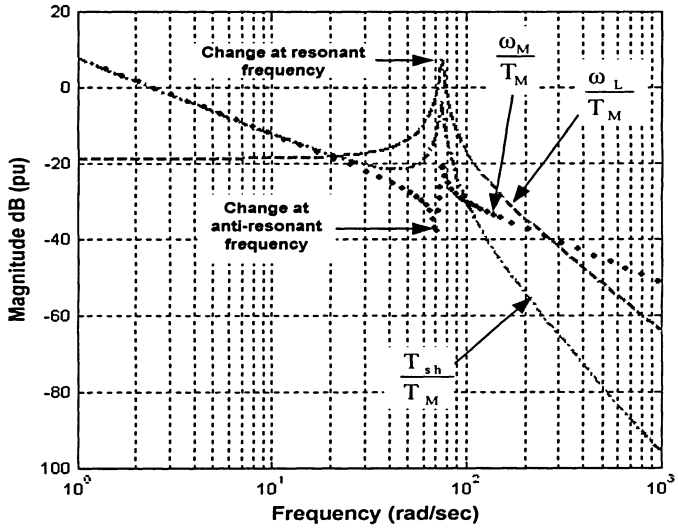

Figure 2-4 Bode plot of the two-mass mechanical system.

2.2.2 Torque Regulator Model

As mentioned earlier, the torque regulator model represents the dynamics of the inner torque regulator loop and can be modeled as a single lag with delay as follows:

$$T_M = \frac{e^{-sT_d}}{1 + sT_r} T_{ref} \qquad (2\text{-}9)$$

where

T_M is the motor torque;
T_{ref} is the motor torque reference;
T_d is the time delay; and
T_r is the regulator time constant and equal to $1/\omega_{CC}$, where ω_{CC} is the torque cut-off frequency.

Figure 2-5 shows a block diagram of the torque regulator model. Usually, the range of torque regulator time constant T_r is between 1ms and 10ms depending on the type of the power converter. The term e^{-sT_d} (linear phase delay) represents the delay from motor torque reference T_{ref} to the motor torque T_M and can be calculated by:

$$\text{Phase Delay} = -\omega_n T_d \frac{180^\circ}{\pi} \tag{2-10}$$

To simplify the analysis, the irrational term e^{-sT_d} of Equation (2-9) is converted to rational transfer function by using Pade approximation.

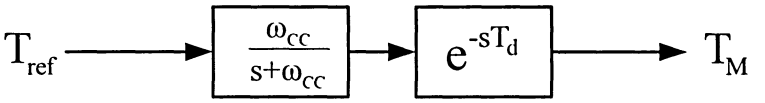

Figure 2-5 Dynamic model of torque regulator.

In this thesis, a second order Pade approximation is used for better accuracy comparing with the actual linear phase delay.

2.2.3 Speed Regulator

The speed regulator used in this project is a conventional PI controller. This type of controller is widely use in industry because it is simple, robust and effective. The transfer function of the PI controller is as follows:

$$G_{PI} = \frac{K_P(\tau s+1)}{\tau s} \tag{2-11}$$

where K_P is the proportional gain and τ is the integration time constant of the PI controller.

This type of controller is usually designed for a rigid mechanical system with no attention paid to the resonant poles.

The rigid mechanical system is given by:

$$G_{rigid} = \frac{1}{J_T s} \tag{2-12}$$

where $J_T = J_M + J_L$ is the total moment of inertia.

The proportional gain K_P is therefore calculated by:

$$K_P = J_T \omega_{cs} \tag{2-13}$$

where ω_{cs} is the cut-off frequency of the speed loop.

The integration time constant of the PI controller, τ, should be much greater than $1/\omega_{cs}$ so that the speed response does not have high overshoot [17]. In the design example system a time constant of $\tau = 5/\omega_{cs}$ is used.

The performance of the speed controller is evaluated according to three performance factors: overshoot, settling time, and impact drop as shown in Figure 2-6.

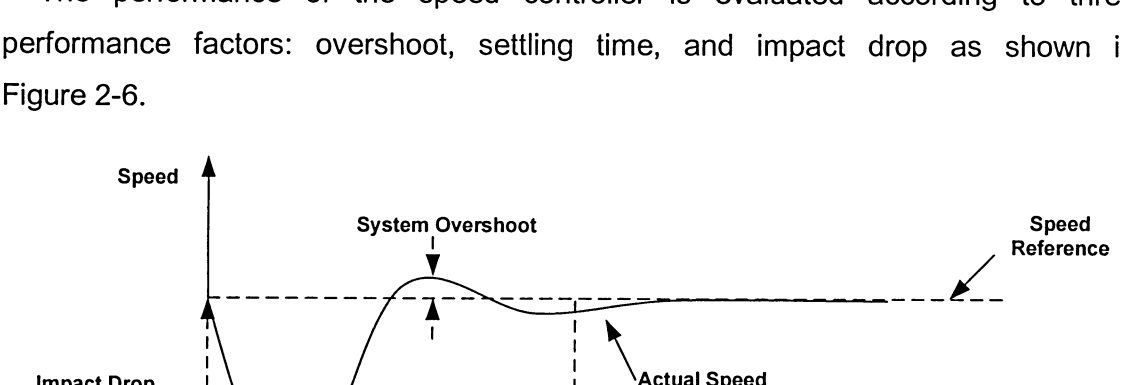

Figure 2-6 Performance factors of the speed controller.

2.3 Case Study of an Industrial Drive

2.3.1 System Parameters and Analysis

The system parameters of the case study are taken from actual rolling mill drive system [15]. This rolling mill system is driven by twin dc motors fed by digitally controlled 12-pulse thyristor converters. This mill system has the capacity to roll 3 million ton/annum of hot steel slabs (maximum size 12.5m long x 1650 mm wide x 230 mm thick weighing up to 31 tons) to transfer bars (130 m long and 30 mm thick) in five to nine passes. Drive data are shown in Figure 2-7 and Table 2-1.

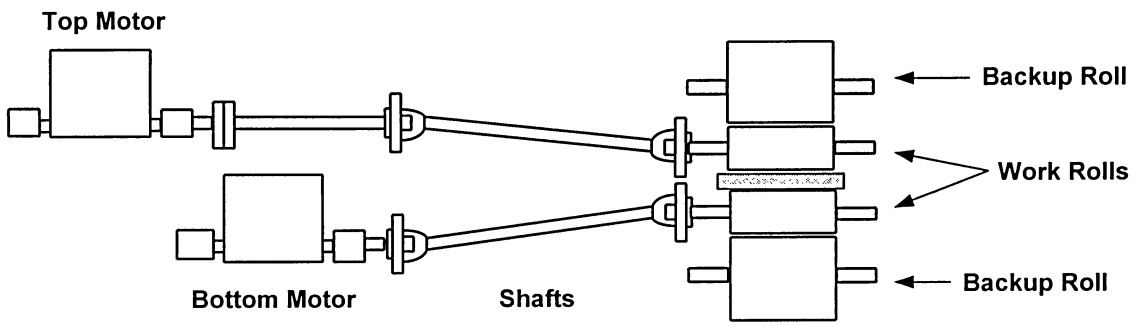

Figure 2-7 Roll mill drive.

Table 2-1 System parameters

DC Motors Data	Shaft (Spindle) data	Roll data
Rated Power: 6000KW Speed: 43/100 rpm Rated Voltage: 1200V Rated Current: 5376A Rated Torque: 1360KN.m Equivalent Inertia(J_M): 110000 Kg.m^2	Length: 10.9 m Equivalent Stiffness(K_{sh}): 70 M N.m/rad Equivalent Damping(D_{sh}): 46 K N.m/rad/sec	Work Rolls: 1200 mm diameter 1800 mm long Backup Rolls: 1400 mm diameter 1800 mm long Rolls+Slab Inertia(J_L): 14000 Kg.m^2

The controller of this drive mill is a conventional speed control system with two loops, one for the torque regulator and the other is for the speed loop. The specification of this controller are shown in Table 2-2

Table 2-2 Controller parameters

Parameters	Value
Speed Regulator Cross-over Frequency :	15 rad/sec
Torque Regulator Cross-over Frequency:	180 rad/sec
Loops Sampling Rate:	3.3 ms
Torque Regulator Time Delay:	20 ms

Table 2-3 shows more data which are calculated from the mechanical system parameters.

Table 2-3 Calculated parameters

Parameters	Value
J_M/J_L Ratio	7.85
Resonant Frequency	75 rad/sec
Anti-resonant Frequency	70.7 rad/sec

Since the system has resonant frequency of 75 rad/sec and time delay around 20 ms, the actual phase delay is equal to -85.94°. Figure 2-8 shows the difference between the actual linear phase delay and the second order approximation of the delay. It is very clear that there is a very small difference of only 0.5 degree at the resonant frequency. This proves the accuracy of phase delay approximation.

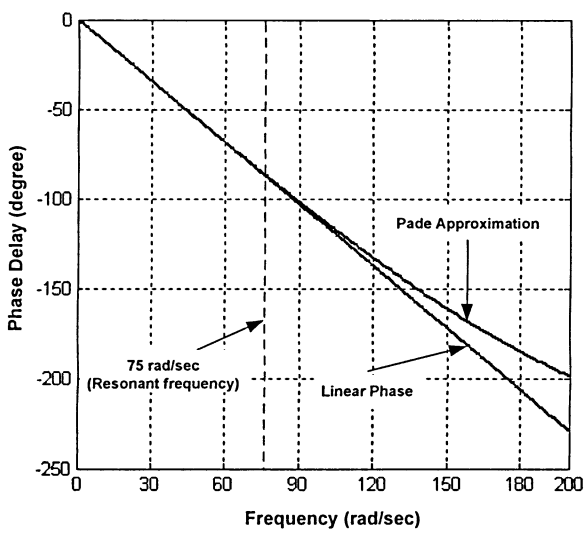

Figure 2-8 Difference between the actual linear phase delay and the second order approximation of the delay.

The dynamic response of the system is analyzed with the aid of Bode plot as shown in Figure 2-9. Using speed crossover frequency of 15 rad/sec, the phase margin of 51° degrees seems satisfactory. However, at 75 rad/sec resonant frequency, the phase angle lag is 80° degrees which causes the system to be unstable due to the resonant peak that hit the 0 dB.

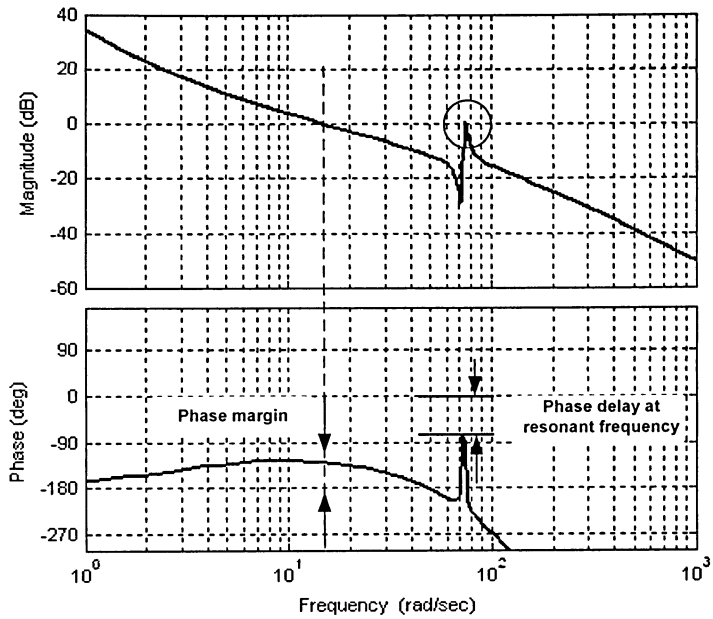

Figure 2-9 Bode plot of the open loop system transfer function.

2.3.2 Simulation Block Diagram

For more realistic simulation model, some extra parts that simulate some practical effect are added to the approximate model of the drive. These extra parts are the continuous time (CT) and the discrete time (DT) models. Figure 2-10 shows the simulation model that is used in this thesis. In this section, the effect and model of these parts are discussed.

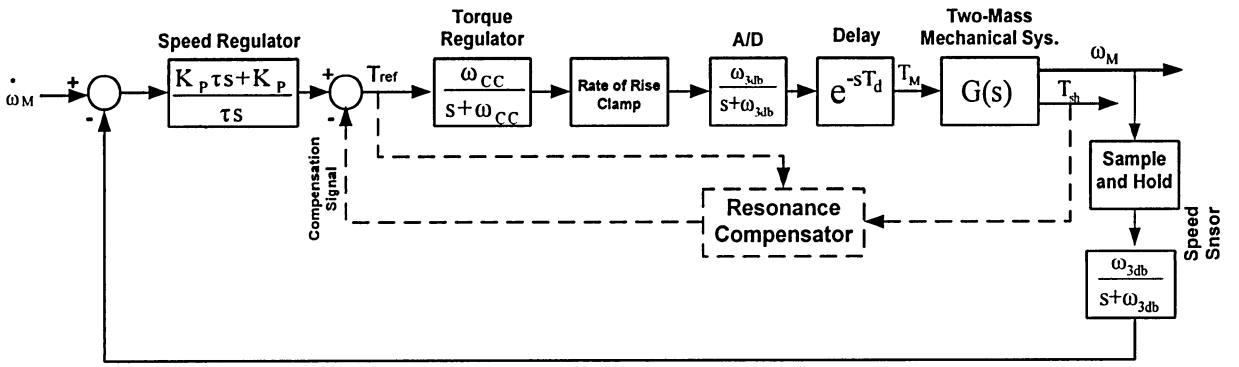

Figure 2-10 Block diagram of simulation model.

a) Speed Sensor (Digital Tachometer)

In most practical applications, a digital tachometer is preferred rather than a analog tachometer due to its low cost and ease to integrate with a digital controller. The effect of the tachometer is to add time or phase delay and finite resolution. Since the time delay is more concerned in this thesis, the model of the tachometer will include the effects that cause time delay such as the limited bandwidth and the discrete nature of the tachometer.

The simplified and effective continuous time model of the digital tachometer is given by:

$$G(s)=\frac{1-e^{-s\Delta T}}{\Delta Ts} \tag{2-14}$$

where ΔT is the time between samples.

The above transfer function can be approximated by:

$$G_{tach}(s)=\frac{\omega_{3db}}{s+\omega_{3db}} \tag{2-15}$$

where $\omega_{3db}=2f_s$

The tachometer model represented by Equation (2-15) simulates the effect of limited bandwidth and the phase delay. In order to simulate the effect of digital time of the

tachometer, a Sample and Hold is added in series with the transfer function of Equation (2-15).

b) A/D Circuits

The principle operation of A/D is to count pulses between sample times. The inherited low pass filter characteristic that is useful for noise reduction can be modeled as a low pass filter with cut-off frequency set to twice the sample rate. The digital time effect of the A/D can be modeled as a Sample and Hold added in series with the transfer function of the A/D circuit. The transfer function of this circuit is as follows:

$$G_{A/D}(s)=\frac{\omega_{3db}}{s+\omega_{3db}} \tag{2-16}$$

c) Rate of Rise Clamps

The rate of rise clamps simulates the digital time approximation of the torque regulator lag with a clamp. Adding this effect will give additional time delay to the system. The setting of rate clamp is based on the compensator change rate with respect to the ripple magnitude. Since the magnitude of the ripple of the case study system is about 0.5 pu (50% of the rated torque), this value will be reasonable for setting the rate of rise clamp. Now, with a linear approximation for 180 rad/sec time constant with a 0.5 pu step, the limit will be as follows:

$$0.5(63\%)/0.0055 = 56.7 \text{ pu/sec} \tag{2-17}$$

Therefore, in simulation of the case study, the rate limit is set to 60 pu/sec (rated torque=1 pu). The result of this limit is simply to place more phase delay at the resonant frequency.

2.3.3 System Simulation

To obtain some elementary features about the behavior of the standard industrial drive system and the two-mass model, step change responses are taken with

system parameters defined in Tables 2-1 and 2-2. For now, simulation does not include any time lag and discrete time effect. The responses are taken by applying 20% speed step change initially and 50% load torque step change at 2 sec. Figure 2-11 shows the step responses of the system with 0.887 J_M / J_T inertia ratio (light load) and Figure 2-12 shows the step responses of the system with 0.5 J_M / J_T inertia ratio (heavy load).

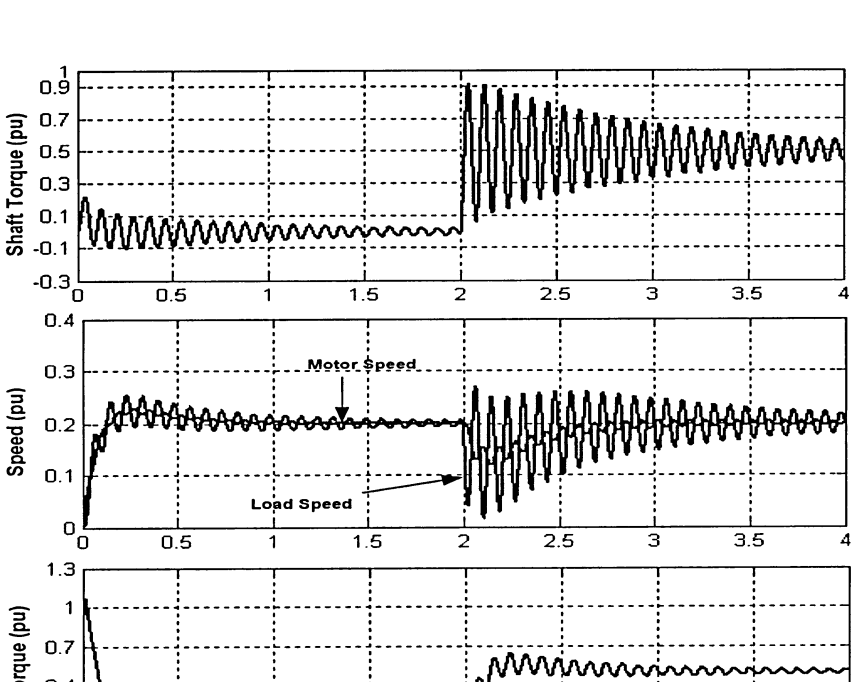

Figure 2-11 Responses of the system for light load case.

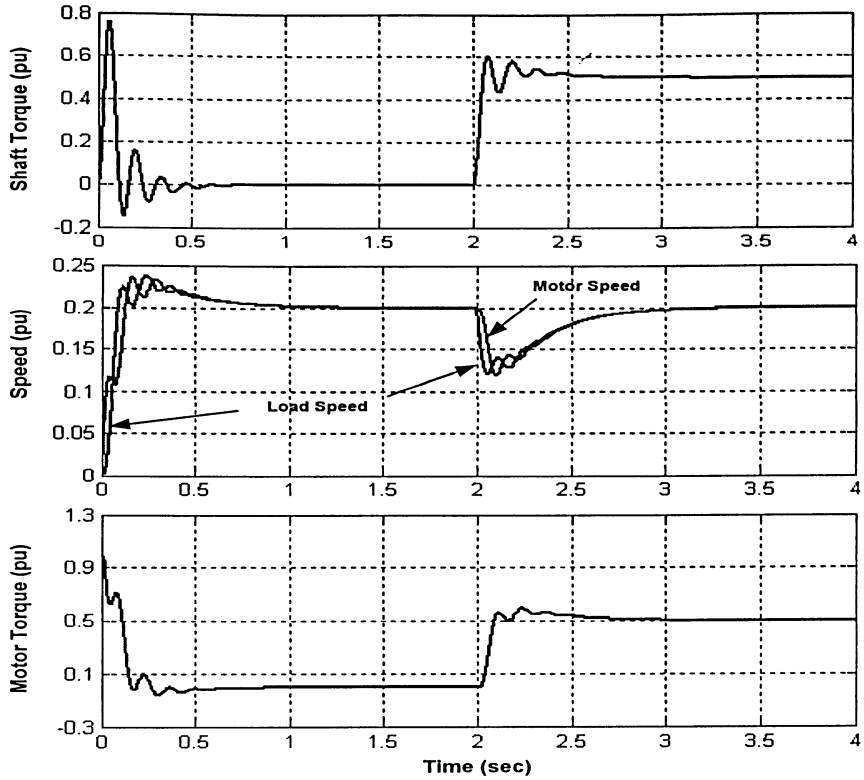

Figure 2-12 Responses of the system for heavy load case.

It is very clear that the response of the shaft torque exhibits large oscillation comparing with the responses of the applied torque, motor speed and load speed. Also, the system responses have more oscillation with large motor-to-total inertia comparing with the system with small motor-to-total inertia.

From the speed responses, it is found that the peak shaft torque with large motor-to-total inertia ratio is less than the case with small motor-to-total inertia ratio. The opposite results are obtained at the load torque step response, which means that the peak is greater at the large motor-to-total inertia ratio while the peak is smaller at the small motor-to-total inertia ratio.

2.4 Effect of System Parameters on Damping

It is important that the effects of system parameters on damping be investigated because system models are based on simplification and assumption. In addition, some parameters encounter variation during the operation.

2.4.1 Effect of the Load Inertia to Motor Inertia Ratio on Damping

To determine the effect of the motor to load inertia ratio on damping, a root locus of the resonant poles and the torque regulator pole of the closed loop control system is plotted with the change of J_M/J_T ratio. This is obtained by keeping the speed crossover frequency, torque regulator pole and total inertia constant. In doing so, the initial resonant frequency of the mechanical system is changed and shift stiffness is kept constant.

Figure 2-13 shows the root locus of the resonant plots as the J_M/J_T ratio changes. As can be seen from the Figure 2-13, the ratio J_M/J_T is decreased from 0.887 to 0.241 by decreasing J_M from 110000 $Kg.m^2$ to 30000 $Kg.m^2$ (10000 $Kg.m^2$ per step) and increasing J_L from 14000 $Kg.m^2$ to 94000 $Kg.m^2$ (10000 $Kg.m^2$ per step). It is found from the root locus plot that when the J_M/J_T ratio is decreased, the damping tends to increase and the torque regulator pole moving towards the right side of the s-plan. Also, it is found that with excessive increase in the J_M/J_T ratio, the torque regulator will move more towards the right, which will impact the speed regulator and cause oscillations in the responses of the system and reduction of damping

The root locus plot is an effective tool to be used to investigate the stability boundary of the inertia ratios and prevent the system from the unstable condition.

2.4.2 Effect of the Torque Regulator Pole

Departure angle of the resonant poles of the system can be a good indication for the damping of the system. To study the effect of the torque regulator pole on damping, the departure angle of the resonant poles for the closed loop speed control is determined first. The departure angle of the resonant poles is given by:

$$\left.\begin{aligned} \theta_{departure} &= 180^\circ - \sum \text{pole angles} + \sum \text{zero angles} \\ &= 180^\circ - (\alpha_r + 90^\circ + 90^\circ + 90^\circ) + (\alpha_o + 90^\circ + 90^\circ) \\ &\text{Lets } \alpha_o \approx 90^\circ \\ \theta_{departure} &= 180^\circ - \alpha_r \end{aligned}\right\} \quad (2\text{-}18)$$

where α_o is angle of the torque regulator zero; and

$\alpha_r = \tan^{-1}(\frac{\omega_n}{\omega_{cc}})$ is the angle of the torque regulator pole to the positive resonant pole.

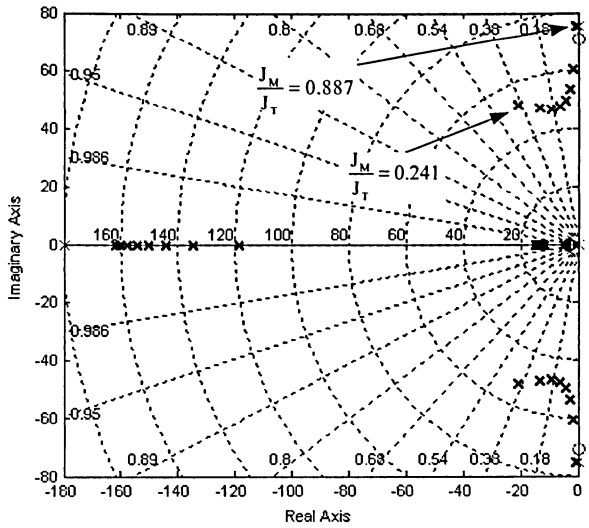

Figure 2-13 Root loci of the closed loop resonant poles with reducing JM/JL ratio.

From the equation of the departure angle, it is noticed that the closer the departure angles to 180 degree the better the damping is. This means that with large torque regulator pole or lower resonant frequency, better damping can be achieved. Figure 2-14 shows the procedure of calculating the departure angle of the resonant poles of the mechanical system.

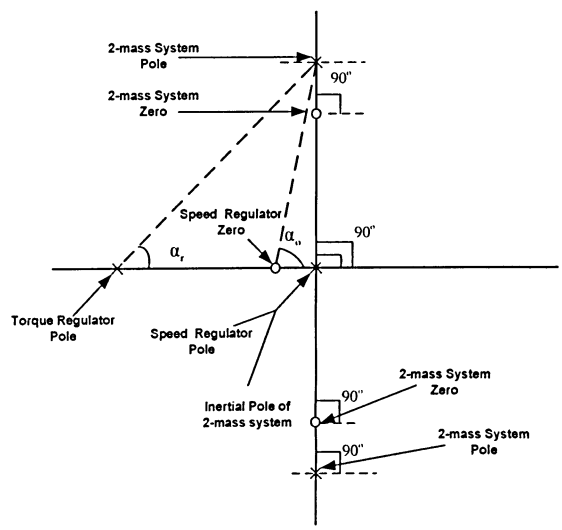

Figure 2-14 Departure angle calculation.

In order to confirm the effect of the torque regulator, root locus of the resonant poles is performed using system parameters of the case study. This is obtained by changing the torque regulator pole and keeping the speed regulator crossover frequency and inertia ratio constant. Figure 2-15 shows the root locus of the resonant poles with increasing the torque regulator pole from 0 to 300 rad/sec with 50 rad/sec step. It is very clear that increasing the torque regulator pole tends to increase the damping of the system.

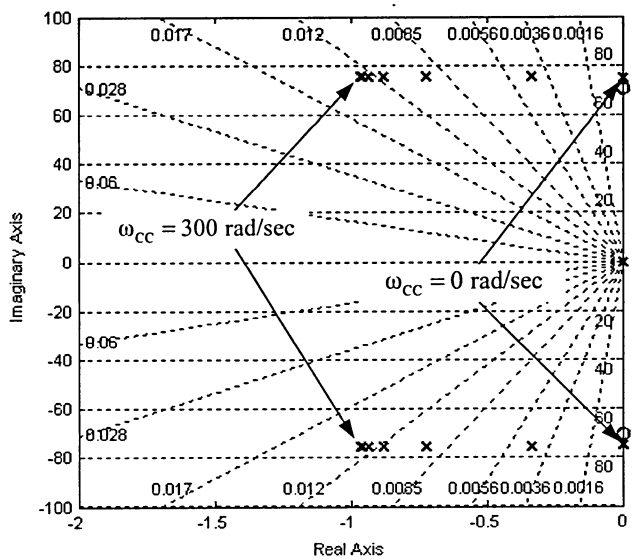

Figure 2-15 Locus of the resonant poles as torque regulator increases from 0 to 300 rad/sec.

2.4.3 Effect of System Time Delay

In case the system has a time delay or phase lag, the equation of the departure angle of the resonant poles should be modified by adding the phase lag to the departure angle. Therefore the departure angle is modified as follows:

$$\theta_{departure} = 180^\circ - \alpha_r - \omega_o T_d \frac{180^\circ}{\pi} \qquad (2\text{-}19)$$

For the system without phase lag, the departure angle is around 157.4° which is close to 180°. With 20 ms time delay, the departure angle is about 71.4° which can cause an unstable system easily.

The time delay causing the departure angle of 90° can be called a significant time delay T_{ds} and can be calculated by:

$$\left.\begin{aligned} 90^\circ &= 180^\circ - \alpha_r - \omega_o T_{ds} \frac{180^\circ}{\pi} \\ T_{ds} &= \left(\frac{90^\circ - \alpha_r}{\omega_o}\right)\frac{\pi}{180^\circ} \end{aligned}\right\} \qquad (2\text{-}20)$$

This time delay will cause the speed control loop to be unstable. Therefore, the time delay of the closed loop speed control system must be less than the significant time delay to ensure the stability of the system.

For case study system parameters, the significant time delay is 15 ms. Figure 2-16 shows Nyquist plot of the closed loop system with three time delay values: 5 ms, 10 ms, and 15 ms. It is very clear that with a 5 ms, and 10 ms time delay, the system is still stable. However, with 15 ms time delay the system becomes unstable as the plot cross -1 limit of Nyquist.

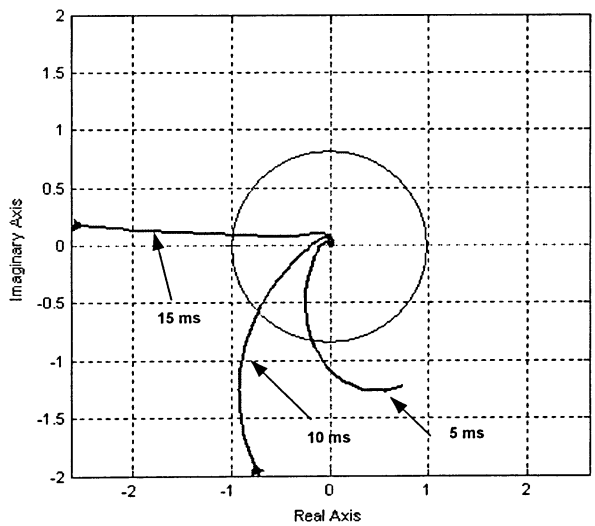

Figure 2-16 Nyquist plot of the closed loop system for three time delay values: 5 ms, 10 ms and 15 ms.

2.5 Torsional Vibration Mitigation Methods

Although the PI-based control system remains the dominant method in the industry, this type of controller can not be used to damp out the torsional vibration.

As mentioned earlier, the design of the PI parameters is based on the rigid system, which does not consider the resonant poles. Therefore, the resonant poles still have high underdamped response, which result in significant amplification of torque ripple at the resonant frequency. Also, the PI-based controller system tries to keep the motor speed constant at sudden load changes and that makes matters worse by enlarging the torsion and the vibration.

Over the years many different control approaches have been used to solve the problem of torsional vibration. Some mitigation methods of torsional vibration are covered in this section. These methods are very important in developing the proposed damping algorithm.

2.5.1 Conventional Methods of Damping

a) Detuning the Speed Regulator Gain

One of the well-known methods to control the resonance vibration is by de-tuning the speed loop. The idea of doing that is simply to attenuate the gain below 0 dB when the phase drops to 180 degree. Detuning the gain of the speed loop is practically not preferable because it reduces the dynamic performance of the speed loop [18].

b) Adding Lag Filter

The principle of using this method is to add single pole lag in the forward path of the speed loop to attenuate the gain below 0 dB at the resonance poles when the phase drops to 180 degree. Using this method looks more practical comparing with the detuning the speed regulator method but it has some conditions need to be met as follows:

(a) There is enough attenuation from the lag to the resonant pole. (If a lag is used, it can not be placed too close to cut-off frequency of the speed regulator because it will impact on the speed response)

(b) The resonance gain must be small enough so it can be reasonably reduced by the lag.

To investigate the effect of adding the single lag filter, the overall open loop gain at the resonance frequency is calculated. Before calculating the overall open loop gain of the system, the resonance gain at the shaft is determined. By taking the frequency response from applied torque to shaft torque and letting $\omega=\omega_n$, the resonance gain can be calculated as follows:

$$G(\omega_n)=\frac{T_{sh}}{T_M}=\frac{J_L}{J_T}\left(\frac{4\xi^2+1}{4\xi^2}\right)^{1/2}\approx\frac{J_L}{J_T}\frac{1}{2\xi} \tag{2-21}$$

where ξ is the damping factor and can be calculated from the decay time of the shaft torque waveform [15]. Since damping factor is around 0.0095, the overall open loop gain at the resonance frequency can be calculated as follows:

$$\left.\begin{aligned} G(\omega_n)&=\underbrace{20\log\left(\frac{\omega_{CS}}{\omega_n}\right)}_{\text{SpeedReg.Pole}}+\underbrace{20\log\left(\frac{1}{\sqrt{1+\left(\frac{\omega_n}{\omega_{CC}}\right)^2}}\right)}_{\text{TorqueReg. Pole}}+\underbrace{20\log\left(\left|\frac{J_L}{J_T}\frac{1}{2\xi}\right|\right)}_{\text{Resonance pole of 2-mass sys.}}+\underbrace{20\log\left(\frac{1}{\sqrt{1+\left(\frac{\omega_n}{\omega_{Lag}}\right)^2}}\right)}_{\text{Lag. Filter Pole}}\\ &=0.8+20\log\left(\frac{1}{\sqrt{1+\left(\frac{\omega_n}{\omega_{Lag}}\right)^2}}\right)\end{aligned}\right\} \tag{2-22}$$

In order to attenuate the gain at the resonance pole, a lag filter of 50 rad/sec cut-off frequency is used. Figure 2-17 shows the Bode plot of the open loop system with the use of lag filter. It is very clear that the gain at the resonant poles have been attenuated below the 0 dB. However, the speed loop is affected as the filter pole collides with the speed regulator pole as shown in Figure 2-18. It is noticed that this method can adversely impact the speed regulator response if large damping is required. Therefore, this method might be effective only for stabilizing the system.

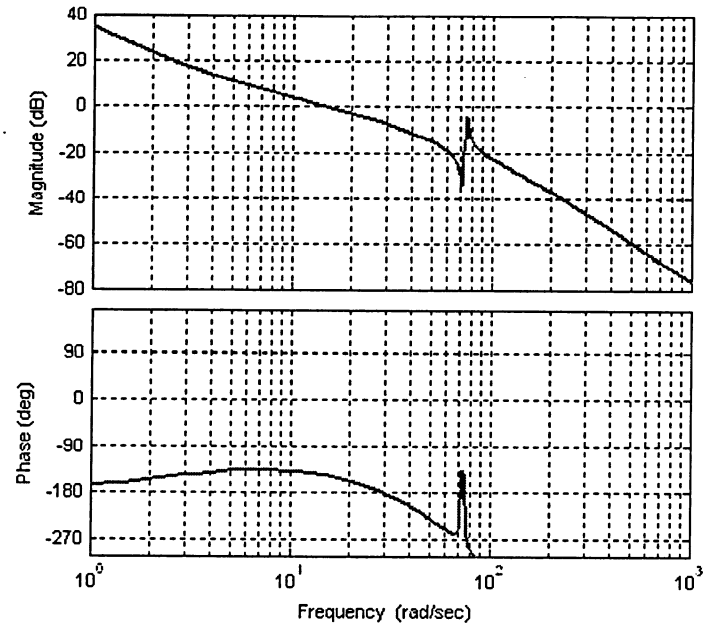

Figure 2-17 Bode plot of the system with Lag filter.

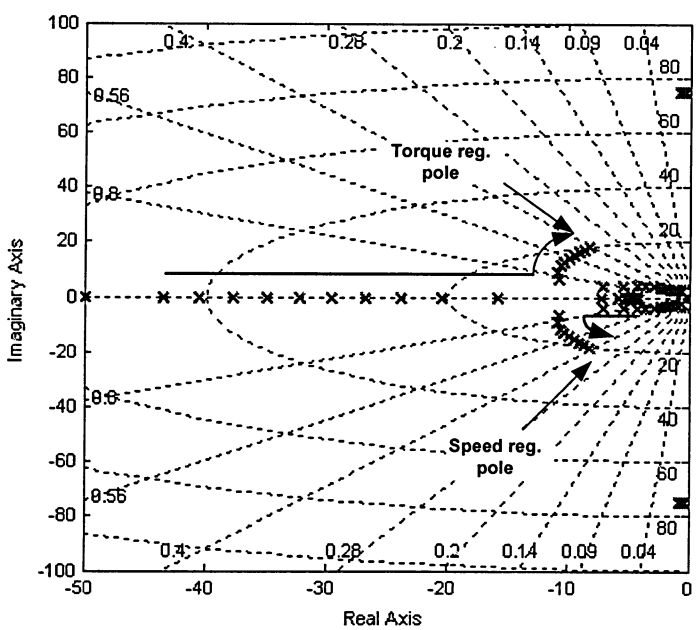

Figure 2-18 Root locus for the system with the use of Lag filter.

c) Adding Notch Filter

Another method that can be used to reduce the gain at the resonance frequency is by adding a notch filter to reduce the phase [18,19]. The notch filter transfer function is as follows:

$$G_{notch} = \frac{s^2 + 2\xi_n \hat{\omega}_n s + \hat{\omega}_n^2}{s^2 + 2\xi_o \hat{\omega}_n s + \hat{\omega}_n^2} \tag{2-23}$$

where

$\hat{\omega}_n$ is the estimated resonant frequency.

ξ_n, ξ_o are the numerator and denominator damping factor.

Typically the notch filter is placed in the forward loop at the output of the speed regulator. By designing the notch filter, phase lead should be as much as possible. For maximum lead, the zeros of the filter have to be on the imaginary axis below the resonant poles ($\xi_n \approx 0$). For minimum lag, the notch filter damping has to be small such that the lag from the upper notch filter pole is small and the lag from the lower pole close to 90 degree. Altogether a maximum net lead of 90 degree is achieved. Using the notch filter, the departure angle will be modified as follows:

$$\theta_{departure} = 180° - \alpha_r - \omega_o T_d \frac{180°}{\pi} + 90 - \alpha_{notch} \tag{2-24}$$

where

$$\left.\begin{aligned} \alpha_{notch} &= \arctan\left(\frac{\omega_n - \hat{\omega}_n\sqrt{1-\xi_o^2}}{\xi_o \hat{\omega}_n}\right) \\ &\approx \arctan\left(\frac{\omega_n - \hat{\omega}_n}{\xi_o \hat{\omega}_n}\right) \end{aligned}\right\} \tag{2-25}$$

For the case study system parameters, the setting of variable are $\xi_o = 0.1$ and $\hat{\omega}_n = 73$ rad/sec. This gives $\alpha_{notch} = 16°$ and $\theta_{departure} = 145.4°$ which insures a stable system. Figure 2-19 shows the Bode plot of notch filter transfer function. Figure 2-20 and Figure 2-21 show Bode plot of open loop transfer function and the root locus of the system with notch filter. It is very clear that using notch filter with more damping will increase the possibility to impact the speed response. Therefore, it is clear that the notch filter cannot do much more than insure the stability without impact the speed regulator response.

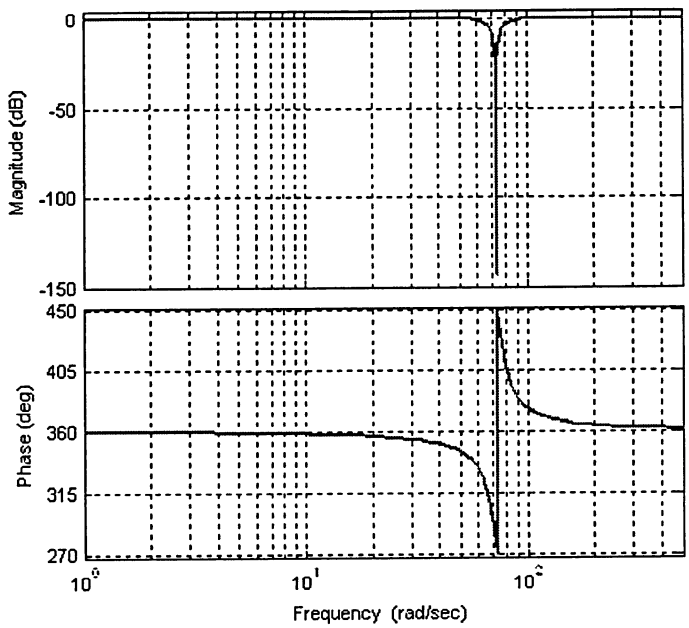

Figure 2-19 Bode plot of the notch filter transfer function.

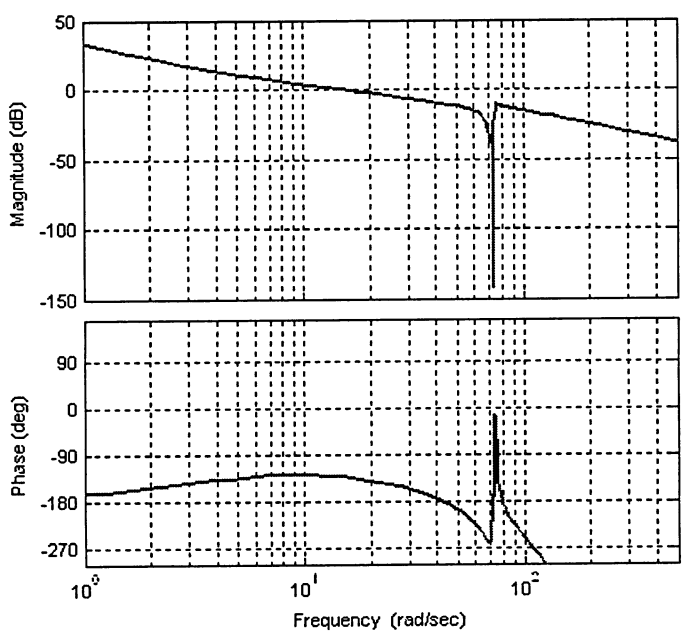

Figure 2-20 Bode plot of open loop transfer function with notch filter.

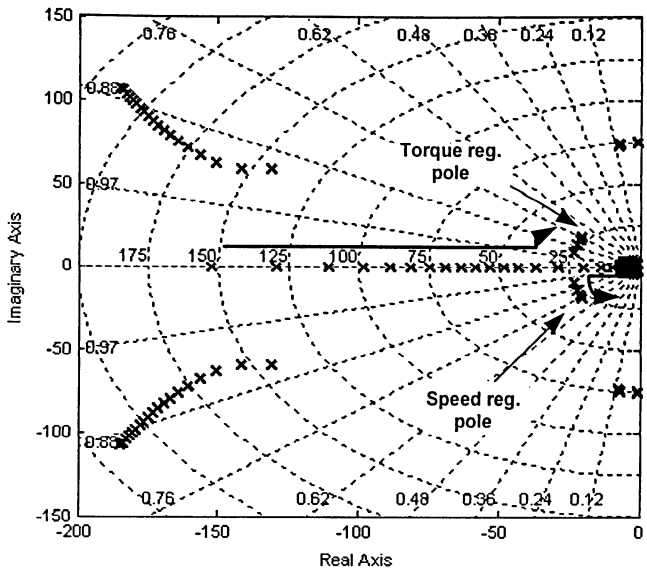

Figure 2-21 Root locus of open loop transfer function with notch filter.

2.5.2 Advanced Methods of Damping

a) Torque Sensor Based Compensator

Shaft torque measured signal based compensator can create feedforward control if this signal fed back into the torque reference. This method can improve the mechanical damping and strongly diminish any tendency to oscillate [15,20]. The shaft torque signal is an excellent signal if a sensor of good quality is used and placed adequately. Figure 2-22 shows the basic block diagram of the Torque Sensor Based compensator method.

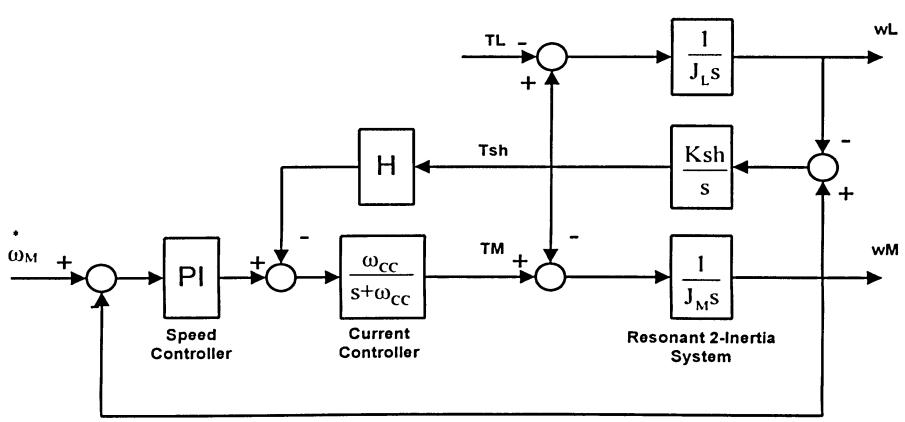

Figure 2-22 Block diagram of the Torque Sensor Based compensator method.

It is easy to prove the damping effect of this method by derive the transfer function from $\dot{T}_m^*$ to ω_M (see Appendix A). This transfer function is equal to:

$$\frac{\omega_M}{\dot{T}_m^*} = \frac{s^2+\omega_o^2}{J_M s\left(s^2+\frac{CK_{sh}}{J_M}s+\omega_n^2\right)} \tag{2-26}$$

where

$$\left.\begin{aligned}\omega_o &= \sqrt{\frac{K_{sh}}{J_L}} \\ \omega_n &= \sqrt{\frac{K_{sh}(J_M+J_L)}{J_M J_L}}\end{aligned}\right\} \tag{2-27}$$

The coefficient of the second term of the denominator represents the damping factor of the system and can be controlled by adjusting the gain C.

Using the case study system parameters as an example, root locus of the closed loop system with shaft torque feedforward path are drawn for two different cases, one with 20 ms time delay and the other without time delay as shown in Figure 2-23 and Figure 2-24 respectively. The condition for these plots is to increase the gain (C) in order to damp the resonant poles 10 % from there initial critical positions. From Figure 2-23, it is clear that increasing the damping will cause big change in the closed loop torque regulator and speed regulator poles (torque regulator pole move to the right and the speed regulator pole move to the left) till they collide. This change in the poles will impact the speed response and cause stability problem. Therefore, it is concluded that torque sensor based compensator method can function very well with systems without significant time delay.

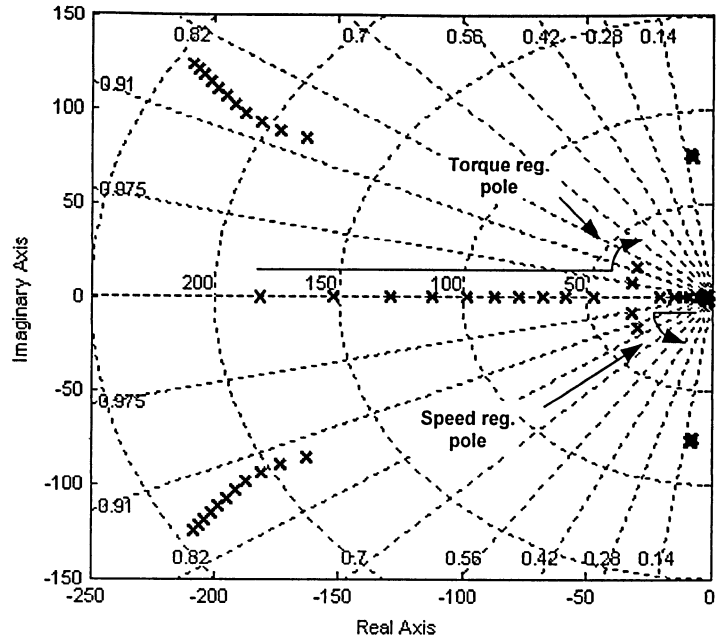

Figure 2-23 Root locus of the Torque Sensor Based compensator method with 20 ms time delay.

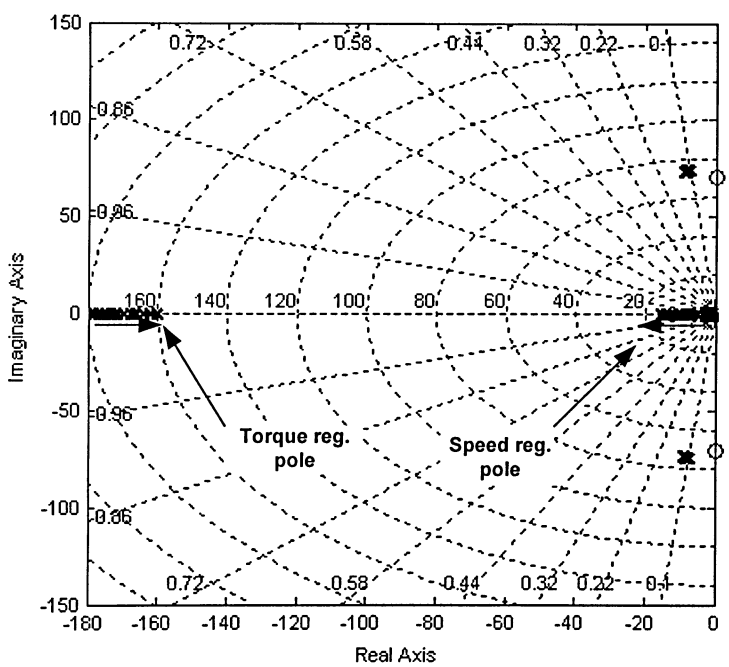

Figure 2-24 Root locus of the Torque Sensor Based compensator method without time delay.

b) Model Following Control Method (MFC)

The principle of this method is simulating the ideal speed of the motor and compares it with the actual speed of the motor [10,11]. The resultant difference of

the two speeds is multiplied by constant gain K. The output of this gain is added to the input of the torque regulator. Figure 2-25 shows the block diagram of the MFC method.

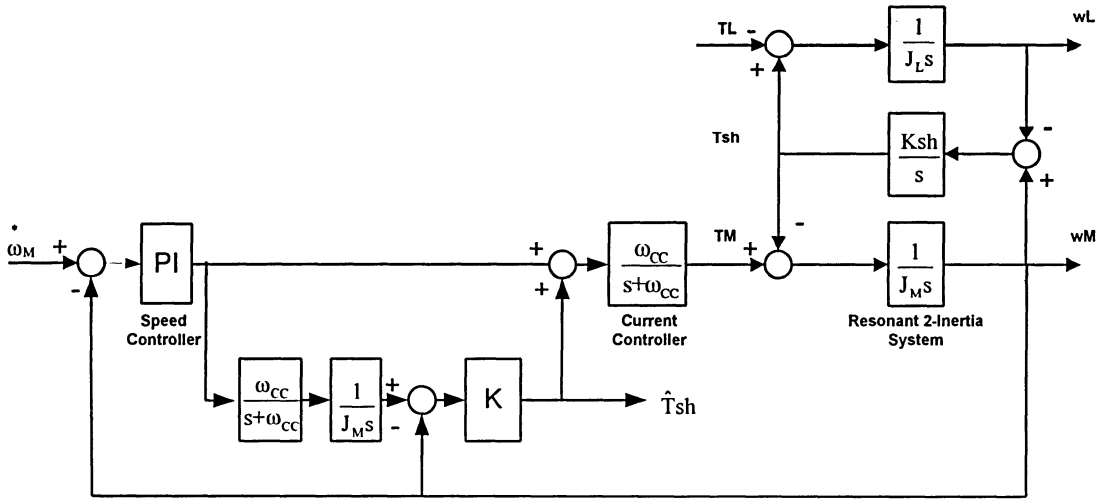

Figure 2-25 Block diagram of the MFC.

The relation between the estimated and the actual shaft torque can be given by the Equation (2-29) [11]:

$$\hat{T}_{sh} = \frac{K(s+\omega_{cc})}{J_M(s^2+\omega_{cc}s+\frac{K\omega_{cc}}{J_M})} T_{sh} \qquad (2\text{-}28)$$

The above equation indicates that the estimation dynamics is adjusted by the gain K.

In general, the MFC is effective and practical method for vibration suppression since it uses the estimated shaft toque as a feedforward signal to compensate the disturbance without using differentiator within the estimator. The drawback of this method is that compensated signal can affect the speed loop because of the offset of the load change.

c) Disturbance Observer

The principle of this method is to estimate the shaft torque using Gopinath's method and feedforward this signal to the torque regulator to compensate the

disturbance [13,21,22,23]. The estimation of the shaft torque is basically based on the motion equation which is equal to:

$$J_M \frac{d\omega_M}{dt} = T_M - T_{sh} \tag{2-29}$$

Given the motor speed feedback and motor applied torque (or measured current in case of DC drive), Equation (2-30) can be rewritten for shaft torque as follows:

$$T_{sh} = T_M - J_M \frac{d\omega_M}{dt} \tag{2-30}$$

Figure 2-26 shows the block diagram of this method. This method can damp the vibration very effectively and does not need prior identification of the mechanical resonant frequency.

The disadvantage of this method is that the observer based on a differentiator and is essentially vulnerable to noise. Simulation and root locus analysis of this method shows that significant time delay could case stability problem.

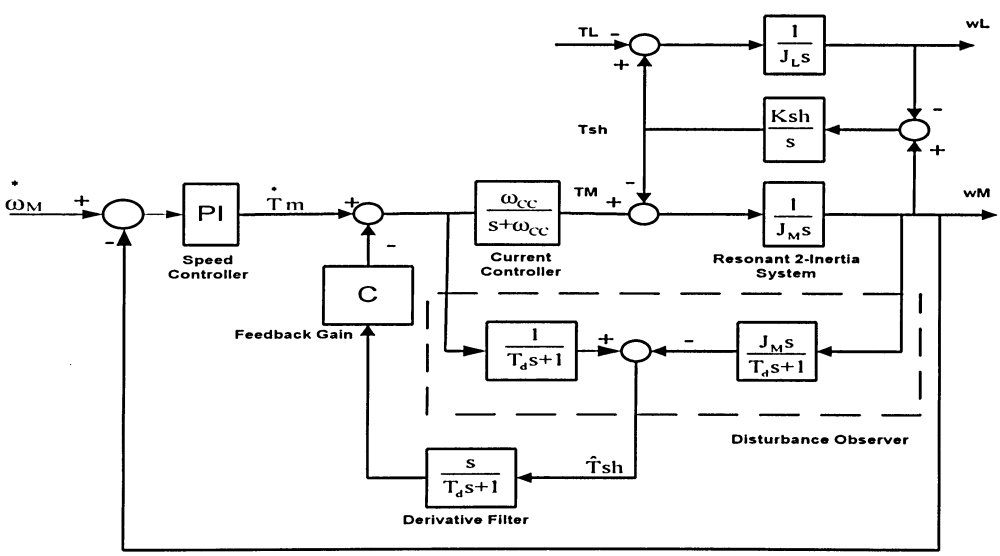

Figure 2-26 Block diagram of the Disturbance Observer.

2.6 Summary

This chapter has provided detailed analysis and modeling of standard drive with the two-mass mechanical model. The dynamic model of the conventional drive

including the two-mass mechanical system was implemented in MATLAB/Simulink. The simulation results verified that the model can accurately describe the dynamic behavior of the drive system. As expected, the conventional drive system cannot damp the torsional oscillation effectively, since the design of this system based on the rigid mechanical system without any attention to the resonance poles. Among various mitigation methods, predictive compensation such as feedforward control seems very promising. It is found that these methods may not work effectively with large value of system time delay. In addition, they may affect the response of the speed loop. These two disadvantages are the main focus in the development of the proposed resonant compensator method. The modeling and the analysis of this chapter are important part of this thesis work. It offers the basis for the proposed resonance compensator design that will be discussed in the next chapter.

CHAPTER 3: TORSIONAL VIBRATION DAMPING USING STATE SPACE METHOD

3.1 Introduction

The conventional torsional vibration mitigation methods outlined in the previous chapter can stabilize a drive system, but resonant poles of the drive still tend to be highly under-damped. Different advanced control schemes of torsional vibration mitigation methods are discussed in Chapter 2 that can solve the problem but not effectively due to the large value of time delay in large drives.

To solve this problem, a proposed damping algorithm that incorporates the time delay in the design is developed. This algorithm is based on State Feedback Control method and Linear Quadratic Regulator/Kalman Filter approach with shaft torque sensor as a feedback element. The main feature in the design of the proposed method is to suppress the torsional vibration without affecting the speed control loop.

In this Chapter, a mathematical analysis and design steps of the proposed method are discussed. The verification of the design and the dynamic performance is accomplished by using time and frequency domain techniques. Robustness with respect to inner and outer loop is also investigated. Simulation results of the entire drive system are presented.

3.2 State Feedback Modeling

As discussed earlier, the plant of the control system is modeled with three transfer functions: torque regulator transfer function, time delay transfer function, which is modeled as a second order Pade approximation, and the second order two-mass mechanical model transfer function. Figure 3-1 shows the block diagram of the plant.

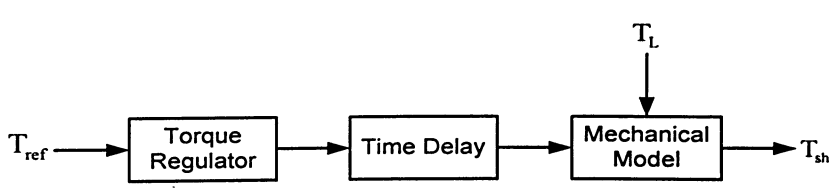

Figure 3-1 Plant Model.

To obtain the state space model of the plant, each transfer function is converted to state space model and then combined together (using Equation (B-2) in Appendix B) to model the entire state space system for the plant as shown in Equation (3-1).

$$\left.\begin{aligned}\dot{x}_s=\begin{bmatrix}\dot{x}_1\\ \dot{x}_2\\ \dot{x}_3\\ \dot{x}_4\\ \dot{x}_5\end{bmatrix}&=\begin{bmatrix}-(\frac{D_{sh}}{J_M}+\frac{D_{sh}}{J_L}) & -(\frac{K_{sh}}{J_M}+\frac{K_{sh}}{J_L}) & -\frac{12}{T_dJ_M} & 0 & \frac{\omega_{CC}}{J_M}\\ 1 & 0 & 0 & 0 & 0\\ 0 & 0 & -\frac{6}{T_d} & -\frac{12}{T_d^2} & \omega_{CC}\\ 0 & 0 & 1 & 0 & 0\\ 0 & 0 & 0 & 0 & -\omega_{CC}\end{bmatrix}\begin{bmatrix}x_1\\ x_2\\ x_3\\ x_4\\ x_5\end{bmatrix}+\begin{bmatrix}0\\ 0\\ 0\\ 0\\ 1\end{bmatrix}u+\begin{bmatrix}0\\ 0\\ 0\\ 0\\ 1\end{bmatrix}T_L\\ T_{sh}&=\begin{bmatrix}D_{sh} & K_{sh} & 0 & 0 & 0\end{bmatrix}x_s\end{aligned}\right\}\quad(3\text{-}1)$$

where

x_1 is the speed difference state ($\Delta\omega=\omega_M-\omega_L$);
x_2 is the angle difference state ($\Delta\theta=\theta_M-\theta_L$);
x_3,x_4 are the Pade approximation states;
x_5 is the torque regulator output state;
T_M,T_L,T_{sh} are the motor, load, shaft and motor reference torques [N.m];
J_M , J_L are the motor and load moment of inertias [kgm^2];
K_{sh} is the shaft Stiffness [Nm/rad];
D_M , D_L , D_{sh} are the motor, load and shaft damping coefficients [Nm/(rad/sec)];
ω_{CC} is the cut-off frequency of the current loop [rad/sec];
T_d is the time delay from T_{ref} to T_M [sec]; and
u is the reference input signal [N.m].

Equation (3-1) can be express in general form as:

$$\left.\begin{aligned}\dot{x}_s&=A_sx_s+B_su+ET_L\\ T_{sh}&=C_sx_s\end{aligned}\right\}\quad(3\text{-}2)$$

where

A_s is the state matrix;
B_s , E are the input matrices; and
C_s is the output matrix.

To design a state feedback compensator for the plant in Equation (3-2), the following control low is selected,

$$u = T_{ref} - K_m x_s \tag{3-3}$$

where T_{ref} is the torque reference and $K_m=[K_1\ K_2\ K_3\ K_4\ K_5]^t$ is the state feedback gain. Substituting Equation (3-3) into Equation (3-2) gives

$$\left.\begin{aligned} \dot{x}_s &= A_s x_s + B_s(T_{ref} - K_m x_s) \\ \text{or}\quad \dot{x}_s &= (A_s - B_s K_m)x_s + B_s T_{ref} \end{aligned}\right\} \tag{3-4}$$

Equation (3-4) can be represented as a block diagram as shown in Figure 3-2. This block diagram can be called as ideal state feedback compensator since the state variables are directly fed back to form the control feedforward signal. The open loop and the closed loop poles of the system of Figure 3-2 can be calculated from the characteristics equations given by (3-5) and (3-6), respectively:

$$\left|(sI - A_s)\right| = 0 \tag{3-5}$$

$$\left|(sI - A_s + B_s K_m)\right| = 0 \tag{3-6}$$

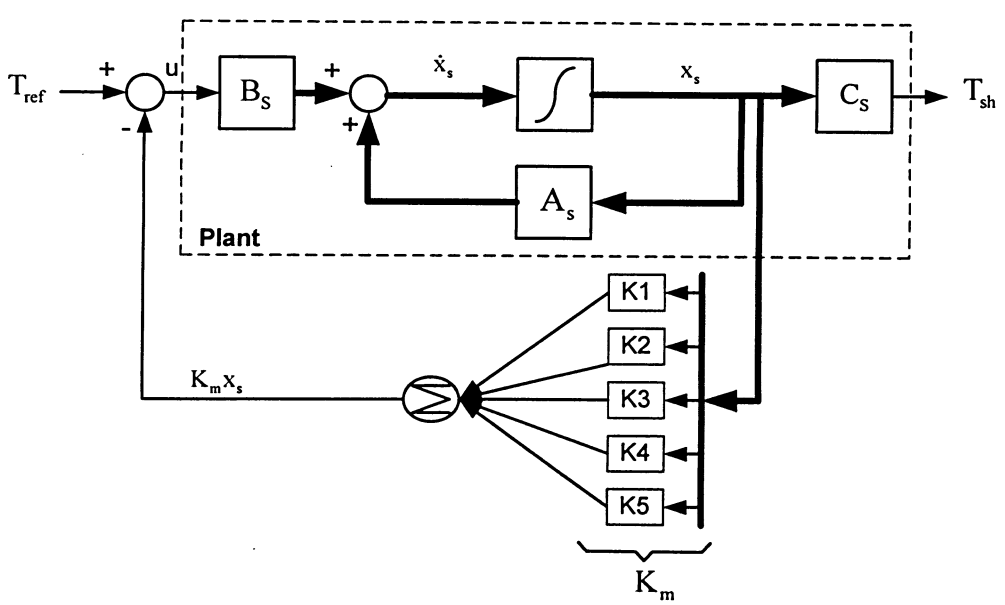

Figure 3-2 Ideal state feedback compensator.

3.3 States and Disturbance Observer

In the previous section where the state feedback design is discussed, it is assumed that all the state variables are available for the control law of the compensator. The control law equation requires that all state variables must be measured. In practice this may not happen for a number of reasons, including inaccessibility to the state variables. Under this condition it becomes necessary to observe or estimate the state variables. Therefore, the control law of the compensator becomes as follows:

$$u = T_{ref} - K_m \hat{x}_S \tag{3-7}$$

where $\hat{x}_S$ are the observed state variables.

In the proposed algorithm, the shaft torque signal is used to estimate not only the plant states but also the load torque which can improve the load response remarkably. The load torque which is unknown input to the plant is added as state variable x_L. Therefore, the state space model in Equation (3-1) is modified by:

$$\dot{x}_o = \begin{bmatrix} \dot{x}_1 \\ \dot{x}_2 \\ \dot{x}_L \\ \dot{x}_3 \\ \dot{x}_4 \\ \dot{x}_5 \end{bmatrix} = \left\{ \begin{bmatrix} -\left(\frac{D_{sh}}{J_M}+\frac{D_{sh}}{J_L}\right) & -\left(\frac{K_{sh}}{J_M}+\frac{K_{sh}}{J_L}\right) & \frac{1}{J_L} & -\frac{12}{T_d J_M} & 0 & \frac{\omega_{CC}}{J_M} \\ 1 & 0 & 0 & 0 & 0 & 0 \\ 0 & 0 & 0 & 0 & 0 & 0 \\ 0 & 0 & 0 & -\frac{6}{T_d} & -\frac{12}{T_d^2} & \omega_{CC} \\ 0 & 0 & 0 & 1 & 0 & 0 \\ 0 & 0 & 0 & 0 & 0 & -\omega_{CC} \end{bmatrix} \begin{bmatrix} x_1 \\ x_2 \\ x_L \\ x_3 \\ x_4 \\ x_5 \end{bmatrix} + \begin{bmatrix} 0 \\ 0 \\ 0 \\ 0 \\ 0 \\ 1 \end{bmatrix} u \right\}$$

$$T_{sh} = \begin{bmatrix} D_{sh} & K_{sh} & 0 & 0 & 0 & 0 \end{bmatrix} x_o \tag{3-8}$$

The modified state space model of the plant can be written in general form as:

$$\left.\begin{aligned} \dot{x}_o &= A_o x_o + B_o u \\ T_{sh} &= C_o x_o \end{aligned}\right\} \tag{3-9}$$

where A_o, B_o, C_o are the modified plant matrices.

Applying Luenberger observer [24,25] to the system of Equation (3-9), the state estimator, often known as observer, is given by:

$$\left.\begin{aligned}\dot{\hat{x}}_o &= A_o\hat{x}_o + B_o u + K_f(T_{sh} - \hat{T}_{sh}) \\ &= (A_o - K_f C_o - B_o K_m)\hat{x}_o + B_o T_{ref} + K_f T_{sh}\end{aligned}\right\} \quad (3\text{-}10)$$

where K_f is the estimator gain. Figure 3-3 shows the block diagram of the closed loop control system with full-order observer-based state feedback controller. As can be seen from Figure 3.3, an extra gain K_L for the load torque state is added to the state feedback law as the state variables modified by adding the load torque state to the plant. The procedure of tuning this gain will be discussed later.

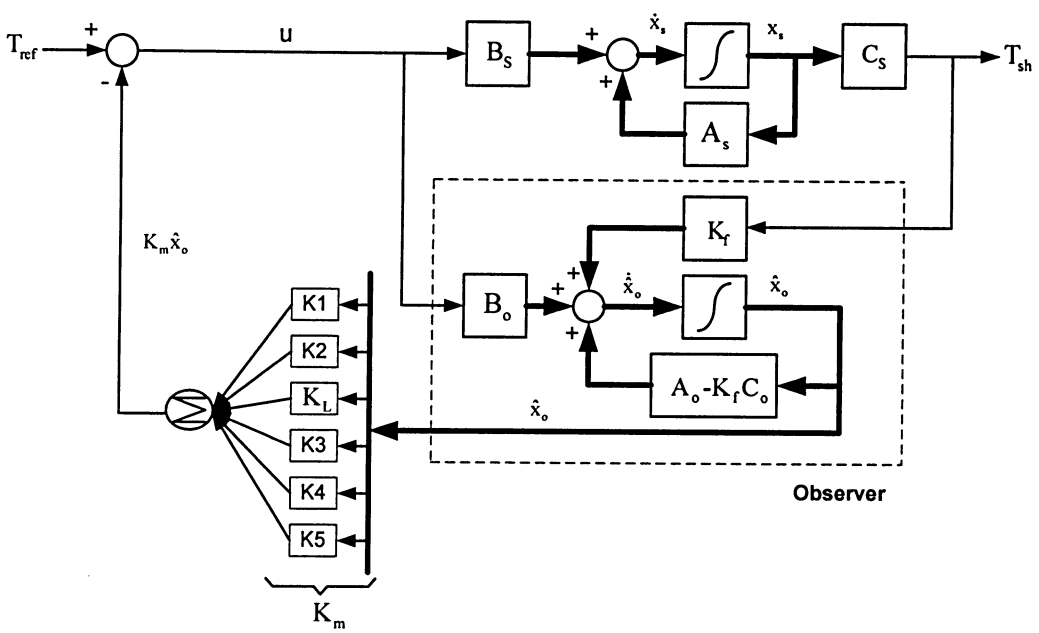

Figure 3-3 State feedback compensator with full-order observer.

3.4 State Feedback Pole Placement

In order to obtain the desired compensation (damping), the required state feedback gain K_m needs to be designed by putting the poles of the system in the desired places. There are different methods for pole placement that can be used in the design. The problem with these methods is that these methods need to know the

exact pole position for the desired design. It is not easy to decide where to put five poles (poles of the plant) at the eigenvalues of$(A_s\text{-}B_sK_m)$. Therefore, Linear Quadratic Regulator (LQR) method [26] is used to place the poles of the system at the desired position. This method provides an optimal control law for a linear system with a quadratic performance index. Assuming the linear system in equation (3-1), the objective of the optimal control is to minimize the quadratic performance index (J) given by Equation (3-11).

$$J = \int (x^T Q_s x + u^T R_s u) dt \tag{3-11}$$

where Q_s and R_s matrices are the state and control action weighting matrices and are always square and symmetric. The advantage of the performance index is that for a linear system it has a mathematical solution that yield an optimal linear control law.

In order to design an optimal state feedback gain K_m, the design start first by selecting the covariance matrices Q_s and R_s as follows:

$$\left.\begin{aligned} Q_s &= \begin{bmatrix} q11 & 0 & 0 & 0 & 0 \\ 0 & 0 & 0 & 0 & 0 \\ 0 & 0 & 0 & 0 & 0 \\ 0 & 0 & 0 & 0 & 0 \\ 0 & 0 & 0 & 0 & 0 \end{bmatrix} \\ R_s &= 1 \end{aligned}\right\} \tag{3-12}$$

Provided that the system is controllable and observable, the state feedback gain K_m can be found from

$$K_m = R_s^{-1} B^T P \tag{3-13}$$

where P is the solution of the Algebraic Ricatti Equation (ARE) as follows:

$$PA_s + A_s^T P + Q_s - PB_s R^{-1} B_s^T P = 0 \tag{3-14}$$

The design procedure is to maintain R_s as unity scalar, and vary the diagonal element $q11$ of matrix Q_s to achieve the performance specification. A 10-15% (from critical position) damping for the resonant poles is chosen for the case study system defined in Tables 2-1 and 2-2. It is reasonable to vary the element $q11$ of the matrix Q_s. This element panelizes the speed difference state $(\omega_m - \omega_L)$ to obtain the desired degree of damping, since speed difference state directly affects the shaft torque and damping.

The instruction (lqr) available in MATLAB is used to solve Equations (3-13) and (3-14) and then find the optimal state feedback gain K_m to give the desired damping.

3.5 State Estimator Pole Placement

Based on the separation theorem principle [26], the state feedback poles and the estimator poles can be solved separately. In previous section, LQR method is used to put the state feedback poles at the desired places. In designing the estimator, there is same problem of placing the estimator poles at the desired place of the eignvalues of $(A_o - K_f C_o)$. Therefore, Kalman Filter (KF) is used to find the estimator gain K_f that can put the poles of the estimator at the desired places.

By using Kalman Filter, the system in Equation (3-8) is subject to various disturbances and modeling errors. Gaussian white noises are used to represent all of these external error sources as follows:

$$\begin{aligned} \dot{x}_s &= A_s x_s + B_s u + G w \\ T_{sh} &= C_s x_s + v \end{aligned} \qquad (3\text{-}15)$$

where w is the process noise added to the state dynamic and v is the measurement noise added to the output. The covariance matrices of these noises can be defined as Q_{of} and R_{of} respectively.

Now, for estimator of Equation (3-10) the goal is to minimize the error between the actual state x_o and the observed one $\hat{x}_o$ as the filter gain K_f varied.

Kalman Filter gain K_f is calculated as follows:

$$K_f = PC_o^T R_f^{-1} \tag{3-16}$$

where P is the solution of the following algebraic Ricatti Equation (ARE):

$$A_o P + PA_o^T + Q_{0f} - PC_o^T R_f^{-1} C_o P = 0 \tag{3-17}$$

The instruction (lqe) available in MATLAB is used to solve Equations (3-16) and (3-17) and then find the estimator gain K_f to give the desired damping.

3.6 Loop Transfer Recovery

A control system that contains a Linear Quadratic Regulator (LQR) together with a Kalman Filter (KF) state estimator is called a Linear Quadratic Gaussian (LQG) control system [26,27] as shown in Figure 3-4. The final LQG controller can be realized by separately implementing the Kalman filter, thus generating $\hat{x}_o$, and then multipling the output of the Kalman filter by K_m (calculated by using LQR) to generate the control input $u=-K_m\hat{x}_o$.

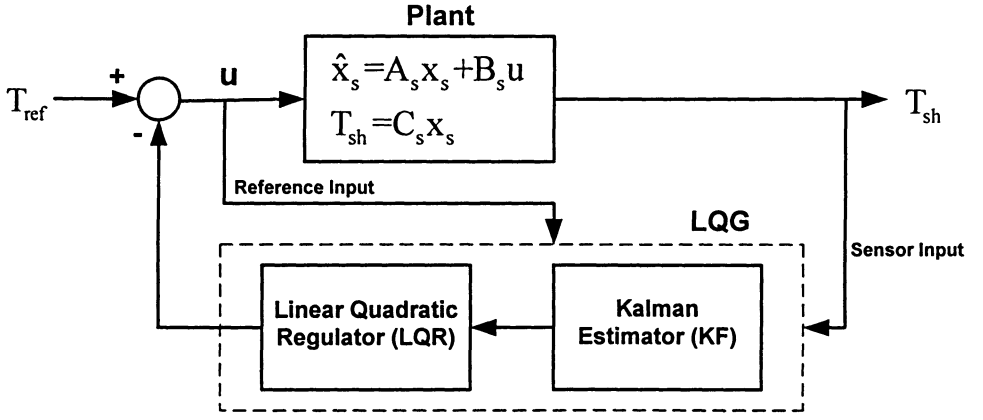

Figure 3-4 Realization of LQG compensator.

Individually the Linear Quadratic Regulator (LQR) and Kalman Filter (KF) have strong robustness properties with gain margin up to infinity and over 60° phase margin. Unfortunately, the LQG has relatively poor stability and therefore, to

overcome the problem of poor compensator, the Loop Transfer Recovery (LTR) method is used to improve the stability. The LTR method was first proposed by Doyle and Stain [28].

The Loop Transfer Recovery (LTR) of the target feedback loop (ideal state feedback loop) is achieved by modifying the design of Kalman Filter, i.e. the uncertainties at the plant input are represented by large amount of process noise as follows:

$$Q_f=(1+q^2)Q_{0f} \tag{3-18}$$

where

$$Q_{0f}=\begin{bmatrix} 0 & 0 & 0 & 0 & 0 & 0 \\ 0 & 0 & 0 & 0 & 0 & 0 \\ 0 & 0 & q_{33} & 0 & 0 & 0 \\ 0 & 0 & 0 & 0 & 0 & 0 \\ 0 & 0 & 0 & 0 & 0 & 0 \\ 0 & 0 & 0 & 0 & 0 & 0 \end{bmatrix} \tag{3-19}$$

where q^2Q_{of} represents the additional fictitious noise and q is the free design parameter. q_{33} is the element of the Q_{of} matrix that affect the load torque input state. The procedure of LTR is as follows: For $q=0$, K_f corresponds to the nominal Kalman Filter gains. To obtain the desired pole placement and optimal K_f, the design parameter q is increased in the iteration. In each iteration, the ideal open loop state feedback compensator of system shown in Figure 3-2 is compared with that of the corresponding plot of current compensator of system shown in Figure 3-3 using either a Nyquist or Bode plot as gauging indices. The iteration process will stop whenever open loop compensator with contain estimator become close to the open loop ideal compensator. In more detail, the open loop transfer function of Figure 3-3 can written as,

$$G_{LQG}(s)=F(s)\,C_s(sI-A_s)^{-1}B_s \tag{3-20}$$

where $F(s)=K_m(sI-A_o+B_oK_m+K_fC_o)^{-1}K_f$. Now, as q approaches infinity, the open loop transfer function $G_{LQG}(s)$ will approach the ideal open loop transfer function (e.g. LQR state feedback loop transfer function),

$$G_{ideal} = K_m(sI-A_s)^{-1}B_s \tag{3-21}$$

Provided that the system is ideally recovered (open loop compensator with estimator is close to open loop ideal compensator), it is found that the system will rely more on the sensor input rather than on the reference input. As a result, the reference input could be removed from the estimator and the compensator is modified from Multi-Input-Single-Output (MISO) to Single-Input-Single-Output (SISO) system. One should keep in mind that by relying on sensor input rather than the reference input, the immunity to the sensor noise will vanish. Therefore, a reasonable compromise between noise performance and recovery should be considered.

In order to justify the possibility of removing the reference input from the estimator, the state space model is redrawn and modeled in terms of transfer function as shown in Figure 3-5. The output of the compensator is given by the following Equation:

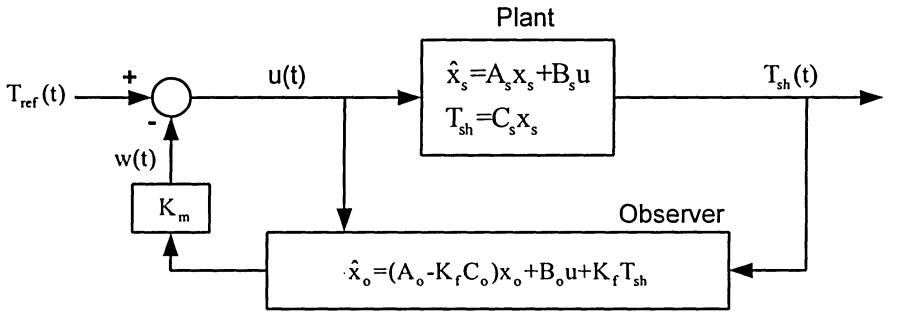

Figure 3-5 Compensator with two inputs.

$$W(s)=H_{Tsh}(s)T_{sh}(s)+H_u(s)U(s) \tag{3-22}$$

where

$$\left.\begin{aligned} H_{Tsh}(s)&=K_m(sI-A_o+K_fC_o)^{-1}K_f \equiv \frac{p(s)}{d(s)} \\ H_u(s)&=K_m(sI-A_o+K_fC_o)^{-1}B_o \equiv \frac{q(s)}{d(s)} \end{aligned}\right\} \tag{3-23}$$

Using Equation (3-22), Figure 3-5 can be redrawn using block diagram manipulation as shown in Figure 3-6. Figure 3-6(b) shows that the system can be represented by feedforward part and feedback part. The feedforward part represents

the reference input transfer function and the feedback part represents the sensor transfer function. Doyle and Stain show that the reference input transfer function becomes unity when the loop recovery is achieved (see Appendix C).

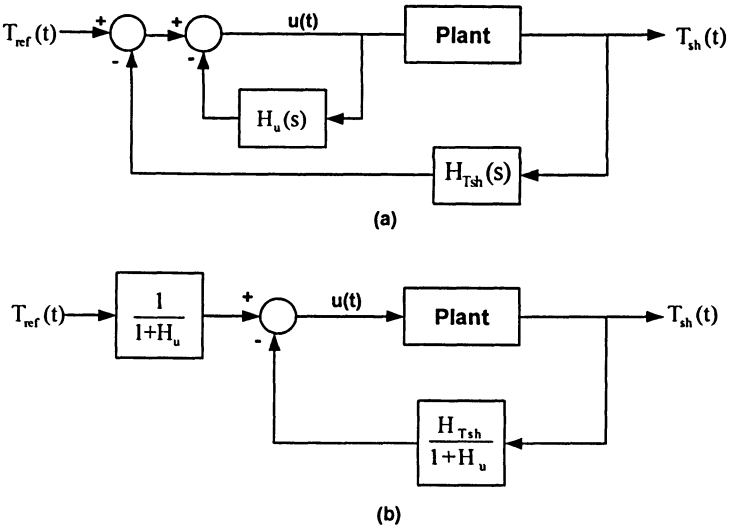

Figure 3-6 Simplification steps of transfer function model of the compensator.

Using the above results, the compensator of Figure 3-5 can be simplified by removing the estimator reference input. This system will tend to be equivalent to ideal state feedback compensator when the loop recovery is achieved. As a result of loop recovery, the compensator becomes transparent and does not affect the outer speed loop.

One more interesting thing happened when the LTR method is applied to the estimator; the order of the estimator is reduce as a direct consequence of pole/zero cancellation resulting from eliminating the reference input. Three poles, the torque regulator output pole and the Pade approximation poles are canceled. Therefore, the compensator is reduced from 6^{th} to 3^{rd} order as shown in Figure 3-7.

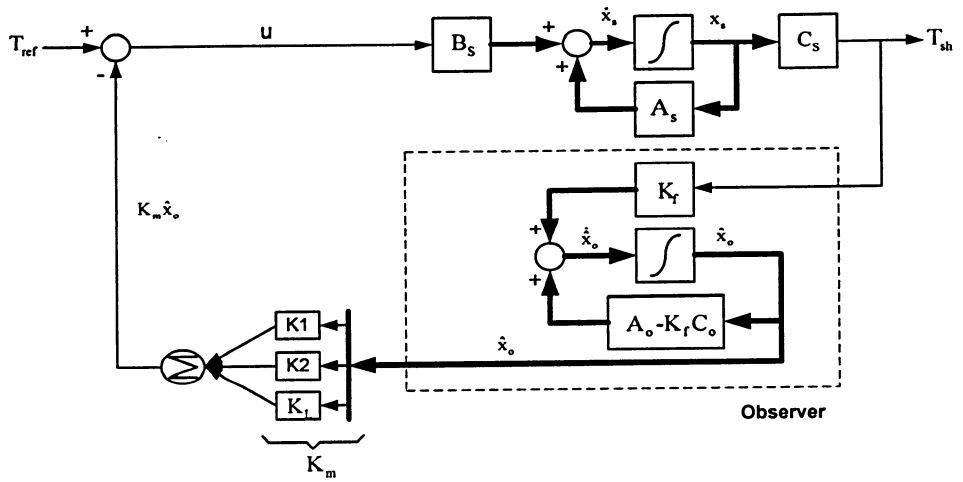

Figure 3-7 Modified model for the compensator.

In order to prove the cancellation of the Pade approximation and torque regulator poles, the estimator model is remodeled as two models in series. One represents the Pade approximation and torque regulator $[A_{pr},B_{pr},C_{pr},D_{pr}]$ and the other represents the mechanical two mass model of the plant $[A_M,B_M,C_M,D_M]$, with states $x=[x_{pr},x_M]$, estimator gains $K_f'=[K_{fpr},K_{fM}]'$ and state feedback $K_m=[K_{mpr},K_{mM}]$. Equations (3-24) and (3-25) represent the rewritten series models of the estimator model.

$$\dot{x}_{pr}=A_{pr}x_{pr}-K_{fpr}C_M x_M+K_{fpr}y \tag{3-24}$$

$$\dot{x}_M=(A_M-K_{fM}C_M)x_M+B_M C_{pr}x_{pr}+K_{fM}y \tag{3-25}$$

Equations (3-24) and (3-25) can be represented as follows:

$$\left.\begin{aligned}\begin{bmatrix}\dot{x}_{pr}\\ \dot{x}_M\end{bmatrix}&=\begin{bmatrix}A_{pr} & -K_{fpr}C_M\\ B_M C_{pr} & (A_M-K_{fM}C_M)\end{bmatrix}\begin{bmatrix}x_{pr}\\ x_M\end{bmatrix}+\begin{bmatrix}K_{fpr}\\ K_{fM}\end{bmatrix}y\\ u&=[K_{mpr}\quad K_{mM}]\begin{bmatrix}x_{pr}\\ x_M\end{bmatrix}\end{aligned}\right\} \tag{3-26}$$

The zeros of the estimator can be found by using the following expression:

$$\begin{vmatrix} sI-\bar{A} & K_f \\ K_m & D \end{vmatrix} = \begin{vmatrix} sI-A_{pr} & K_{fpr}C_M & K_{fpr} \\ -B_M C_{pr} & sI-(A_M-K_{fM}C_M) & K_{fM} \\ K_{mpr} & K_{mM} & 0 \end{vmatrix} = 0 \qquad (3\text{-}27)$$

Since, the estimator gains of the Pade approximation and torque regulator states are essentially zero, Equation (3-27) can be simplified as follows:

$$(sI-A_{pr})K_{mM} = 0 \qquad (3\text{-}28)$$

Equation (3-28) shows that the estimator zeros will place at the eigenvalues of the Pade approximation and torque regulator. This proves the cancellation of the Pade approximation and torque regulator poles due to eliminating the reference input.

3.7 Design Example

In order to demonstrate our proposed algorithm, system parameters defined in Tables 2-1 and 2-2 are used as an example. Bode plot, Nyquist plot, root locus and time domain responses are used in the design procedure to verify the dynamic performance of the proposed resonant compensator.

3.7.1 Design of State Feedback Gains

According to the procedure of penalizing the speed difference $(\omega_M-\omega_L)$ outlined in Section (3.4), initial penalty matrix is first set by selecting q_{11} equal to $33*10^8$. This matrix is then multiplied by scalar gain (h) which is increased as per in each iteration. When the desired degree of damping is achieved, the iteration is stopped and the designed state feedback gain is obtained. Figure 3-8 shows root locus of the resonant poles as the scalar gain changes in the iteration. As can be seen from the figure, the resonant poles move to the left till desired damping of 10% of their critical position is achieved (see the position of the resonant poles with respect to damping lines). There is a slight change in the original position of torque regulator. Pade approximation poles are stay in their original position.

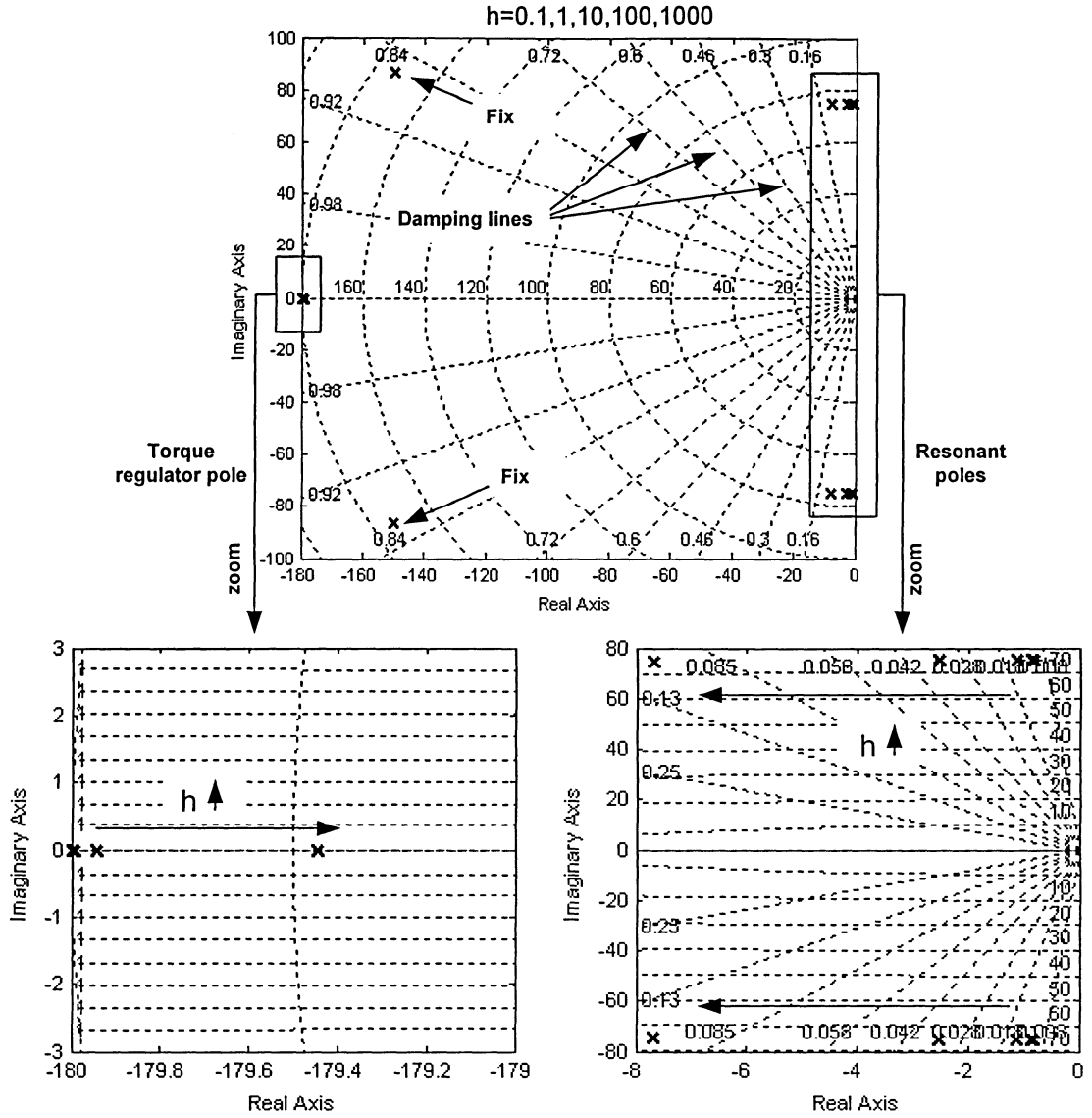

Figure 3-8 Loci of the state feedback poles.

3.7.2 Design of Observer Gains

Using the design procedure outlined in Sections (3.5) and (3.6), an iteration design method is used for selecting the covariance matrix (Q_f). Again, initial penalty matrix (Q_{of}) is selected first with element (q_{33}) equal to 1000. This matrix is then multiplied by scalar gain ($1+q^2$) which is increased by factor 10 in each iteration. Figure 3-9 shows the root locus of the estimator dynamic as the free design parameter q changes in the iteration. While q increases, one has to consider that

the magnitude of the poles should not exceed the sampling rate of the compensator. It is noticed that the magnitudes of the poles are in the range less than 300 rad/sec which is acceptable for compensator running at 3.33 ms sampling rate.

To gauge system loop recovery, Bode and Nyquist plots are used as shown in Figure 3-10 and Figure 3-11 respectively. Figure 3-10 shows the open loop Bode plots that represent the comparison between the compensators that contain estimator and the ideal state feedback loop with the use LTR methodology. As can be seen from the figure, a good recovery is achieved from 0 rad/sec to around 200 rad/sec. This represents large bandwidth compensation. Figure 3-11 shows Nyquist plots comparison of the compensator dynamics with reference input, without reference input and the ideal compensators. It is noticed that the compensator with reference input has better dynamic behavior (80° phase margin and 14 dB gain margin). Compensator without reference input has good performance as well.

Figure 3-12 and Figure 3-13 show the plant and observer responses of the load torque and shaft torque, with and without LTR, for compensator closed loop. As can be seen, the damping is improved after the LTR as the estimated states track the plant states. In other word, a good system recovery is achieved.

Figure 3-14 shows the root locus plot of the estimator dynamic. It is clear that that there is zero/pole cancellation due to eliminating the reference input of the estimator.

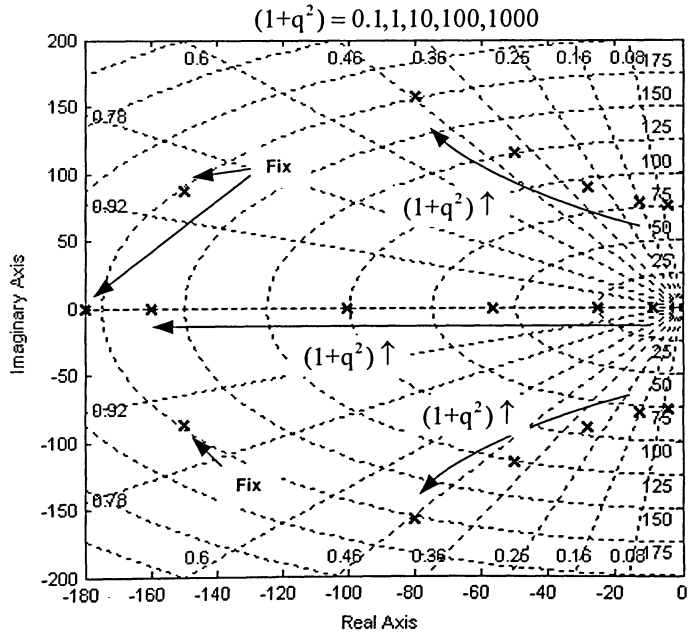

Figure 3-9 Loci of the estimator poles.

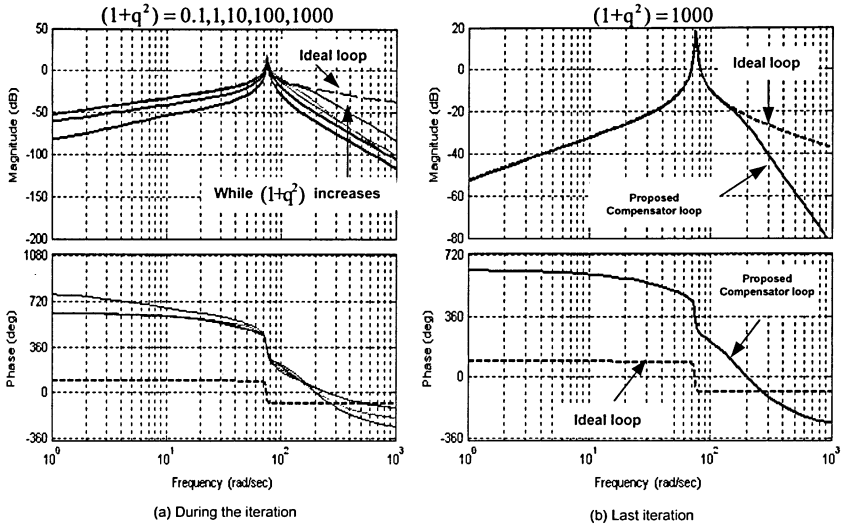

Figure 3-10 Comparison between the open loop Bode plot of ideal state feedback loop and the open loop Bode plot of compensator that contains estimator using LTR.

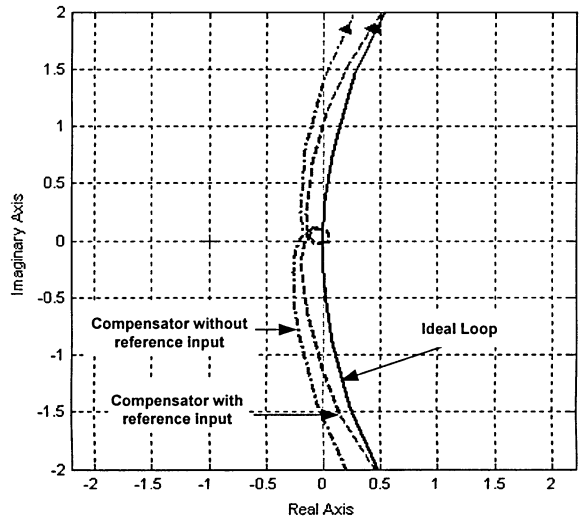

Figure 3-11 Nyquist plots comparison of the compensator with estimator (with and without the reference input) and the ideal compensator.

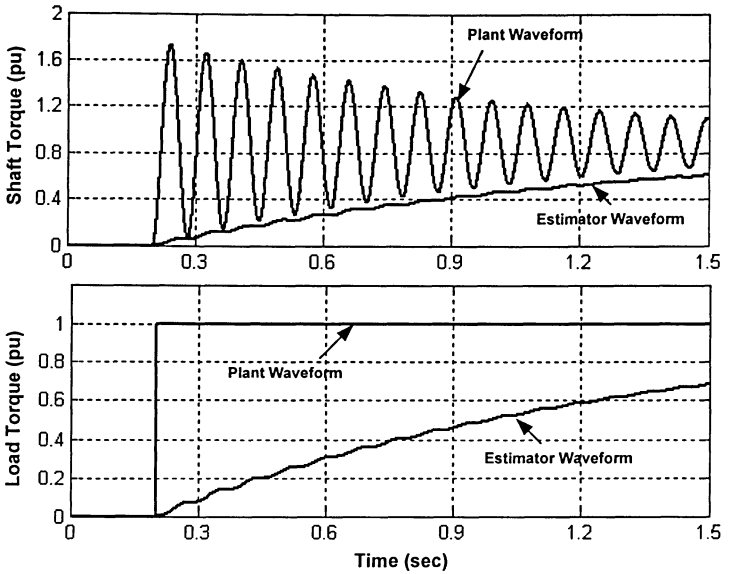

Figure 3-12 Plant and observer responses of the load torque and shaft torque without LTR for the inner closed loop compensator.

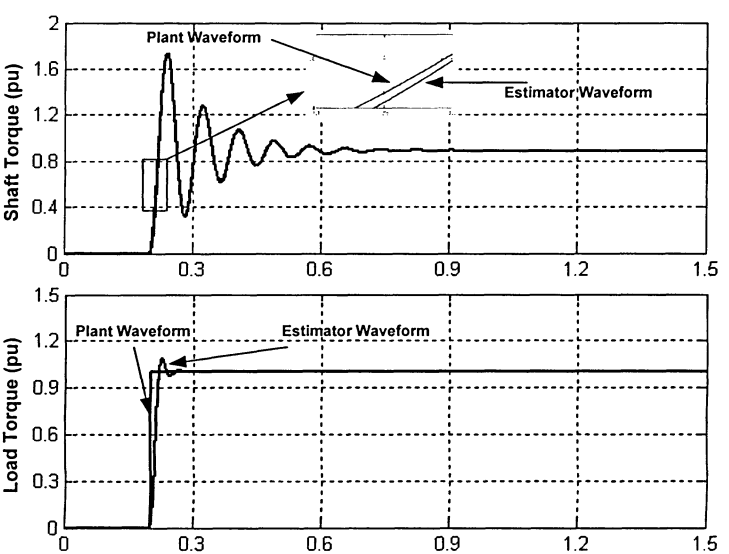

Figure 3-13 Plant and observer responses of the load torque and shaft torque with LTR for the inner closed loop compensator.

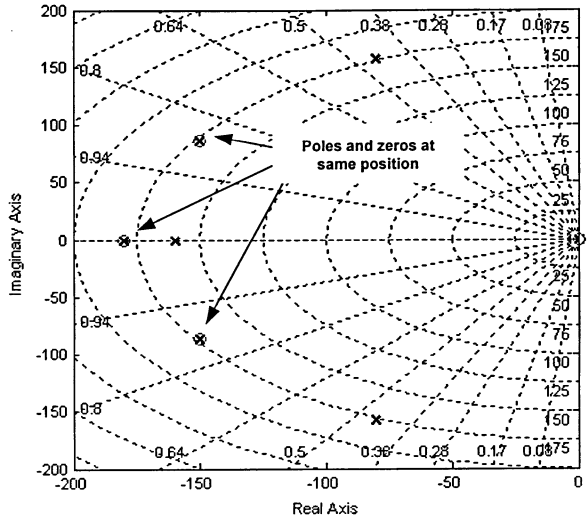

Figure 3-14 Loci of the estimator zeros/poles.

3.7.3 Design of Load Torque State Gain

As mentioned earlier, the state feedback gain K_m is modified to include the gain of load torque state K_L as shown in Figure 3-3. This gain is set to increase the bandwidth of the recovery which leads to remove any dc offset due to load change and minimize the interference with the motor acceleration and deceleration in response of speed reference. This factor is adjusted by iteration with the use of Bode or Nyquist plot as gauge indices.

Figure 3-15 and Figure 3-16 show the Bode plot and Nyquist plot before and after the adjustment of the load torque state gain K_L. From Nyquist plot one can notice that the dc bias (a) is reduced with the adjustment of load torque state gain K_L. Once the factor (a) becomes zero, the iteration stopped and the required load torque state gain K_L is obtained. Figure 3-17 shows the Bode plot of the feedforward (series) transfer function (1/(1+Hu)). It is very clear that there is zero gain with almost

zero phase at the low frequency. This proves the zero dc bias and the transparency of the recovered system.

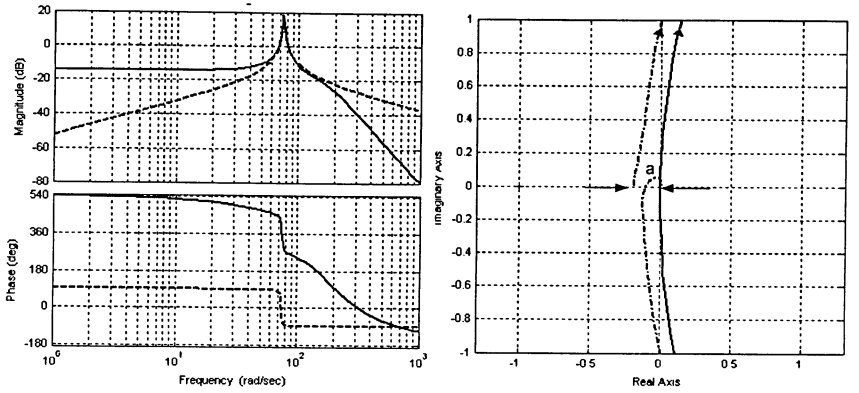

Figure 3-15 Plots before the adjustment of the load torque state gain K_L.

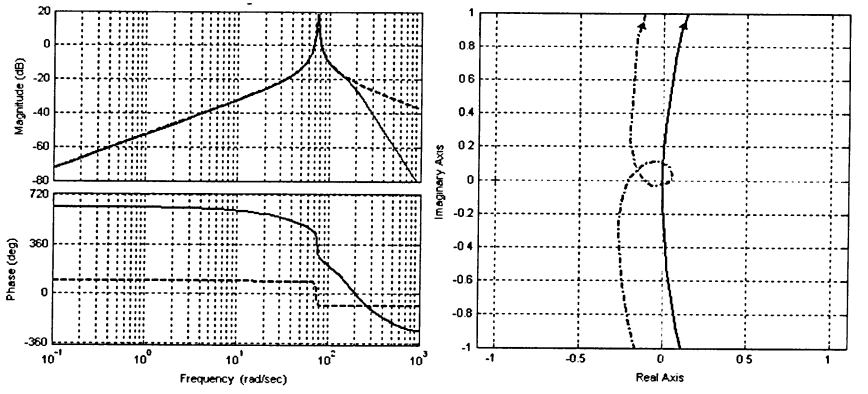

Figure 3-16 Plots after the adjustment of the load torque state gain (KL).

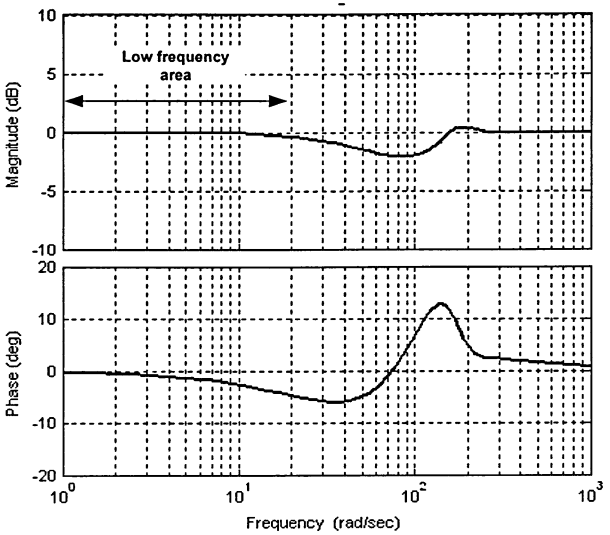

Figure 3-17 Bode plot of the feedforward (series) transfer function 1/(1+Hu).

3.8 Robustness With Respect to Inner Loop

Although the compensation of torsional vibration using state feedback method has proven to be very effective, it is necessary to evaluate the robustness of the compensation technique to physical parameter variation. This variation may be produced by changes in the parameters due to the operating conditions or due to errors in the measurement or estimation of these parameters.

3.8.1 Robustness to Uncertain Time Delay

In practice, the procedure of determining the time delay is usually based on estimation. Therefore, it is important to investigate the impact of the uncertainty in the estimation of the time delay. Nyquist plot is used as a tool for determining the uncertainty due to the time delay. First, the time delay of the compensator is set to the nominal value of 20 ms. Then the plant time delay is varied above and below the nominal time delay. The compensator dynamics of the proposed algorithm are as shown in Figure 3-18. This figure shows Nyquist plots of the compensator dynamics with three values of plant time delay 18 ms, 20 ms, and 22 ms. Results shows that

there is more margin for system with less time delay. Also, the plot of 22 ms time delay still has good stability margin. From the results, it is concluded that system with time delay less than the estimated nominal value is better than greater value.

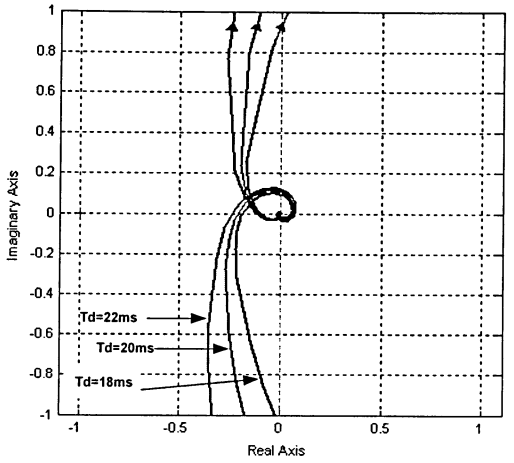

Figure 3-18 Nyquist plots of the compensator dynamics with three values of plant time delay.

3.8.2 Robustness to Uncertain Torque Regulator Bandwidth

A closed loop system for the inner compensator loop is formed to perform the root locus in order to examine the effect of inaccurate estimation of torque regulator bandwidth. The root locus is performed by varying the torque regulator from 20 rad/sec to 400 rad/sec. Figure 3-19 shows the root locus of the upper resonant pole as the torque regulator changes. As can be seen from the results, the resonant poles damp out as the torque regulator gain is increased till the nominal value and then decreases. The conclusion is that torque regulator bandwidth greater than the nominal is better.

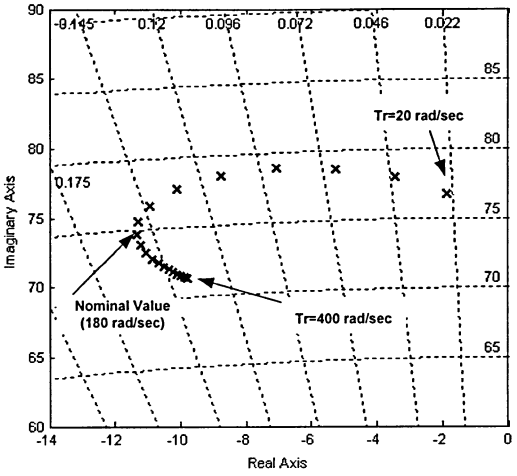

Figure 3-19 Locus of the upper resonant pole as the torque regulator changes.

3.8.3 Robustness to Uncertain Resonant Frequency

To examine the effect of uncertain resonant frequency on the compensator, root locus is performed by varying the spring stuffiness of the shaft which varies the resonant frequency. Figure 3-20 shows the root locus of the upper resonant pole as the shaft stiffness varies from one-half nominal to twice the nominal value. This varies the resonant frequency from 71% to 139% of nominal.

As shown, if the desire is to maintain the damping within bound of 10-15% of critical damping, the stiffness can vary from 78% to 128% of nominal which varies the nominal resonant frequency from 88% to 113%. This turns out to be from about 10.5 to 13.5 Hz. This is good result as estimating the open loop resonant frequency in the field is difficult. From the result, it is noticed that system with resonant frequency greater than the nominal value is better.

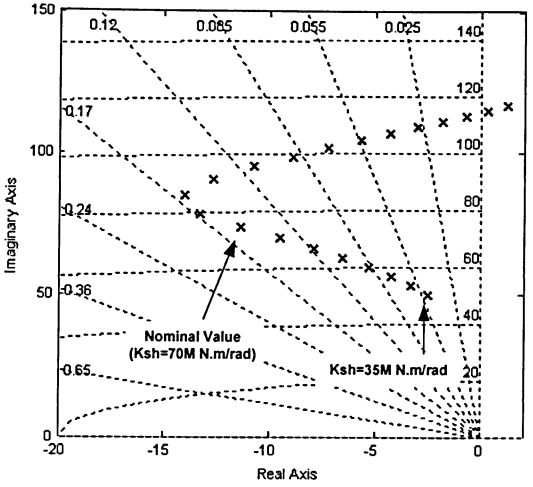

Figure 3-20 Locus of the upper resonant pole as the spring stiffness changes.

3.9 Robustness With Respect to Speed Outer Loop

It is very important to study the effect of the speed loop on the compensator dynamics and vise versa. To do this study, root locus of resonant compensator loop and the outer speed loop is performed. As another alternative, frequency responses and time simulation can also be performed for each resultant closed loop.

Based on the block diagram of Figure 3-21, the open loop state equation and system matrices are derived. Once the open loop system matrices are determined, it is easy to perform the root locus using MATLAB.

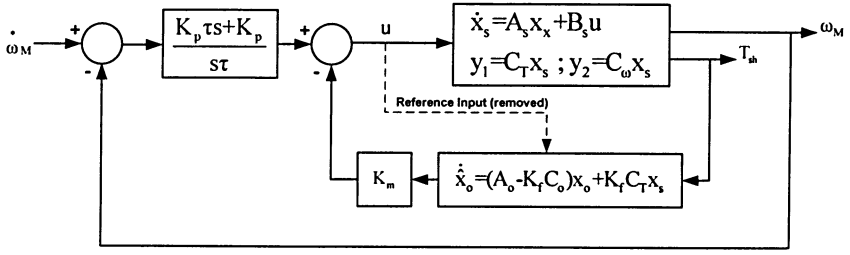

Figure 3-21 Resonance compensator loop with outer closed loop.

For the inner compensator loop, the open loop state equation is as follows:

$$\left.\begin{aligned} \dot{x}_{op} &= \begin{bmatrix} \dot{x}_s \\ \dot{\hat{x}}_o \end{bmatrix} = \begin{bmatrix} A_s & 0 \\ K_f C_T & A_o - K_f C_o \end{bmatrix} \begin{bmatrix} x_s \\ \hat{x}_o \end{bmatrix} + \begin{bmatrix} B_s \\ 0 \end{bmatrix} u \\ y_{TI} &= [0 \quad -K_m] x_{op} \qquad \text{(close loop with } T_{sh}) \\ y_{\omega I} &= [-C_m \quad 0] x_{op} \qquad \text{(close loop with } \omega_M) \end{aligned}\right\} \tag{3-29}$$

To perform the root locus, the open loop is closed with shaft torque output and varies the root locus gain from 0 to 1. The closed loop system of the inner loop is as follows:

$$\left.\begin{aligned} \dot{x}_{op} &= \begin{bmatrix} \dot{x}_s \\ \dot{\hat{x}}_o \end{bmatrix} = \begin{bmatrix} A_s & -B_s K_m \\ K_f C_T & A_o - K_f C_o \end{bmatrix} \begin{bmatrix} x_s \\ \hat{x}_o \end{bmatrix} + \begin{bmatrix} B_s \\ 0 \end{bmatrix} T_{ref} \\ y_{TI} &= [0 \quad -K_m] x_{op} \qquad \text{(close loop with } T_{sh}) \\ y_{\omega I} &= [-C_m \quad 0] x_{op} \qquad \text{(close loop with } \omega_M) \end{aligned}\right\} \tag{3-30}$$

Figure 3-22 shows root locus of the resonance compensator loop as the root locus gain increases from 0 to 1. It is very clear that the resonant poles move to the range of desired damping 10-15% from their initial position.

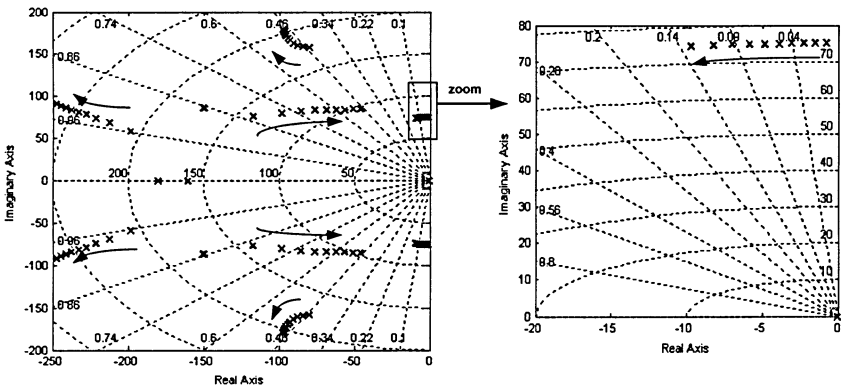

Figure 3-22 Root locus of the resonance compensator loop as the root locus gain increases from 0 to 1.

To perform the root locus of the outer loop, first cascade the speed regulator equation with the resultant equation of the inner closed loop to form the open loop system. Next, close the loop with the motor speed output and vary the root locus gain from 0 to 1. The open loop and the closed loop state equation are shown in Equation (3-31) and Equation (3-32).

$$\left.\begin{aligned} \dot{x}_{CL} &= \begin{bmatrix} \dot{x}_{op} \\ \dot{x}_{sp} \end{bmatrix} = \begin{bmatrix} A_s & -B_sK_m & B_sK_p/\tau \\ K_fC_T & A_o-K_fC_o & 0 \\ 0 & 0 & 0 \end{bmatrix} \begin{bmatrix} x_{op} \\ x_{sp} \end{bmatrix} + \begin{bmatrix} B_sK_p \\ 0 \\ 1 \end{bmatrix} u \\ y_{\omega 2} &= [-C_\omega \quad 0 \quad 0] x_{CL} \quad \text{(close loop with } \omega_M\text{)} \end{aligned}\right\} \tag{3-31}$$

$$\left.\begin{aligned} \dot{x}_{CL} &= \begin{bmatrix} \dot{x}_{op} \\ \dot{x}_{sp} \end{bmatrix} = \begin{bmatrix} A_s-B_sK_pC_\omega & -B_sK_m & B_sK_p/\tau \\ K_fC_T & A_o-K_fC_o & 0 \\ -C_\omega & 0 & 0 \end{bmatrix} \begin{bmatrix} x_{op} \\ x_{sp} \end{bmatrix} + \begin{bmatrix} B_sK_p \\ 0 \\ 1 \end{bmatrix} \omega_{ref}^* \\ y_{\omega 2} &= [-C_\omega \quad 0 \quad 0] x_{CL} \quad \text{(close loop with } \omega_M\text{)} \end{aligned}\right\} \tag{3-32}$$

Figure 3-23 shows root locus of the outer speed loop as the root locus gain varies from 0 to 1. It is noticed that the inertial pole (pole at origin) has moved to 15 rad/sec and there is a change at the resonant poles.

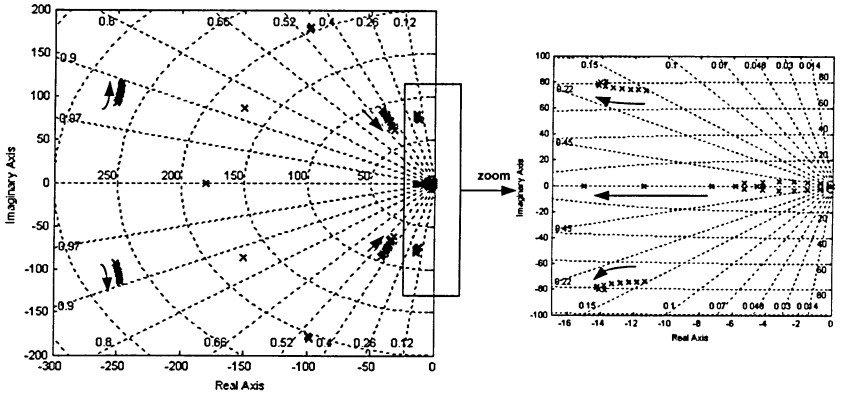

Figure 3-23 Root locus of the outer speed loop as the root locus gain increases from 0 to 1.

As can be seen from Figure 3-23, the speed regulator pole position is at 15 rad/sec which is the desired position for the pole of speed regulator. Also, it is very

clear that the damping is increased as the resonance pole shifted more to the left. This means that the speed loop has some effect on the compensator dynamic.

3.10 Time Domain Simulation

The performance of the proposed state feedback method is simulated by using MATLAB. Load step and speed step responses are examined for two cases: with and without the proposed resonant compensator. System parameters defined in Chapter Two are used in the simulation. Unless otherwise stated, the parameters are: 15 rad/sec speed regulator bandwidth; 180 rad/sec torque regulator bandwidth; 300 Hz torque and speed sampling rate; 60 pu/sec rate limit of the full load torque (1360KN.m=1pu); 100% load step of the full load torque (1360KN.m=1pu); 5% speed step of the rated speed (4.5 rad/sec=1pu); 3^{rd} order discrete time compensator without reference input. The mechanical system damping (Ds) is adjusted only to stabilize the system.

3.10.1 Load Torque Step Response

Load torque step can be considered as an excellent test to excite the resonant vibration. Figure 3-24 shows torque and speed waveforms with 1 pu load torque step change (100% of rated torque) for system without compensator. From the results, one can notice a large oscillation on the shaft torque waveform. The motor speed and the applied torque waveforms have small ripple comparing with the shaft torque waveform. Figure 3-25 shows the torque and speed waveform with load torque step change for system with the effect of compensator. It is very clear that the compensator has very effective damping for the oscillation. The oscillation lasts for only around six cycles.

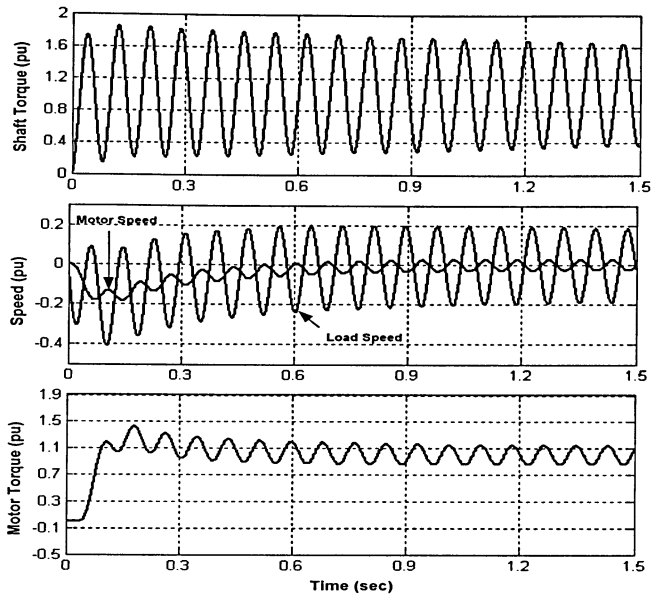

Figure 3-24 Torque and speed waveforms with 1 pu load torque step change for system without compensator.

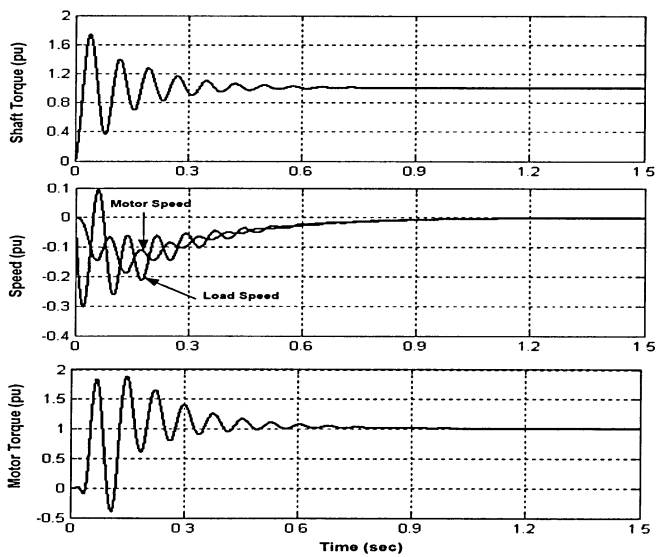

Figure 3-25 Torque and speed waveforms with 1 pu load torque step change with the compensator.

3.10.2 Speed Step Response

Step response shows the effect of the resonance compensator on the speed regulator. Ideally, the speed response should be same in the presence or absence the compensator. Figure 3-26 shows the torque and speed waveforms with 5% speed step change for system without compensator. From the result, one can notice a larg oscillation on the shaft torque comparing with the speed and applied torque waveforms. Figure 3-27 shows the torque and speed waveforms with 5% speed step change with the use of compensator. It is very clear that the compensator has removed the oscillation very effectively. The compensator has almost no effect on speed response and that verify the theoretical robustness analysis of the compensator with respect to outer loop.

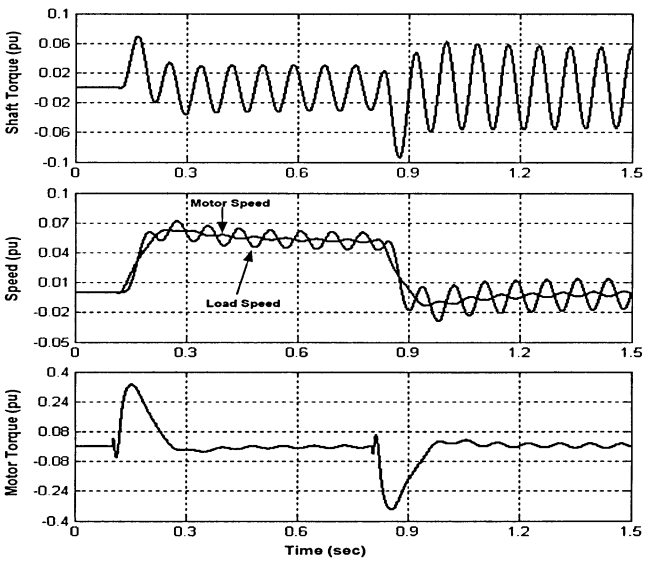

Figure 3-26 Torque and speed waveforms with 5% speed step change for system without compensator.

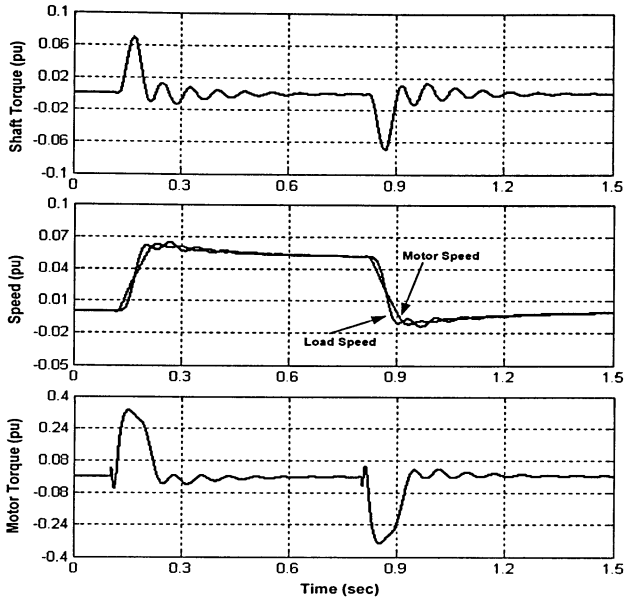

Figure 3-27 Torque and speed waveforms with 5% speed step change for system with compensator.

3.11 Summary

In this chapter, the resonant compensator based speed control using torque sensor signal as a feedback is developed. Theoretical analysis and time domain simulation are carried out to verify the effectiveness of the proposed control algorithm.

The developed resonant compensator has the following features:

- Suppresses the torsional vibration of the mechanical resonant frequency without affecting the speed loop response.
- Solves the limitation of torsional vibration damping due to the large value of system time delay.
- Improves the load torque disturbance rejection response.
- Robust controller against load torque disturbances and the uncertainties in the system.

To achieve the above features, State Feedback Control method is developed. The incorporation of time delay in the design and the feedforward compensation of

estimated load torque disturbance solve the problem of the large time delay on damping and improve the load torque disturbance rejection response respectively. The compensation of the load torque disturbance adds extra feature to the proposed compensator. This feature is to remove any effect on the speed loop by adjusting the gain of the estimated load torque. The (LTR) design methodology is found to be a useful design tool and provided a systematic approach to the design of the rolling mill drive train system and to the enhancement of system robustness properties.

From the primary analysis, it is found that the resulting structure of the designed compensator is a multiple-input single-output (MISO) system. This structure of compensator can be represented as a feedback part which effects the pole placement and feedforward part which serves the closed loop zeros to cancel out the poles of the observer. With LTR methodology, it is noted that the reference input signal can be eliminated. Therefore, the MISO structure of the compensator can be modified to single-input single-output (SISO) structure. Eliminating the reference input leads to reduce the order of estimator from 6^{th} order to 3^{rd} order compensator. The reduction in the structure order minimizes the computation time of the controller and the potential design error. This improvement in the controller structure is one of the contributions in this thesis.

Apart from the outer speed loop, it is found that the compensator loop with its designed gain can produce the internal and disturbance states and damp out the resonant poles with good robustness. Also, it is noticed that the load disturbance rejection response is remarkably improved by the feedforward compensation of the estimated load torque.

Time domain simulation shows that even with modest rate limiting action, the resonant compensator performs well in suppressing the resonant oscillation even with large value of time delay. The load step responses are very good along with reduced shaft torque oscillation. This proves the effectiveness of the resonance compensator for the steel mill drive as the steel mill application expose a continuous load step changes due to the entrance of metal between the rolls. Also, the results show that the compensator has almost no effect on the outer speed loop which proves the transparency of the compensator to the outer speed loop.

CHAPTER 4: HARDWARE IMPLEMINTATION AND RESULTS

4.1 Introduction

To verify the performance of the proposed resonance damping algorithm, a laboratory prototype of two-mass drive system is constructed. This chapter introduces the experiment setup, including the mechanical system, variable speed drive and the digital controller. The experimental results of the system will be discussed in association with the theoretical expectation of Chapter 3. The experimental waveforms of the shaft torque, motor speed, load speed and motor torques are compared to the simulation results. The design procedure and the performance of the resonant compensator are confirmed by the experimental results.

4.2 Experimental Setup

4.2.1 Forming the Mill Drive Train System

To verify the performance of the proposed resonance compensator control method of mill drive system model presented in Chapter 3, an experimental setup is constructed to act as a test bench for the proposed method. The prototype system used in the experiment is shown in Figure 4-1 and Figure 4-2. The experimental setup consists of two identical dc machines, one operating as motor driven by a four quadrant dc chopper and the other as a generator (load machine) to represent the mechanical system (roll and steel load). The two machines are coupled through a long elastic shaft designed with 450 mm long and 9.52 mm diameter to provide mechanical resonant frequency of close to 24 Hz. A dc inductor of 10mH is used to reduce the armature current ripple generated by the dc chopper. The dc chopper is controlled by a TI F2812 DSP controller connected to a PC. Table 4-1 gives the rating and parameters of the experiment system.

Table 4-1 Parameters of experimental Setup

Motor Ratings	Motor Parameters	Shaft Parameters
Rated Output Power: 1 hp	Arm. Resistance (Ra): 0.66 Ω	Shaft Long: 450 mm
Rated Speed: 1750 rpm	Arm. Inductance (La): 1.66 mH	Shaft Diameter: 9.52 mm
Rated Input Voltage: 90 V	Moment of Inertia (J_M): 0.0138 Kg.m^2	Resonant Frequency: 24 Hz
Rated Output Torque: 4 N.m	Torque Constant (K_T): 0.478 N.m/A	Damp. Coeffi.(D_{sh}): 0.0043 N.m/r/s
Rated Arm. Current: 10 A	Damping Coeffi. (D_M): 0.0043 N.m/r/s	

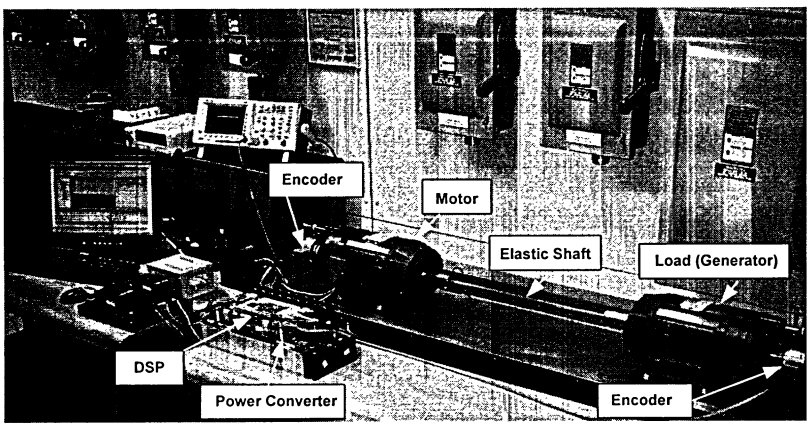

Figure 4-1 Experimental setup.

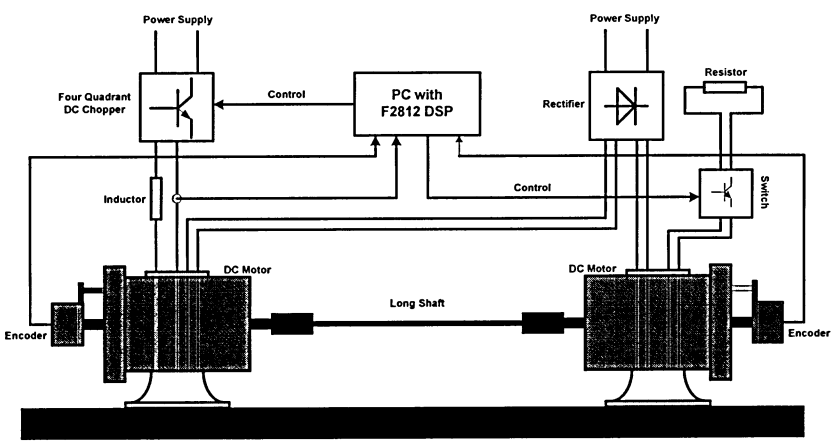

Figure 4-2 System diagram of the experimental setup.

4.2.2 Controller Implementation

The control method proposed in Chapter 3 is implemented using the DSP-FPGA platform. The controller system used in this experiment consists of the analogue signal conditioning board, DSP and FPGA as shown in Figure 4-3.
The system voltages and currents are sensed and inputted to the conditioning circuit to be converted into the appropriate voltage signals for the analogue-to-digital converter (A/D). These are received by the DSP and FPGA to be used for control algorithm implementation and protection respectively.

The outputs of the DSP board consist of the PWM commands for appropriate chopper switches. The role of the FPGA is to provide instantaneous protection for the switches of the chopper by disabling the PWM signal generated by the DSP. Therefore, under this arrangement all of the computing functions are implemented in the DSP, while the FPGA fulfills the protection function.

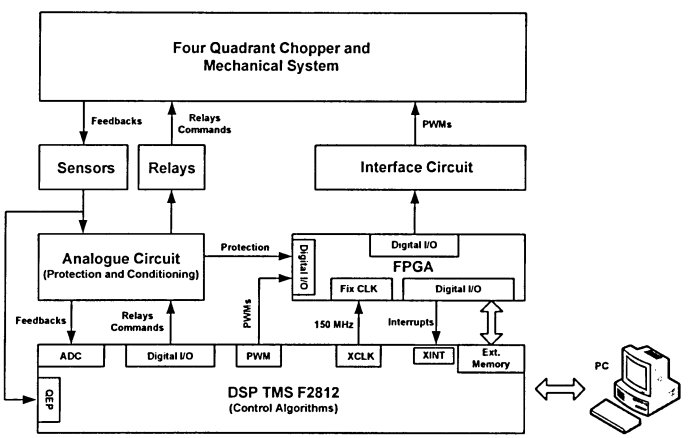

Figure 4-3 Controller Structure.

The control algorithm of Chapter 3 is implemented in the DSP by converting the state space equation of the compensator dynamic into discrete time using MATLAB's C2DM command with bilinear conversion option with 0.333 ms sample rate. The discrete time state space equation is converted to transfer function which is implemented into DSP as difference equation using C programming language with

the assistance of the powerful DSP development tool- Code Composer Studio™ (CC Studio 2.1) provided by Texas Instrument. All the computation in the program is carried out using IQ math format which allows high precision manipulation with the floating type variables. The complete code for the controller is given in Appendix (D).

The raw data for the speed and shaft toque is obtained using two incremental encoders attached to the motor and load machine shafts. The encoders have a resolution of 5000 pulses per revolution resulting an accuracy of 0.018 degrees. Such a performance allows the system to match closely with the model used in the simulation.

The sampling time of the loops is selected to be equal to 0.333ms. The choice is based on the degree of damping and the accuracy of the observation of the state feedback variables of the proposed algorithm.

4.3 Time Delay Estimation

One of the important parameters in the design procedure of the resonant compensator is the time delay of the system. According to the resonant compensator algorithm, the time delay represents the delay from the torque reference to the measured shaft torque. Figure 4-4 shows the system blocks that produce the delays from the reference torque to the measured shaft torque.

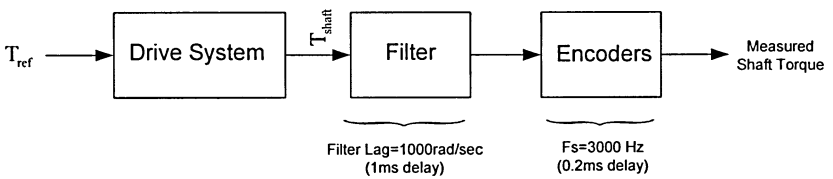

Figure 4-4 System blocks that produce the delay from reference torque to measured shaft torque.

The time delay of the experiment setup model is estimated by comparing the measured shaft torque with shaft torque waveform of the simulation model as the time delay parameter of the simulation model is tuned. When the shaft torque waveforms match each other, the tuning is stopped and the estimated time delay can be obtained. After the estimation procedure, it is found that the experiment setup

model has 8 ms time lag from reference torque to measured shaft torque. It is very important to mention that the estimation procedure of time delay is performed after adjusting all the mechanical parameters of the system at the open loop test which will be discussed in Section 4.5.1.

4.4 Experimental Setup Resonant Compensator Design

Based on the parameters of the experimental setup, the proposed resonant compensator is designed to obtain the optimal gains of K_m and K_f that can damp the resonant poles 17% of their original critical position. A second order Pade approximation is used to model the estimated 8ms time lag. The cut-off frequency of the torque regulator and the speed regulator are set to 70 rad/sec and 5 rad/sec respectively. Following the procedure discussed in Chapter 3 and using ratings and parameters of Table 4-1, satisfactory design can be achieved with some iteration.

Figure 4-5 shows the state feedback poles as the state feedback gains are iterated. It can be observed that the final damping factor for the resonant poles is equal to 17% of its original critical position (see the position of the resonant poles with respect to damping lines). Also, the torque regulator poles moves slightly to the right while the Pade approximation poles stay at the same position.

Figure 4-6 shows the locus of the estimator poles as the estimator gains are iterated. As mentioned earlier, the satisfactory selection for the estimator gains is based on comparing the Bode plot of the proposed system loop with the open loop of ideal compensator.

Figure 4-7 shows the Bode plot of the series transfer function [1/(1+Hu)]. This figure illustrates that the designed resonant compensator does not affect the speed loop as the low frequency gain is equal to 0 dB. This proves the transparency of the proposed compensator with respect to outer speed loop. This will remove any dc offset due to load step change and minimize the interference of the proposed compensator with the motor acceleration and deceleration in response of speed reference.

Figure 4-8 shows the comparison between the open loop Bode plot of the ideal compensator and the open loop Bode plot of the proposed compensator. As the LTR method is by nature an iterative method, this comparison work as a gauge for the recovery process. As can be seen from Figure 4-8, a good recovery is achieved

from 0 rad/sec to 700 rad/sec. This proves that the estimated states track the plant states accurately.

To investigate the robustness of the resonant compensator of the experimental setup model to the outer speed loop, a root locus is performed for the entire closed loop system (from $\omega_{ref} \rightarrow \omega_M$) with root locus gain changed from 0 to 1 as shown in Figure 4-9. As can be seen from the Figure 4-9, the final damping of the resonant poles is more than 17% of the critical which is excellent result as the speed pole is on the ideal position of 5 rad/sec.

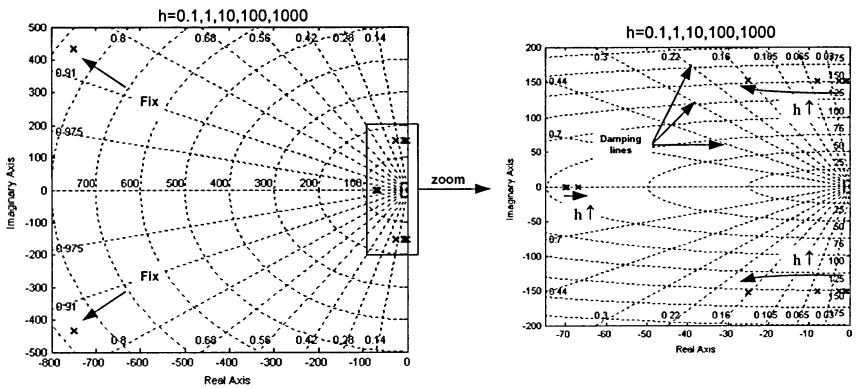

Figure 4-5 Loci of the state feedback poles during the design of optimal K_m.

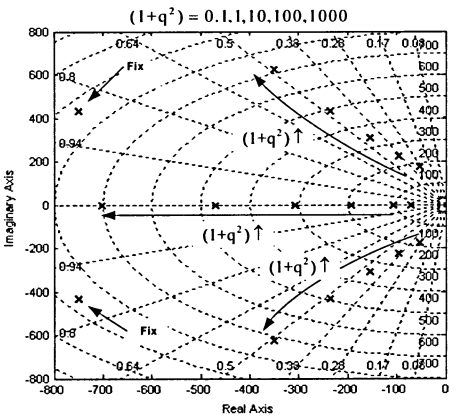

Figure 4-6 Loci of the estimator poles during the design of optimal K_f.

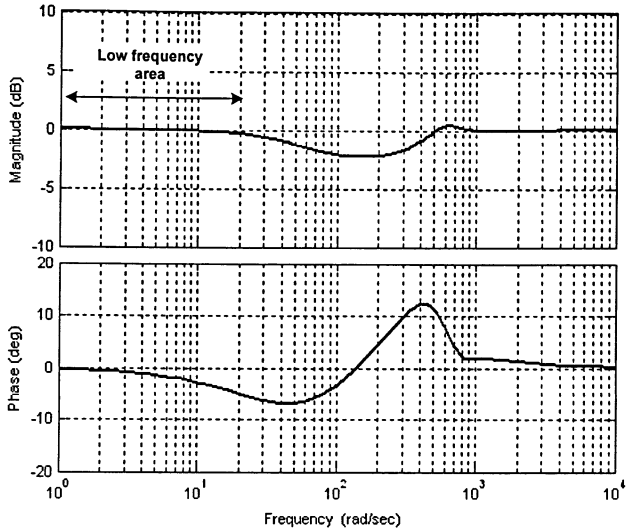

Figure 4-7 Bode plot of the feedforward (series) transfer function (1/(1+Hu)).

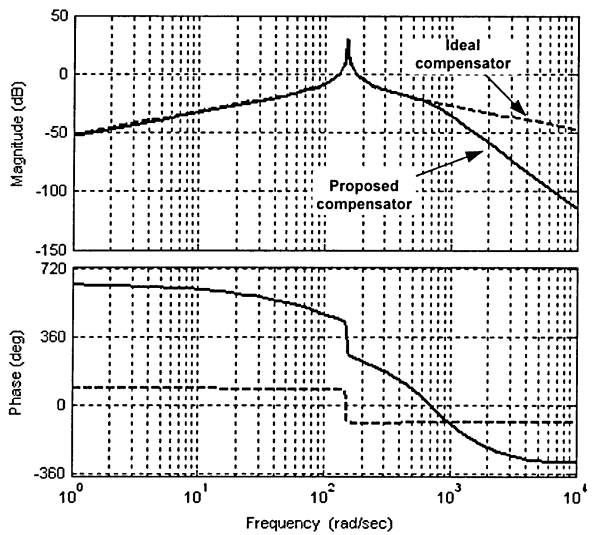

Figure 4-8 Bode plots of the open loop proposed compensator and open loop ideal compensator after the LTR method.

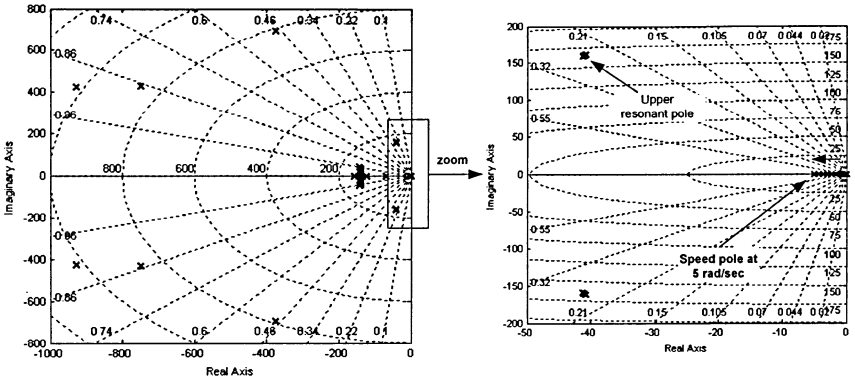

Figure 4-9 Root locus of entire closed loop system (from $\omega_{ref} \rightarrow \omega_M$) as the root locus gain change from 0 to 1.

4.5 Testing Results and Analysis

The testing of the resonant compensator is carried out using the experiment setup described in Section 4.2. The performance of the proposed compensator is evaluated by speed and load step responses, as well as by the harmonic spectrum of the shaft torque waveform as the operating speed frequency match with the mechanical resonant frequency under steady state operation. For comparison, each test has performed using conventional drive system without compensation and then with compensation using the proposed resonant compensator.

As initial experiment, open loop test is performed to make the required adjustment for the simulation parameters of the mechanical system with respect to the experiment mechanical model.

All the experiment test waveforms (except the armature current measured by using oscilloscope) have been measured and calculated during the test and then exported to a file, which could be imported to MATLAB for comparison with the simulation results.

4.5.1 Open Loop Test

The open loop test is performed first by running the motor at rated speed and rated voltage without closing the control loops. Then, a step load change of 100% rated torque is applied to the system by connecting an external resistor to the load machine. Figure 4-10 to Figure 4-13 shows the waveforms of the shaft torque, motor armature current and the speed responses. As can be seen from the figures, the step load test has excited the mechanical resonant frequency of the mechanical system and is equal to around 24 Hz. Another frequency is noticed at the waveforms. This frequency is due to armature reaction and is changeable with the speed and equal to 28.6 Hz at rated speed. It is very clear that the waveforms have experienced the beat phenomena which results from the main two frequencies: the resonant frequency (24 Hz) and the speed frequency (28.6 Hz). After a very small adjusting to the shaft damping of the simulation model, it is noticed that the simulation results are very close to the experimental results.

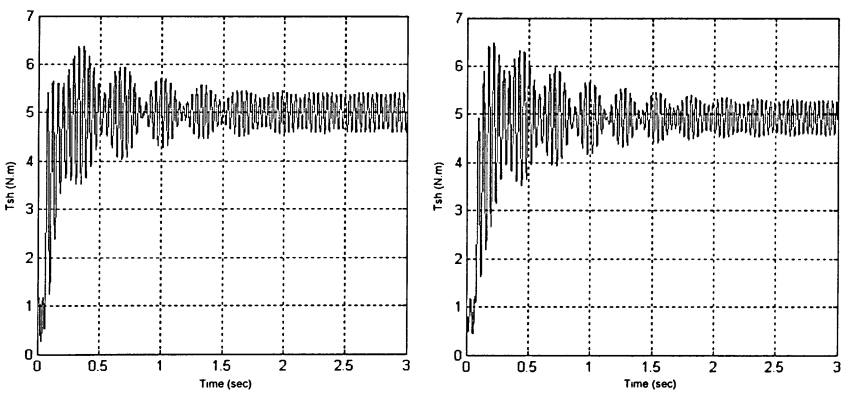

(a) Experimental Result (b) Simulated Result

Figure 4-10 Shaft torque waveform after 1 pu load step change under open loop test.

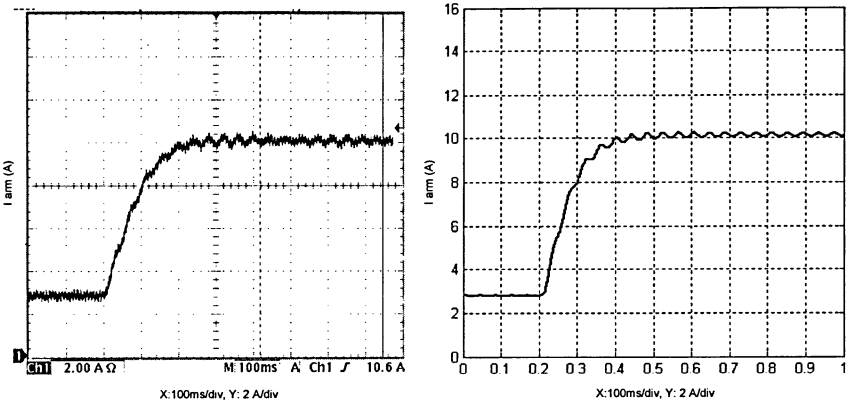

(a) Experimental Result (b) Simulated Result

Figure 4-11 Armature current waveform after 1 pu load step change under open loop test.

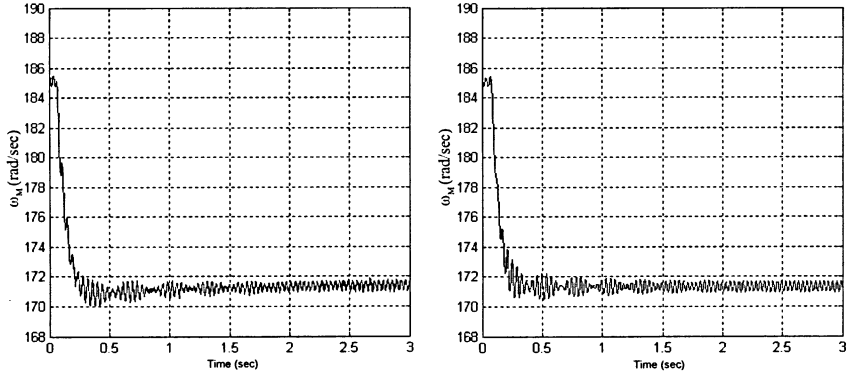

(a) Experimental Result (b) Simulated Result

Figure 4-12 Motor speed waveform after 1 pu load step change under open loop test.

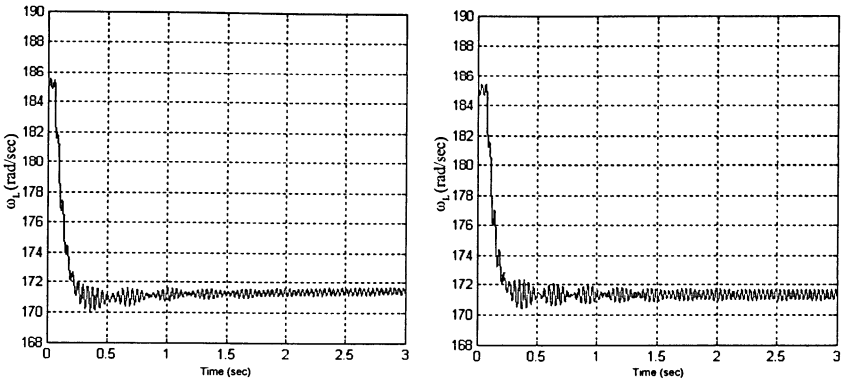

(a) Experimental Result (b) Simulated Result

Figure 4-13 Load machine speed waveform after 1 pu load step change under open loop test.

4.5.2 Speed Steps Response

As mentioned earlier, the speed response can gauge the effect of the resonance compensator on the speed response. In this test, the conventional two loop drive is set to 5 rad/sec for the speed regulator and 70 rad/sed for the current regulator. The reason for the lower bandwidth of the response is to avoid any damage in the mechanical system and to get suitable oscillation with certain mechanical damping. The speed step response test is performed with a 10% step of rated speed. Figure 4-13 to Figure 4-14 and Figure 4-15 to Figure 4-16 show the waveforms of the system without and with the compensation respectively. From the waveforms the shaft torque of the two cases, one can notice that the decay rate of the resonant frequency oscillation is improved from around 3 sec to 0.2 sec with the use of compensator. In addition, the peak shaft torque (also known as Torque Amplification Factor or TAF) is improved too. Also, one can notice that there is reduction of around 50% on the steady state peak oscillation that result from armature reaction. From the speed waveform, it is very clear that the speed responses stay same in the presence and absence the compensator. This proves the transparency of the proposed resonance compensator. Armature current waveforms show how the compensator injects an extra current at the presence of vibration.

As can be seen from the above, the resonant compensator is very effective at mitigation the shaft torque ripple without affecting the speed responses.

The simulation has good match with the measured values.

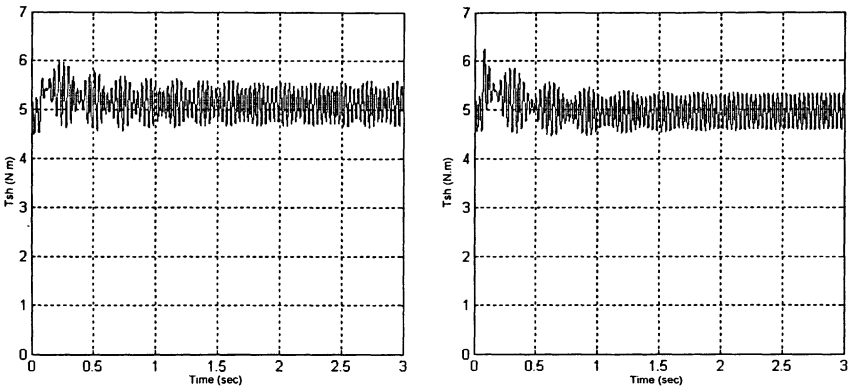

(a) Experimental Result (b) Simulated Result

Figure 4-14 Shaft torque waveform as the speed changes from 170 rad/sec to 180 rad/sec without compensation.

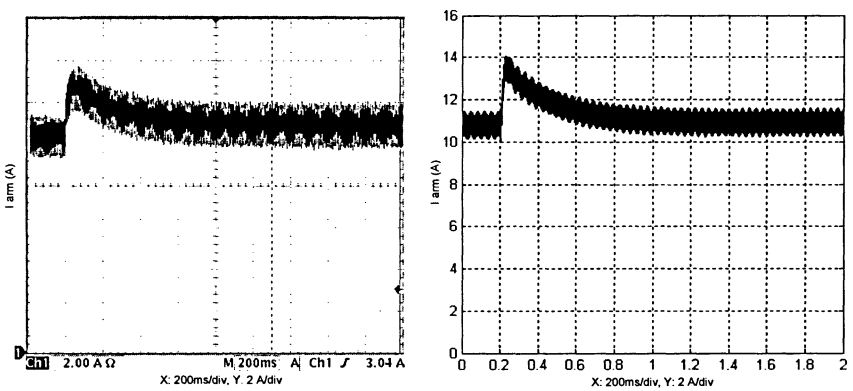

(a) Experimental Result (b) Simulated Result

Figure 4-15 Armature current waveform as the speed changed from 170 rad/sec to 180 rad/sec without compensation.

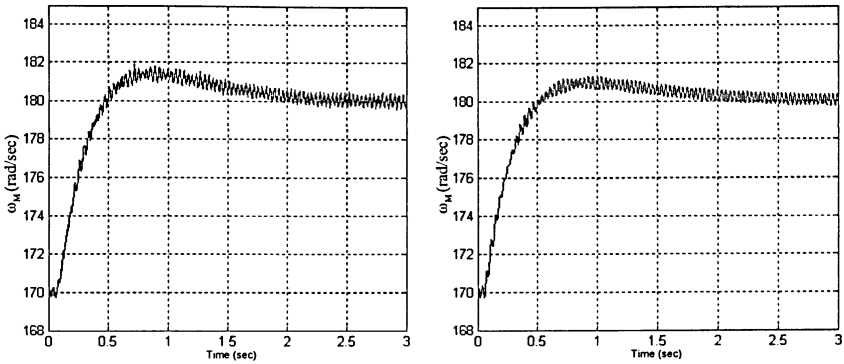

(a) Experimental Result (b) Simulated Result

Figure 4-16 Motor speed waveform as the speed changed from 170 rad/sec to 180 rad/sec without compensation.

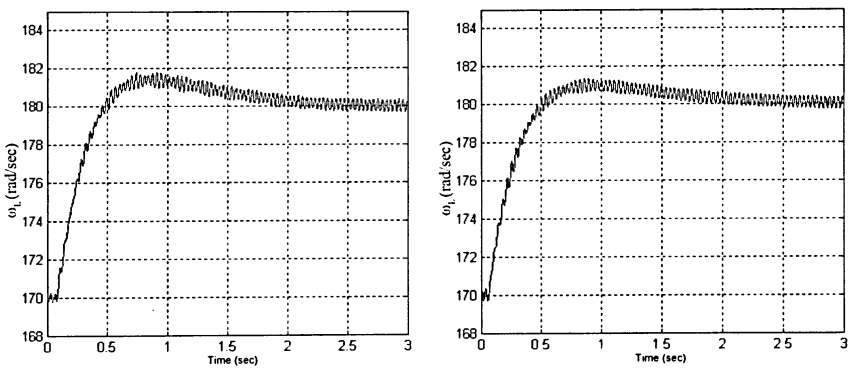

(a) Experimental Result (b) Simulated Result

Figure 4-17 Load machine speed waveform as the speed changed from 170 rad/sec to 180 rad/sec without compensation.

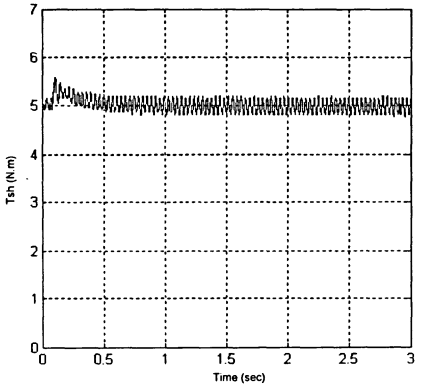

(a) Experimental Result

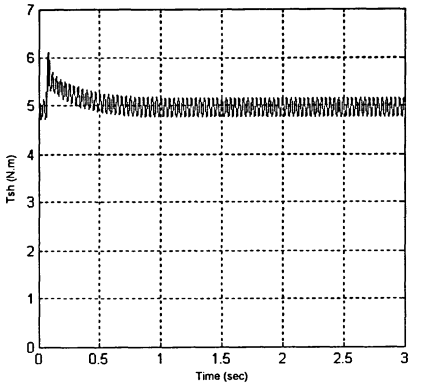

(b) Simulated Result

Figure 4-18 Shaft torque waveform as the speed changed from 170 rad/sec to 180 rad/sec with effect of resonant compensator.

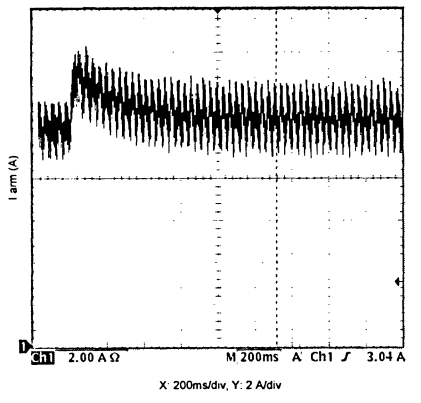

(a) Experimental Result

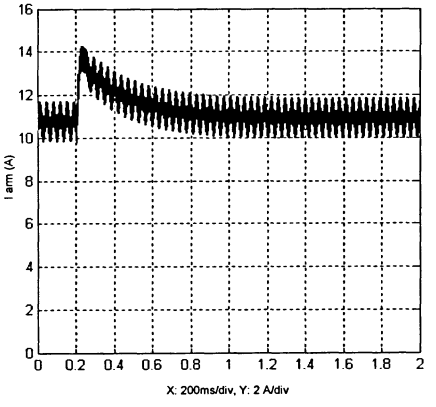

(b) Simulated Result

Figure 4-19 Armature current waveform as the speed changed from 170 rad/sec to 180 rad/sec with effect of resonant compensator.

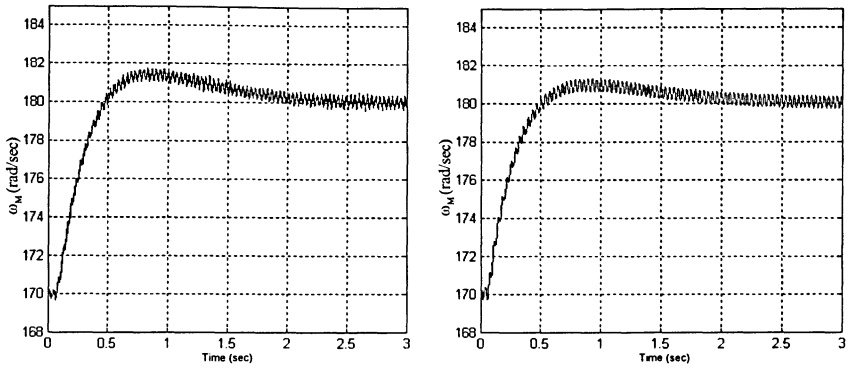

(a) Experimental Result (b) Simulated Result

Figure 4-20 Motor speed waveform as the speed changed from 170 rad/sec to 180 rad/sec with effect of resonant compensator.

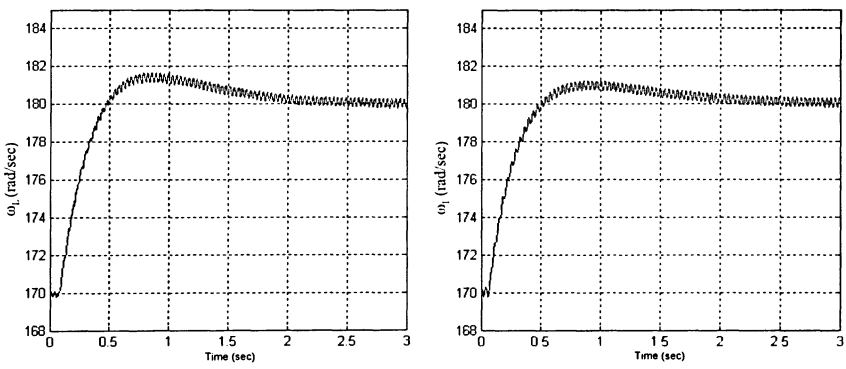

(a) Experimental Result (b) Simulated Result

Figure 4-21 Load machine speed waveform as the speed changed from 170 rad/sec to 180 rad/sec with effect of resonant compensator.

4.5.3 Steady State Test

Steady state test for the drive is performed with two operation conditions. The first operating condition is to run the motor at speed 180 rad/sec without and with the resonant compensator under full load condition. Figure 4-21 shows the experimental waveforms of the armature current and the shaft torque without and with the use of the resonant suppression algorithm. Figure 4-22 shows the frequency spectrum of the measured shaft torque with and without the compensation under steady state operation with 180 rad/sec motor speed. As can be seen from Figure 4-21 and Figure 4-22 the shaft torque ripple is minimized effectively with the use of compensation. However, there is some oscillation of speed frequency of 28.6 Hz in the shaft torque waveform after compensation because the resonant compensator is mainly designed to damp effectively the mechanical resonant frequency of 24 Hz. The high ripple in the armature current with the use of compensation results from the residual oscillation of the speed frequency. The frequency spectrum of Figure 4-22 shows clearly the ripple component (the resonant frequency and the speed frequency) of the shaft torque and how effectively damped by using the resonant compensator.

The second operation condition is carried out by running the motor at speed 150 rad/sec (23.8 Hz) which is near the resonant frequency. This test simulates the case when the mechanical resonant frequency coincides with the motor torque ripple which generated from certain operation condition in ac drives. Also, simulate the case when the motor speed passes the mechanical resonant frequency at the acceleration and deceleration. Figure 4-23 shows the waveform of the armature current and the shaft torque without and with the use of the resonant suppression algorithm at 150 rad/sec motor speed. Figure 4-24 shows the frequency spectrum of the shaft torque with and without the compensation under steady state operation at 150 rad/sec motor speed. From the Figure 4-23 and Figure 4-24, it is very clear that the shaft ripple is damped effectively and there is almost no speed frequency oscillation because it lies on the damping design area (24 Hz).

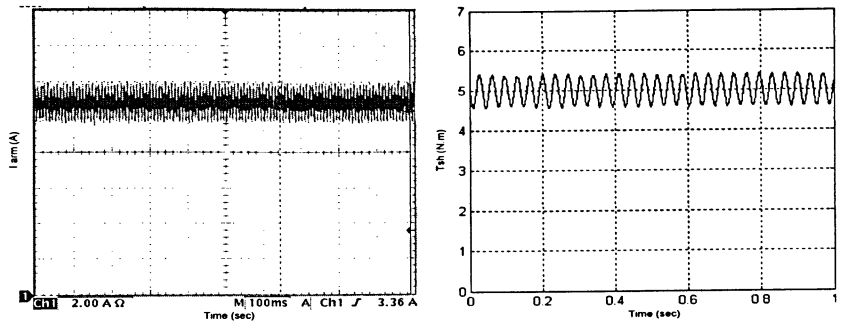

(a) Without Compensation

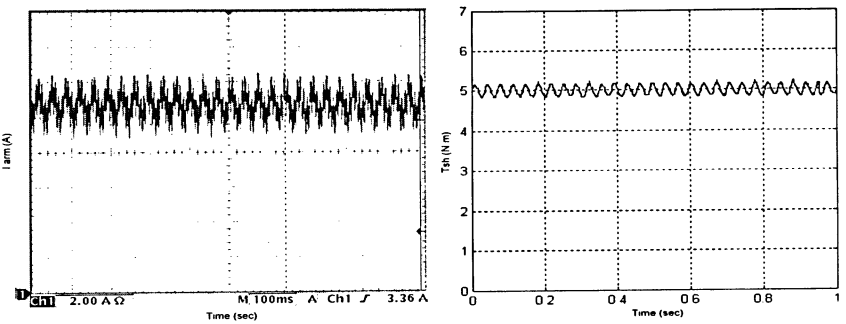

(b) With Compensation

Figure 4-22 Experimental waveforms of the shaft torque and armature current under steady state condition with 180 rad/sec motor speed.

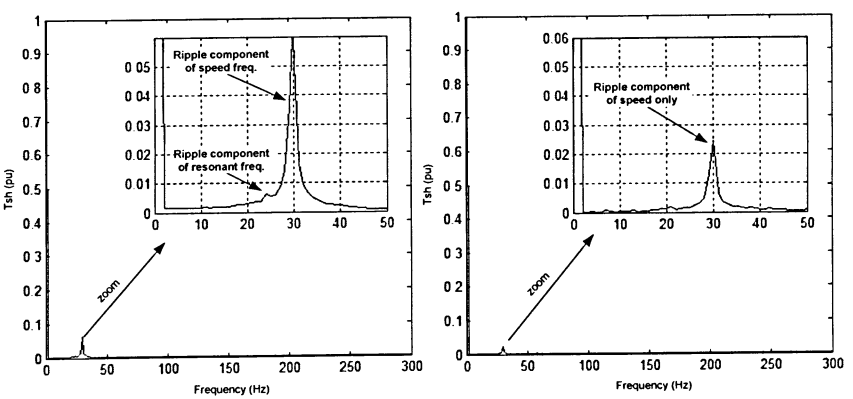

(a) Without Compensation

(b) With Compensation

Figure 4-23 Frequency spectrum of the measured shaft torque as the motor run at 180 rad/sec.

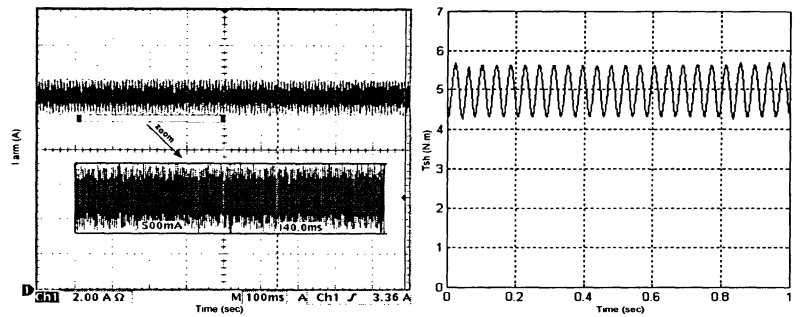

(a) Without Compensation

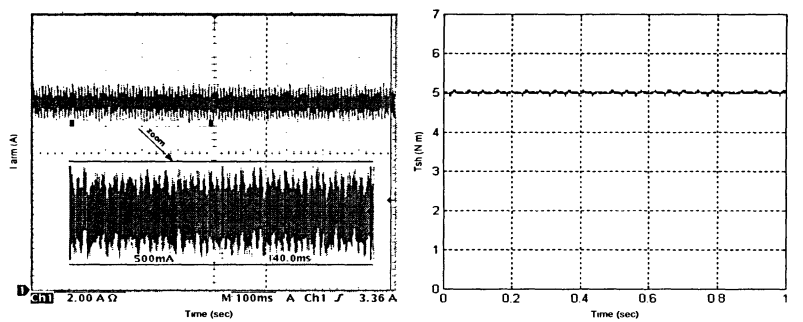

(b) With Compensation

Figure 4-24 Experimental waveforms of the shaft torque and armature current under steady state condition with 150 rad/sec motor speed.

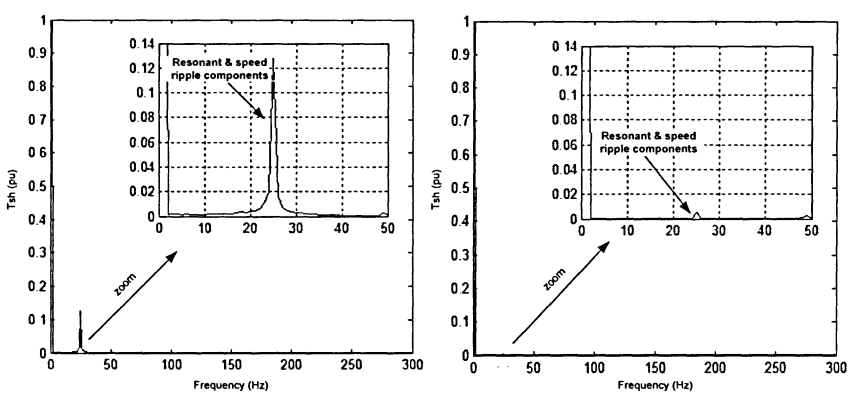

(a) Without Compensation (b) With Compensation

Figure 4-25 Frequency spectrum of the measured shaft torque as the motor run at 150 rad/sec.

4.5.4 Load Torque Response

The load test is performed by applying an external resistor to the machine load to give 100% step of rated torque. Again, the conventional drive is set to 5 rad/sec for the speed regulator and 70 rad/sec for the current regulator. Figure 4-25 to Figure 4-28 and Figure 4-29 to Figure 4-32 show the waveforms of the system without and with the compensation respectively. These figures show that the decay rate of the shaft torque ripple is improved from 3 sec to 0.25 sec and the peak shaft torque (TAF) is minimized significantly. Also, the speed responses of the motor and the load machine stay same in the presence and absence the compensator. This demonstrates that the compensator works as a filter for the oscillation without affecting the speed responses. Armature current waveforms show clearly how the compensator injects an extra current to compensate the sudden load change.

It is very clear that the proposed compensator perform very well in damping the vibration of the shaft torque without affecting the speed responses.

The simulation results has good match with the measured values.

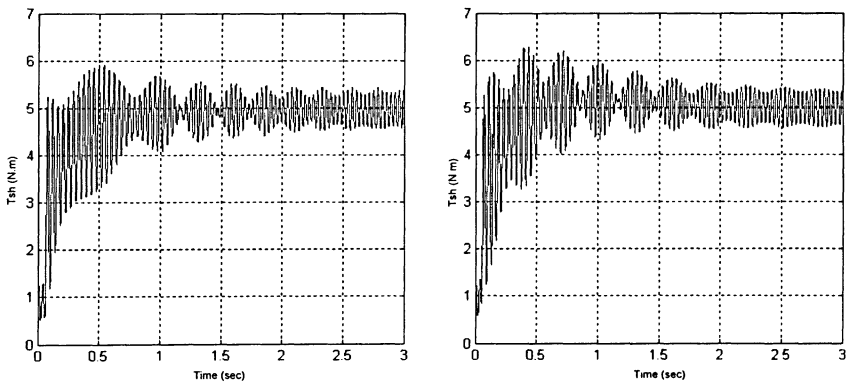

(a) Experimental Result (b) Simulated Result

Figure 4-26 Shaft torque waveform with 100% load step without compensation.

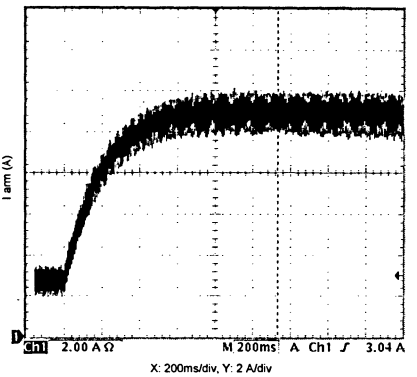

(a) Experimental Result

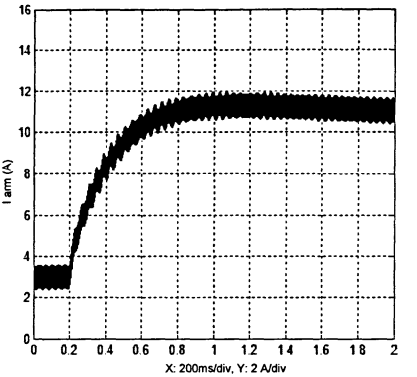

(b) Simulated Result

Figure 4-27 Armature current waveform with 100% load step without compensation.

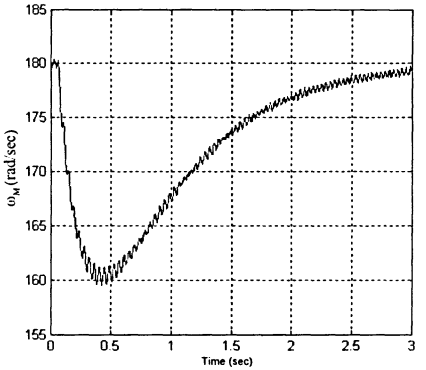

(a) Experimental Result

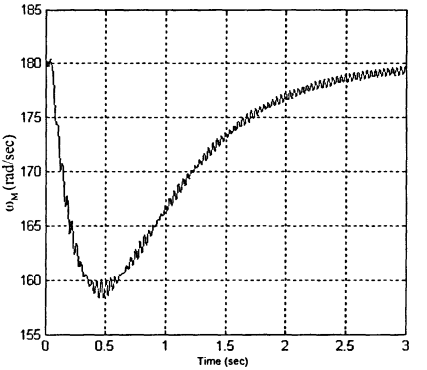

(b) Simulated Result

Figure 4- 28 Motor speed waveform with 100% load step without compensation.

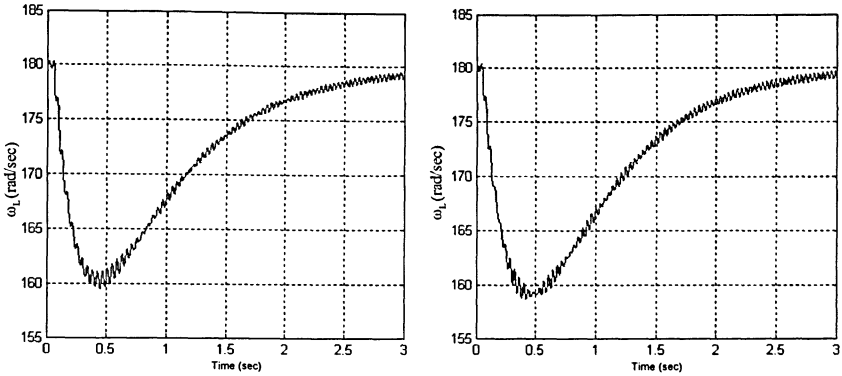

(a) Experimental Result (b) Simulated Result

Figure 4-29 Load machine speed waveform with 100% load step without compensation.

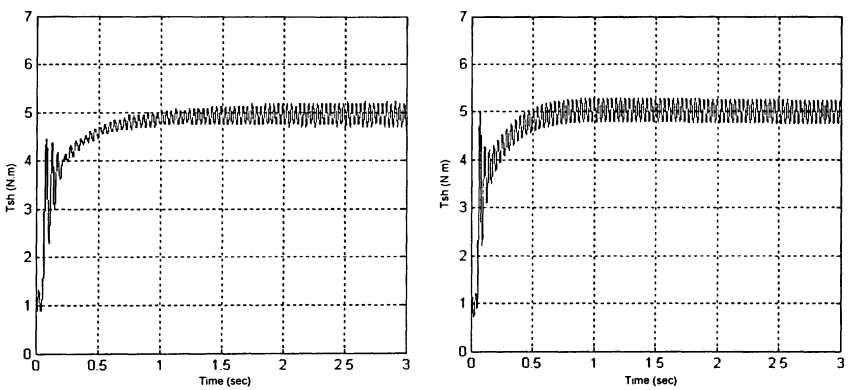

(a) Experimental Result (b) Simulated Result

Figure 4-30 Shaft torque waveform with 100% load step with effect of resonant compensator.

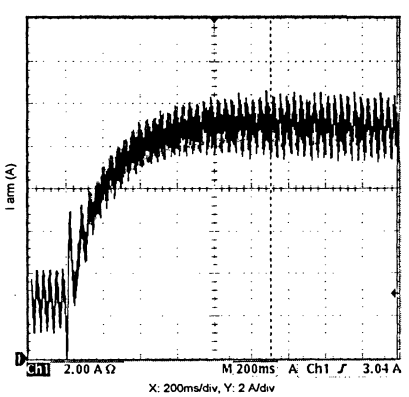

(a) Experimental Result

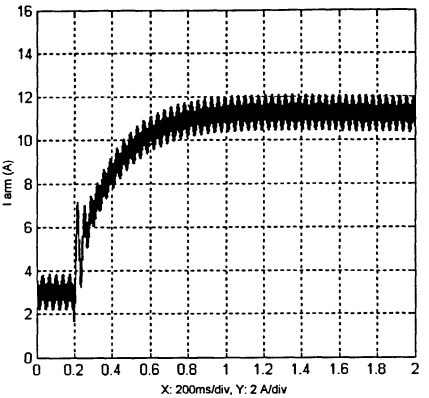

(b) Simulated Result

Figure 4-31 Armature current waveform with 100% load step with effect of resonant compensator.

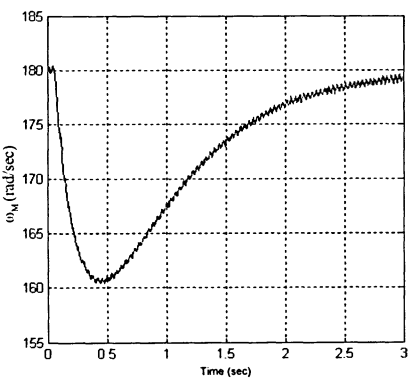

(a) Experimental Result

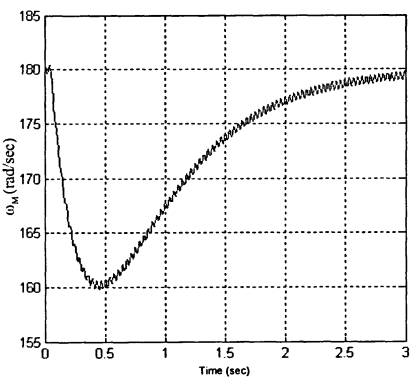

(b) Simulated Result

Figure 4-32 Motor speed waveform with 100% load step with effect of resonant compensator.

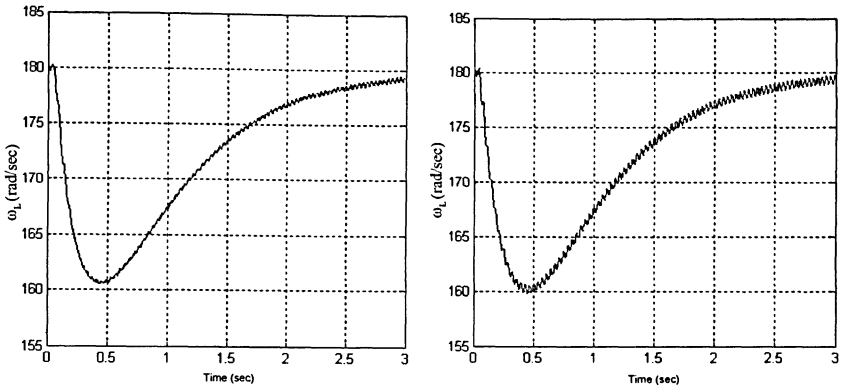

(a) Experimental Result (b) Simulated Result

Figure 4- 33 Load machine speed waveform with 100% load step with effect of resonant compensator.

4.6 Summary

The results of the experiment prototype system support the theoretical results of the proposed resonant compensator for high performance drives discussed in Chapter 3. The results show that the resonance compensator reduces the effect of shaft torque ripple by increasing the mechanical damping without affecting the speed regulator performance. The steady state performance is very good as the steady state oscillation can be damped out effectively. This proves the effectiveness of the compensator for suppressing the torsional vibration when the operating speed frequency (or the multiple of operating frequency) matches with or is close to the mechanical resonant frequency. The speed and load step responses are very good as the decay rate of the shaft torque ripple and the peak shaft torque are reduced significantly. This proves the effectiveness of the resonance compensator for the mill drive application.

CHAPTER 5: CONCLUSIONS

5.1 Conclusions

This thesis is devoted to the research and development of an effective torsional vibration damping method for high performance variable speed drives. Torsional vibration limits the speed loop response bandwidth of industrial drives, deteriorating the transient response to commands and disturbances. Torsional vibration may affect the quality of the end product and also may cause damage to the rolling mill system. Therefore, more effort should be made to eliminate the mechanical torsional vibration in drive systems.

The research started with a thorough investigation of different conventional and advanced mitigation methods. Among various mitigation methods, predictive compensation approach such as the feedforward control seemed very promising. It was found that this approach had certain limitations due to the large value of drive system time delay. Therefore, the proposed resonant compensator is developed with the following features:

- Damp the torsional vibration of the mechanical resonant frequency without affecting the speed loop response.
- Solve the limitation of torsional vibration damping due to the large value of system time delay.

To achieve the above features, a state feedback control method is developed. Shaft torque signal is used in the algorithm to estimate not only the state variables of the system but also the load torque input. Also, the system time delay is incorporated in the design. Linear Quadratic Regulator (LQR) and Kalman Filter (KF) with Linear Transfer Recovery (LTR) are used to design the state feedback and state estimator gains. Analysis, design, simulation and experiment of the proposed method are discussed in detail.

The **major contribution** of this thesis is the development of an effective damping algorithm based on state feedback control method for the resonant torsional vibration. This control algorithm is effective even with large time delay and does not affect the speed regulator loop. The details of the major contributions are provided as follows:

- **Incorporate the time delay in the design:** From the research study, it is found that the time phase delay plays an important role in causing the oscillation of the resonant poles of the mechanical system. Therefore, two states representing the system time delay are added to the design to solve the problem of large time delay on damping. The analysis, simulation and experimental results show that the proposed algorithm is very effective even with large system time delays.
- **Compensate Load torque input:** The compensator is developed to compensate not only the states of the plant but also the load torque input. The compensation of the estimated load torque disturbance improves the load torque disturbance rejection response remarkably. Also, by developing a design procedure for the estimated load toque gain, any dc offset on the speed loop due to step load change can be perfectly removed. Therefore, the compensator will not affect the outer speed loop.
- **Reduce compensator order from 6^{th} to 3^{rd} order:** The extensive study in the state feedback control method with Kalman Filter (KF) and Linear Transfer Recovery (LTR) methodology leads to the modification in the structure of the resonant compensator by eliminating the reference input of the estimator, which results in a reduction of the order of the estimator from 6^{th} to 3^{rd} order compensator.
- **Develop systematic design procedure:** Tuning procedure of weighting matrix Q and R of LQR/Kalman Filter is developed. This procedure is based on different gauging tools such as Bode and Nyquist plots to obtain the desired compensator gains according to design specification.
- **Design robust control system:** Robustness studies show that the modified compensator gives satisfactory margin with respect to variation of torque regulator response, time delay and resonant frequency. Also, the study shows that the compensator has almost no effect on the outer speed loop response. This is very important result as there is no need to retune the PI-regulator parameters of the existing system.

Overall, the research work has given a solution for damping the vibration result from the excessive time delay with only three tuning parameter controller. This improvement in the design reduces the computation time and the potential design error.

5.2 Future Work

As there is some limitation in using direct sensing of shaft torque signal in rolling mill industries, the research study of this thesis can be extended by using the proposed algorithm of the resonant compensator with observed shaft torque signal. The primary investigation of using observed shaft torque signal shows some success and needs to be followed by a study of real time implementation issues taking into account the additional time delay due to the observed shaft torque.

Another important issue that needs to be included in the future research is the identification of the system parameters (the mechanical resonant frequency, drive torque regulator response and latency) of the mill drive train system. The results of this work have shown that the design and the performance of the resonant compensator very much depend on system parameters. Therefore, to enhance the algorithm of resonant compensator, further research is required in the application of system identification techniques to identify the system parameters accurately.

APPENDICES

Appendix A

In order to determine the transfer function from the reference torque to the motor speed $\dot{T}_M \rightarrow \omega_M$, Figure 2-20 is simplified as shown in Figure A-1:

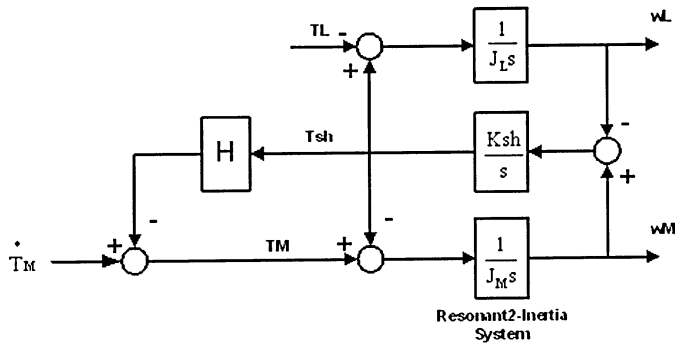

Figure A-1 Simplified system block diagram.

Figure A-1 can be redrawn and simplified by using block diagram simplification method as shown in FigureA-2.

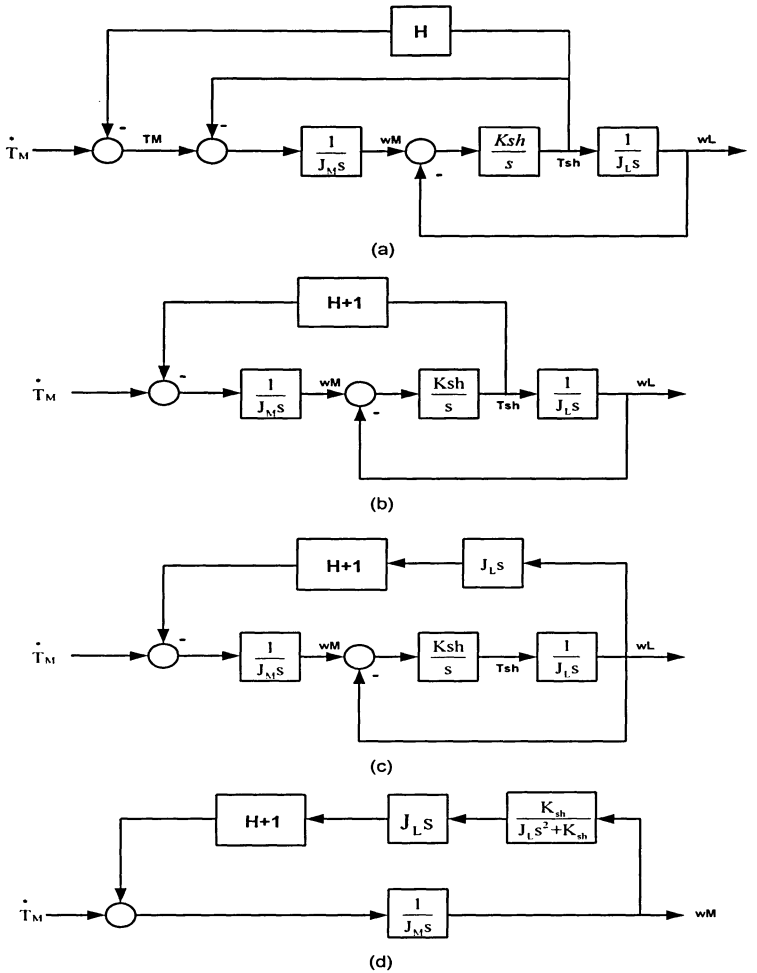

Figure A-2 Simplification steps of block diagram.

From Figure A-2, the transfer function from $\dot{T}_M$ to ω_M can be written as shown in Equation (A-1)

$$\left.\begin{aligned}\frac{\omega_M}{T_M} &= \frac{\frac{1}{J_M}}{1+\frac{1}{J_L s}(1+H)J_L s\frac{K_{sh}}{J_L s^2+K_{sh}}} \\ &= \frac{s^2+\omega_o{}^2}{J_M s[s^2+\frac{HK_{sh}}{J_M}+\omega_n{}^2}\end{aligned}\right\} \quad \text{(A-1)}$$

where

$$\left.\begin{aligned}\omega_o &= \sqrt{\frac{K_{sh}}{J_L}} \\ \omega_n &= \sqrt{\frac{K_{sh}(J_M+J_L)}{J_M J_L}}\end{aligned}\right\} \quad \text{(A-2)}$$

Since the transfer function H is the differentiator of the shaft torque, the final transfer function from the reference torque to motor speed is as follows:

$$\frac{\omega_M}{T_M} = \frac{s^2+\omega_o{}^2}{J_M s[s^2+\frac{CK_{sh}}{J_M}s+\omega_n{}^2]} \quad \text{(A-3)}$$

Appendix B

Suppose that G1 and G2 are two subsystems with state space representations:

$$\left.\begin{aligned}G_1 &= \left[\begin{array}{c|c} A_1 & B_1 \\ \hline C_1 & D_1 \end{array}\right] \\ G_2 &= \left[\begin{array}{c|c} A_2 & B_2 \\ \hline C_2 & D_2 \end{array}\right]\end{aligned}\right\} \quad \text{(B-1)}$$

The series or cascade connection of two subsystems is a system with the output of the second subsystem as the input of the first subsystem as shown in the following diagram:

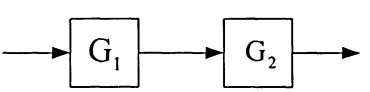

Figure B-1 Series or cascade connection of two subsystems.

This operation in terms of the transfer matrices of the two subsystems is essentially the product of two transfer matrices. Hence, a representation for the cascaded system can be obtained as:

$$G_1G_2 = \left[\begin{array}{c|c} A_1 & B_1 \\ \hline C_1 & D_1 \end{array}\right]\left[\begin{array}{c|c} A_2 & B_2 \\ \hline C_2 & D_2 \end{array}\right] = \left[\begin{array}{cc|c} A_1 & B_1C_2 & B_1D_2 \\ 0 & A_2 & B_2 \\ \hline C_1 & D_1C_2 & D_1D_2 \end{array}\right] = \left[\begin{array}{cc|c} A_2 & 0 & B_2 \\ B_1C_2 & A_1 & B_1D_2 \\ \hline D_1C_2 & C_1 & D_1D_2 \end{array}\right] \quad \text{(B-2)}$$

Appendix C

Doyle and Stein mention that there is no uncertainty with loop broken from point xx (see Figure C-1, while broken point x is a physically important point for testing the robustness of the system since the two points can be assume do not see the same signal. Therefore, the transfer function from u' and u" to the estimated states $\hat{x}$ can be written as follows:

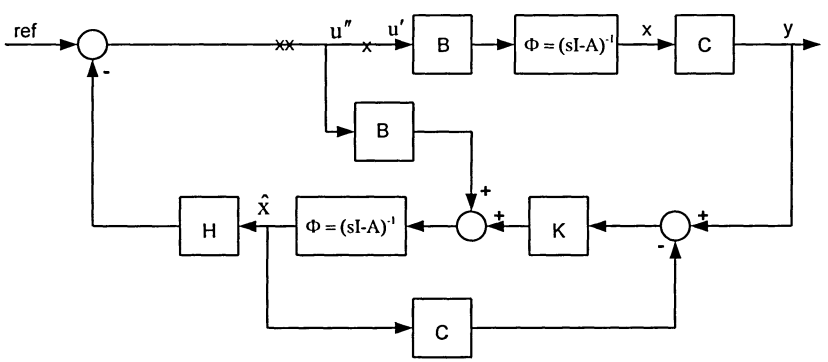

Figure C-1 State Feedback base observer implementation.

$$\hat{x} = \underbrace{\Phi(I+KC\Phi)^{-1}}_{\text{Reference Input part}}u' + \underbrace{\Phi K(I+C\Phi K)^{-1}}_{\text{Sensor Input Part}}y \quad \text{(C-1)}$$

Equation (C-1) shows that the estimated state is equal to two parts, the sensor and the reference transfer function.

Since $y=C\Phi Bu''$, Equation (C-1) can be written as follows:

$$\hat{x}=\Phi(I+KC\Phi)^{-1}u'+\Phi K(I+C\Phi K)^{-1}C\Phi Bu'' \qquad \text{(C-2)}$$

After some manipulations, Doyle and Stein show the following:

$$\hat{x}=\Phi[B(C\Phi B)^{-1}-K(I+C\Phi K)^{-1}]C\Phi Bu'+\Phi[K(I+C\Phi K)^{-1}]C\Phi Bu'' \qquad \text{(C-3)}$$

Also, they point out that if the estimator dynamic satisfies, the following Equation can be achieved:

$$B(C\Phi B)^{-1}=K(I+C\Phi K)^{-1} \qquad \text{(C-4)}$$

Therefore, Equation (C-3) becomes as follows:

$$\hat{x}=\Phi[B(C\Phi B)^{-1}]C\Phi Bu''=\Phi Bu'' \qquad \text{(C-5)}$$

Equation (C-5) is identical to:

$$x=\Phi Bu'' \qquad \text{(C-6)}$$

Equation (C-5) and (C-6) show the system is recovered or in other word the estimated and actual states are the same. It is very clear from Equation (C-5) that the reference input part has been vanished which proves that the reference input can be removed when the system recovered.

Appendix D

DSP Program Code

```
#include      "DSP281x_Device.h"
#include      "DSP281x_Examples.h"
#include      "FPGA_csr.h"
#include      "Display.h"
#include      <stdio.h>
#include      "IQmathLib.h"

#define ADC_usDELAY  8000
#define ADC_usDELAY2  40

// USEFUL DEFINETION

#define Sw_freq 3000.0 //sampling frequency

#define AVE_SAMPLE   8
#define AVE_SHFT     3
#define AVE_SAMPLE_DC 16
#define AVE_SHFT_DC  4

#define w_DC        1000.0
#define w_AD        1000.0
#define w_speed     1000.0
#define w_torque    1000.0
#define w_speed_w   70.0//
#define w_torque_reg  75.0//
#define Kf      0.478
#define Kp_Iarm     0.0041
#define Ki_Iarm     0.231

#pragma DATA_SECTION(graph_data,
        "graph_data");
#pragma DATA_SECTION(graph_data1,
        "graph_data1");
#pragma DATA_SECTION(graph_data2,
        "graph_data2");
#pragma DATA_SECTION(graph_data3,
        "graph_data3");
#pragma DATA_SECTION(graph_data4,
        "graph_data4");
#pragma DATA_SECTION(graph_data5,
        "graph_data5");
# pragma DATA_SECTION(graph_data6,
        "graph_data6");

//VARIABLE DECLARATION

/* ADC  */
Sample_ch7[AVE_SAMPLE],
Sample_ch8[AVE_SAMPLE_DC],

Uint16 ConversionCount=0;
Uint16 ConversionCount1=0;
 int32 AD_BIAS7,AD_BIAS8,

/* PWM*/
Uint16 Ts=50000;//PWM period in counter value

/*Low-pass filter*/
_iq28 LPFa,LPFb,LPFa_DC,LPFb_DC,
      LPFa_speed,LPFb_speed,LPFa_torque,
      LPFb_torque;

/*Copper*/
_iq18 D_inv,D_inv1;
_iq18 Iarm, Iarm_ref,
      Iarm_err, Iarm_err1,I_test;
_iq18 If,If0,If_L,If_L0;
_iq28 kp_Iarm, ki_Iarm;  //PI controller

/*Motor position and speed*/
_iq18 Speed_CNT_L,Speed_CNT_L0;
_iq18 Speed_w,Speed_w0,Speed_w_ref,
      Speed_w_err,Speed_w_err1,Speed_n,
      Delta_speed;
_iq18 Speed_CNT_L1,Speed_CNT_L01;

_iq18 Speed_w1,Speed_w01,Speed_w_ref1,
      Speed_w_err1,Speed_w_err11,Speed_n1,
      Delta_speed1;
_iq18 Te,Tm;

Uint16 Angle_CNT[33],Speed_CNT,
       Speed_CNT0;
Uint16 Angle_index=0,Angle_index1=0;
```

```
Uint16 Angle_CNT1[33],Speed_CNT1,
       Speed_CNT01;
Uint16 Angle_inde=0,Angle_inde1=0;

/*Motor Torque*/

_iq18 torque_motor=0,torque_motor_ref=0,
      torque_G=0,torque_G0=0,torque_G_L=0,
      torque_G_L0=0;

/*Key input*/
int16 key_value, key_value1,
     key_monitor, key_monitor1,key1;


/* Display*/
Uint16 display_counter,display_counter1;

/*Control flags*/
Uint16 CONTACTOR,INTERRUPT, FAULT,
       Fault_info_A,Fault_info_B,

/*Graph of waveform*/
int16  graph_data[3000];
int16  graph_data1[3000];
int16  graph_data2[3000];
int16  graph_data3[3000];
int16  graph_data4[3000];
int16  graph_data5[3000];
int16  graph_data6[3000];

Uint16 graph_index=0;
Uint16 graph_index1=0;
Uint16 graph_index_flag=0;
Uint16 data_shift_times=0;
Uint16 JJ=0;

/*Shaft Torque & Kalman*/
_iq18 shaft_Torque0=0,shaft_Torque1=0,
      shaft_Torque2=0,shaft_Torque=0;
_iq18 Obs_out0=0,Obs_out1=0,
      Obs_out2=0,Obs_out=0;
_iq18 State_out=0;
_iq18 State_out0=0;
_iq18 State_outL0=0,State_outL=0;
```

// FUNCTION DECLARATION

```
interrupt void  adc_isr(void);
interrupt void  pdpinta_isr(void);
interrupt void  t1cint_isr(void);
void get_adc_V(void);
void get_speed(void);
void get_speed1(void);
void Speed_dif(void);
void Kalman_Obs(void);
void Motor_drive(void);
void Speed_control(void);
void Enable_Inv(void);
void Disable_Inv(void);
void Key_input(void);
void Close_Relay(void);
void Open_Relay(void);
void Delay_mili_second (int delay);
void Init_variable(void);
void InitGpio(void);
void InitXintfClocks(void);
void InitPeripherals(void);
void InitEVA(void);
void InitEVB(void);
void InitAdc(void);
void init_fpga(void);
```

// MAIN FUNCTION

```
void main(void)
{
// Step 1. Initialize System Control:
// PLL(PLLCR=0xA), WatchDog(disable), enable
   Peripheral Clocks
   InitSysCtrl();

// Step 2. Initialize the Xintf clocks
   InitXintfClocks();

// Step 3. Initalize GPIO:
   InitGpio();

// Step 4. Clear all interrupts and initialize PIE
vector table:
   DINT; // Disable CPU interrupts
   InitPieCtrl(); // Initialize the PIE control
//registers to their default state.
// The default state is all PIE interrupts
//disabled and flags are cleared.

IER = 0x0000; // Disable CPU interrupts
IFR =0x0000; // Clear all CPU interrupt flags
```

```
InitPieVectTable(); // Initialize the PIE vector
table

// Interrupts  used are re-mapped to ISR
functions
  EALLOW;
  PieVectTable.PDPINTA = &pdpinta_isr;
  PieVectTable.ADCINT = &adc_isr;
  PieVectTable.T1CINT = &t1cint_isr;

 //PieVectTable.T1UFINT = &t1ufint_isr;
  EDIS;

// Step 5. Initialize all the Device Peripherals:
  InitPeripherals();

// Step 6. User specific code, enable interrupts:
  PieCtrlRegs.PIEIER1.bit.INTx1 = 1;
  //Enable PDPINTA
  PieCtrlRegs.PIEIER1.bit.INTx6 = 1;
  //EnableADCINT
  PieCtrlRegs.PIEIER2.bit.INTx5 = 1;
  // Enable t1cint

  IER |= M_INT1; // Enable CPU INT1:
  IER |= M_INT2; // Enable CPU INT2:

  EINT;// Enable Global interrupt INTM
  ERTM;// Enable Global realtime interrupt
DBGM;

 Clear_LED();
 AD_bias16();
 Manu_display();
 AdcRegs.ADCTRL2.bit.INT_ENA_SEQ1=1;

// Step 7. Infinite loop
  while(1)
  {
   if (FAULT == 0) Key_input ();
   display_counter++;
    if(display_counter==20000)
     {
      display_counter1++;
      display_counter=0;
     }
      if (display_counter1==30)
       {
         LED_display();
         display_counter1=0;
         display_counter=0;
       }
  }

} /*End Main*/
```

```
// INTERRUPT SERVICE ROUTINES



interrupt void  t1cint_isr(void)
{
  Angle_CNT1_A1=Angle_CNT0_A1;
  CAP_CNT_A1=CAP_CNT0_A1;
  Angle_CNT1_B1=Angle_CNT0_B1;
  CAP_CNT_B1=CAP_CNT0_B1;

  EINT;
  watch1= EvaRegs.T1CNT;

  get_speed();
  get_speed1();
  get_adc_V();

  switch (INTERRUPT)
  {
    case 1:
    break;
    case 2:
    if((Iarm>_IQ18(30))||(Iarm<_IQ18(-30)))
    {Disable_Inv();INTERRUPT = 1;}

    Speed_control(); //Speed Control to give
Iarm_ref
    Speed_dif(); //To determine Tsh
    Kalman_Obs();
    Motor_drive();
    break;
  }


 /*for waveforms display*/
   graph_data[graph_index]= Speed_w1>>11;
   graph_data1[graph_index]= State_out>>8;
   graph_data2[graph_index]= torque_G>>8;
   graph_data3[graph_index]= Iarm>>8;
   graph_data4[graph_index]= torque_G_L>>8;
   graph_data5[graph_index]= Speed_w>>11;
   graph_data6[graph_index]=
shaft_Torque>>8;


  JJ=JJ+1;
  if (JJ==3)
  {
  graph_index++;
```

```
if((shaft_Torque>_IQ18(2))&&(Speed_w>_IQ18(
110))&&(INTERRUPT==1))
{graph_index_flag=1;}

if((shaft_Torque>_IQ18(3.4))&&(Speed_w>_IQ1
8(110))) {graph_index_flag=1;}

if(Speed_w_ref==_IQ18(180))
{graph_index_flag=1;}
if(Speed_w_ref==_IQ18(160))
{graph_index_flag=1;}

 if(graph_index== 3000) graph_index=0;
 if(graph_index_flag==1) graph_index1++;
 if(graph_index1==2930){graph_index--;
   graph_index1--;}

  JJ=0;
  }
  EvaRegs.EVAIFRA.bit.T1CINT=1;// Clear INT
  PieCtrlRegs.PIEACK.all=PIEACK_GROUP2;

} /*End of t3cint_isr*/


interrupt void  adc_isr(void)
{

Sample_ch7[ConversionCount]=((AdcRegs.AD
              CRESULT7>>4) );

 if  (ConversionCount==AVE_SAMPLE-1)
    {ConversionCount=0;}
 else ConversionCount++;

Sample_ch8[ConversionCount1]=((AdcRegs.AD
              CRESULT8>>4));

 if  (ConversionCount1==AVE_SAMPLE_DC-1)
    {ConversionCount1=0;}
 else ConversionCount1++;

AdcRegs.ADCTRL2.bit.RST_SEQ1=1;
AdcRegs.ADCST.bit.INT_SEQ1_CLR=1;
PieCtrlRegs.PIEACK.all = PIEACK_GROUP1;

} /*End of Adc_isr*/



interrupt void pdpinta_isr(void)
{
 Open_Relay ();
 Disable_Rec();
 Disable_Inv();

 INTERRUPT = 0;
 FAULT = 1;
 CONTACTOR = 0;
Fault_info_A=*FAULT_DETECT_A;
Fault_info_B=*FAULT_DETECT_B;
Display_Fault ();
PieCtrlRegs.PIEACK.all = PIEACK_GROUP1;


} /*End of Pdpinta_isr*/



//SUBPROGRAM ROUTINES



void get_speed(void)
{
Angle_CNT[Angle_index]=EvaRegs.T2CNT;
Speed_CNT0=Speed_CNT;


if (Angle_index==32)
    {
 if(Angle_CNT[32]<Angle_CNT[0])
  {Speed_CNT=Angle_CNT[32]+20000-
   Angle_CNT[0];}
    else{Speed_CNT=Angle_CNT[32]-
        Angle_CNT[0];}
 Angle_index=0;
   }
 else
{
if(Angle_CNT[Angle_index]<Angle_CNT[Angle_i
n
   dex+1])
{Speed_CNT=Angle_CNT[Angle_index]+20000-
   Angle_CNT[Angle_index+1];}
else{Speed_CNT=Angle_CNT[Angle_index]-
     Angle_CNT[Angle_index+1];}
     Angle_index++;
   }
Speed_CNT_L0=Speed_CNT_L;
Speed_CNT_L=_IQ18mpyI32(LPFa_speed>>10
,
(Speed_CNT0+Speed_CNT));
Speed_CNT_L+=_IQ18mpyIQX(LPFb_speed,28
, Speed_CNT_L0,18);
Speed_n=_IQ18mpy(Speed_CNT_L>>5,
  _IQ18(Sw_freq*60/20000));
```

```
 if (Angle_index1==31)
   {
    Speed_w0=Speed_w;
    Speed_w=_IQ18mpy(Speed_CNT_L>>5,
    _IQ18(Sw_freq*2*PI/20000)); (rad/s)
    Angle_index1=0;
 }
    else Angle_index1++;

}//END get_speed(void)


void get_speed1(void)
{
 Angle_CNT1[Angle_inde]=EvbRegs.T4CNT;
 Speed_CNT01=Speed_CNT1;

 if (Angle_inde==32)
  {
 if(Angle_CNT1[32]<Angle_CNT1[0])
{Speed_CNT1=Angle_CNT1[32]+20000-
  Angle_CNT1[0];}
else{Speed_CNT1=Angle_CNT1[32]-
  Angle_CNT1[0];}
  Angle_inde=0;}
 else
  {


if(Angle_CNT1[Angle_inde]<Angle_CNT1[Angle
_i
   nde+1])

{Speed_CNT1=Angle_CNT1[Angle_inde]+2000
0-
      Angle_CNT1[Angle_inde+1];}
else{Speed_CNT1=Angle_CNT1[Angle_inde]-
      Angle_CNT1[Angle_inde+1];}
      Angle_inde++;
}
Speed_CNT_L01=Speed_CNT_L1;
Speed_CNT_L1=_IQ18mpyl32(LPFa_speed>>1
0,(Speed_CNT01+Speed_CNT1));
Speed_CNT_L1+=_IQ18mpylQX(LPFb_speed,2
8,                    Speed_CNT_L01,18);
Speed_n1=_IQ18mpy(Speed_CNT_L1>>5,
_IQ18(Sw_freq*60/20000));
if (Angle_inde1==31)
  {
   Speed_w01=Speed_w1;
   Speed_w1=_IQ18mpy(Speed_CNT_L1>>5,
   _IQ18(Sw_freq*2*PI/20000));
   Angle_inde1=0;
  }
else Angle_inde1++;

}//END get_speed1(void)


void Motor_drive(void)
{
  Uint32 a,b;

  //Iarm_err=(Iarm_ref-AState_Out)-Iarm;
  Iarm_err = (Iarm_ref-State_out)-Iarm;
  //Iarm_err = Iarm_ref-Iarm;
  //Iarm_err=(Iarm_ref+torque_G_HP)-Iarm;

Iarm_err1 +=_IQ18mpylQX( ki_Iarm, 28,
              Iarm_err, 18);
  if  (Iarm_err1>_IQ18(0.95))
     {Iarm_err1=_IQ18(0.95);}
  if  (Iarm_err1<_IQ18(0.05))
     {Iarm_err1=_IQ18(0.05);}

D_inv=_IQ18mpylQX(kp_Iarm,28,
        Iarm_err,18)+Iarm_err1;
if   (D_inv>_IQ18(1)) {D_inv=_IQ18(1);}
if   (D_inv<_IQ18(0.5))
   {D_inv=_IQ18(0.5);}

  a= Ts>>2;
  a= D_inv*a;
  a= a>>16;
  b=27000;
  EvaRegs.CMPR3=a;//Positive(A)
  EvaRegs.CMPR2=Ts-a;//Negative(B)
  EvaRegs.CMPR1 = b;//field(C)
}


void Speed_control(void)
{
 /*outter speed control loop */
Speed_w_err=Speed_w_ref-Speed_w;
Speed_w_err1+=_IQ18mpylQX(
  _IQ28(0.3609/3000),28,Speed_w_err, 18);
  if (Speed_w_err1>_IQ18(20))
    {Speed_w_err1=_IQ18(20);}
  if (Speed_w_err1<_IQ18(0.1))
    {Speed_w_err1=_IQ18(0.1);}
Iarm_ref=_IQ18mpylQX(_IQ28(0.2887),28,
          Speed_w_err,18)+Speed_w_err1;
if (Iarm_ref>_IQ18(20))
 {Iarm_ref=_IQ18(20);}
if (Iarm_ref<_IQ18(0.1))
 {Iarm_ref=_IQ18(0.1);}
}
```

```
void Speed_dif(void)
{
int16 a;

 Angle_1=EvaRegs.T2CNT;
 Angle_2=EvbRegs.T4CNT;

 if ((Angle_1>Angle_2)&&((Angle_1-
              Angle_2)<(20000.0/2)))
   {Angle_delta=Angle_1-Angle_2;}
 if((Angle_2>Angle_1)&&((Angle_2-
              Angle_1)>=(20000.0/2)))
   {Angle_delta=Angle_1+20000-Angle_2;}
 if((Angle_2>Angle_1)&&((Angle_2-
              Angle_1)<(20000.0/2)))
   {Angle_delta=Angle_2-Angle_1;}
 if((Angle_1>Angle_2)&&((Angle_1-
             Angle_2)>=(20000.0/2)))
    {Angle_delta=Angle_2+20000-Angle_1;}
 a=Angle_delta;
Angle_diff_Degree=_IQ18(0.0174/55.5)*a;//(pi/1
80)
                  /(20000/360)
 shaft_Torque=_IQ18mpy(Angle_diff_Degree,
              _IQ18(152));

} //END Speed_dif(void)



void Kalman_Obs(void)
 {

  State_out0=State_out;
  State_outL0=State_outL;

  // Using shaft torque (shaft_Torque)


Obs_out=_IQ18mpyIQX(_IQ28(4.76),28,
        (shaft_Torque-shaft_Torque1),18)-
         _IQ18mpyIQX(_IQ28(4.813),28,
        (shaft_Torque2-shaft_Torque0),18);

Obs_out+=_IQ18mpyIQX(_IQ28(2.532),28,

Obs_out2,18)_IQ18mpyIQX(_IQ28(2.169),28,

Obs_out1,18)+_IQ18mpyIQX(_IQ28(0.6266),28,
    Obs_out0,18);

State_out=_IQ18mpyIQX(_IQ28(1.0),28,
          Obs_out,18);

State_outL=_IQ18mpyIQX(LPFa,28,
     (State_out0+State_out),18);  //filter  w_AD
=1000
State_outL+=_IQ18mpyIQX(LPFb,28,
      State_outL0,18);

  shaft_Torque0=shaft_Torque1;
  shaft_Torque1=shaft_Torque2;
  shaft_Torque2=shaft_Torque;
  Obs_out0=Obs_out1;
  Obs_out1=Obs_out2;
  Obs_out2=Obs_out;

 }//END Kalman_Obs(void)


void Key_input(void)
{
 {
  if(key_value)
  {
   switch (key_value)
   {
    case 1:
     if (CONTACTOR==0)
    {SCREEN=1;Close_Relay();
    Display_Relay_Close();*FAN_CONFIG      =
0x1F;}
     else
      switch (INTERRUPT)
       {
        case 0:
        Enable_Rec();
        INTERRUPT = 1;
        break;
        case 1:
    if(test_flag==1)
          {D_inv= _IQ18(1);test_flag1=1;}
           Enable_Inv();
           INTERRUPT = 2;
           Display_ENB_INV();
           break;
           case 2:
            if (test_flag==1)
            {D_inv= _IQ18(0.5);test_flag1=0;}
             Disable_Inv();
             INTERRUPT = 1;
             Display_DISAB_INV();
             break;
       }
         break;
         case 2:
         switch (INTERRUPT)
         {
          case 0:
          key1++; if (key1>9){key1=0;}
```

```
            break;
            case 1:
            key1++; if (key1>9){key1=0;}
            break;
            case 2:

Speed_w_ref=Speed_w_ref+_IQ18(10);
          if (Speed_w_ref> _IQ18(180))
          Speed_w_ref= _IQ18(180);
               break;
        }
    break;

    case 4:
         switch (INTERRUPT)
    case 0:
    key1--;
    if (key1<0||key1>9){key1=9;}
         break;
         case 1:
         key1--;
         if  (key1<0||key1>9){key1=9;}
         break;
         case 2:              ]
         Speed_w_ref=Speed_w_ref-_IQ18(10);
          if(Speed_w_ref<_IQ18(0.1))
            {Speed_w_ref= _IQ18(0.1);}
            break;
             }
         break;

    case 8:
          if (CONTACTOR==1)
          {
           Disable_Rec();
           INTERRUPT=0;Open_Relay();
           SCREEN=0;
           test_flag1=0;Iarm_ref= 0;
           Delay_mili_second(500);
           Disable_Inv();
           D_inv=_IQ18(0.5);
           Manu_display();
           *FAN_CONFIG=0x1D;
           }
          break;
      }
       }
   }
   key_value=0;

} // End of Key_input


void Init_variable(void)
 {
  /*ADC*/
  ConversionCount=0;

  /*Low pass filter*/
  LPFa=_IQ28(1-2.0/(2.0+w_AD/Sw_freq));
  LPFb=_IQ28(1)-(LPFa<<1);
  LPFa_DC=_IQ28(1-2.0/(2.0+w_DC/Sw_freq));
  LPFb_DC=_IQ28(1)-(LPFa_DC<<1);
  LPFa_speed=_IQ28(1-
2.0/(2.0+w_speed/Sw_freq));
  LPFb_speed=_IQ28(1)-(LPFa_speed<<1);
  LPFa_torque=_IQ28(1-
  2.0/(2.0+w_torque/Sw_freq));
  LPFb_torque=_IQ28(1)-(LPFa_torque<<1);


  /*PI controller*/
  kp_Iarm=_IQ28(Kp_Iarm);
  ki_Iarm=_IQ28(Ki_Iarm/Sw_freq);

 /*Motor Control */
  Iarm_ref= 0;
  Iarm_err = 0;
  Iarm_err1= 0;
  Speed_w_ref=0;

  /* Duty cycle of inverter*/
  D_inv=_IQ18(0.5);
  D_inv1=_IQ18(0.5);

   /* Key input*/
  key_value = 0;
  key_monitor = 0;
  key_monitor1 = 0;
  key1=0;

  /*system flags*/
  CONTACTOR = 0;
  INTERRUPT = 0;
  FAULT = 0;
  PLL = 0;
  SCREEN = 0;
  display_counter=0;
  display_counter1=0;

  //*Shaft Torque*//
  Speed_diff1=0;
 Speed_diff=0;
 Y=0;
Angle_1=0;
Angle_2=0;
Angle_delta=0;
shaft_Torque=0;
Angle_diff_Degree=0;
```

```
} /*End of Init_variable*/


void InitXintfClocks(void)
{
  XintfRegs.XTIMING0.all=0x000358AC;
  XintfRegs.XTIMING6.all=0x0003E746;
  XintfRegs.XINTCNF2.all=0x00000007;
} /*End of InitXintfClocks*/

void InitPeripherals(void)
{
  //Text_LCD_initiate();
  InitAdc();
  InitEVA();
  InitEVB();
  init_fpga();
  Init_variable();
}


void InitEVA(void)
{
  // Configure EVA
  // EVA Clock is already enabled in
InitSysCtrl();

  EvaRegs.EVAIMRA.bit.PDPINTA=1;
 // Enable compare for PWM1-PWM6
  EvaRegs.CMPR1 = 0x0000;
  EvaRegs.CMPR2 = 0x0000;
  EvaRegs.CMPR3 = 0x0000;
  // Compare action control. Action that takes
place
  EvaRegs.ACTRA.all = 0x0999;
  EvaRegs.DBTCONA.all = 0x0FF4;
  EvaRegs.COMCONA.all = 0xA000;

/* Initalize EVA Timer1*/
   EvaRegs.T1PR = Ts;
   EvaRegs.T1CNT = 0x0000;
   // Timer enable
   EvaRegs.T1CMPR=Ts>>1;
   EvaRegs.T1CON.all = 0x0802;
   EvaRegs.EVAIMRA.bit.T1CINT=1;
   //EvaRegs.EVAIMRA.bit.T1UFINT=1;
 /* Initalize EVA Timer2*/
   EvaRegs.T2CNT = 0x0000;
   EvaRegs.T2PR =19999;
   EvaRegs.T2CON.all = 0x1870;

 EvaRegs.T1CON.bit.TENABLE=1;
}

void InitEVB(void)
{
 // Configure EVA
 // EVB Clock is already enabled in InitSysCtrl();
 EvbRegs.EVBIMRA.bit.PDPINTB=1;
 // Enable compare for PWM7-PWM12

/* Initialize QEP circuits*/
  EvbRegs.CAPCONB.all = 0x9004;

/* Initalize the timers*/
/* Initalize EVB Timer4*/

   /* Initalize EVA Timer4*/
   EvbRegs.T4CNT = 0x0000;
   EvbRegs.T4PR =19999;
   EvbRegs.T4CON.all = 0x1870;

 /* Initalize EVB Timer3*/
   EvbRegs.T3CNT = 0x0000;
   EvbRegs.T3PR =Ts>>4;
   EvbRegs.GPTCONB.bit.T3TOADC = 1;
   EvbRegs.T3CON.all = 0x0800;

   EvbRegs.T3CON.bit.TENABLE=1;

}/*End of InitEVB(void)*/


void InitAdc(void)
{
  /*Start ADC*/
  AdcRegs.ADCTRL3.bit.ADCBGRFDN = 0x3;
  Delay_micro_second (ADC_usDELAY);
  AdcRegs.ADCTRL3.bit.ADCPWDN = 1;
  Delay_micro_second (ADC_usDELAY2);

  /*Configure ADC*/
   AdcRegs.ADCTRL1.bit.ACQ_PS = 0x1;
   AdcRegs.ADCTRL3.bit.ADCCLKPS = 0x5;
   AdcRegs.ADCTRL1.bit.SEQ_CASC = 1;
   AdcRegs.ADCTRL1.bit.CONT_RUN = 0;

   AdcRegs.ADCMAXCONV.all = 0x000B;
   AdcRegs.ADCCHSELSEQ2.bit.CONV07      =
0xC;
   AdcRegs.ADCCHSELSEQ3.bit.CONV08      =
0xD;

   AdcRegs.ADCTRL2.bit.EVB_SOC_SEQ = 1;

} /*End of InitAdc*/


void init_fpga(void)
 {
```

```
   /*Hardware Protection*/
*FAULT_CLEAR_A = 0x0;
 *FAULT_ENABLE_A = 0x1ff;

 *FAULT_CLEAR_B = 0x0;
 *FAULT_ENABLE_B = 0x1ff;

 /*Thermal Protection (disabled)*/
 *FAULT_THERMO_ENABLE = 0x0;

 *FAN_PERIOD = 14999;
 *FAN_COUNT = 0x0;
 *FAN_COMPARE_A = 0x0;
 *FAN_COMPARE_B = 12180;
 //*FAN_CONFIG = 0x1F;

 /*Fault signal distribution*/
*FAULT_DISTRIBUTE = 0xffff;
/*Zero-crossing detection */
*PHASE_SHIFT_A = 0x4DDC;
*PHASE_SHIFT_CONFIG_A = 0x0118;

/*IO pin configuration*/
*GPIOA6_CONFIG = 0x0A;
*GPIOB6_CONFIG = 0x0B;

 /*XINT interrupt configuration*/
 *XINT1_CONFIG = 0x0;
 *XINT2_CONFIG = 0x0;

 /*KeyinputText LCD displace interface*/
 *KEY_IN = 0xf;

 *SWITCH_IN = 0x00;

  /*FPGA LED*/
 *FPGA_LED = 0x0;
} /*End of Init_fpga*/


void get_adc_V(void)
{
    Uint16 i;

   Uint32 Sum_ch7=0;
   Uint32 Sum_ch8=0;
   for(i = 0; i<AVE_SAMPLE; i++)
     {
       Sum_ch7+=Sample_ch7[i]
     }
  for(i = 0; i<AVE_SAMPLE_DC; i++)
     {
      Sum_ch8+=Sample_ch8[i];
     }
```

```
   /*Chanel 12*/
Iarm=Sum_ch- (AD_BIAS7<<(AVE_SHFT));
Iarm=(Iarm<<(18-AVE_SHFT)); format)
Iarm=Iarm/2050;
Iarm=-Iarm*50; /*current sensor 5:1 */


   /*Chanel 13*/
If=Sum_ch8-(AD_BIAS8<<(AVE_SHFT_DC));
 If=(If<<(18-AVE_SHFT_DC));
 If=If/2050;
 If=-If*50; /*current sensor 5:1 */
 If+=_IQ18(0.14);

  /*Low pass filtering for If*/
  If_L0=If_L;
  If_L=_IQ18mpyIQX(LPFa_DC,28, (If0+If),18);
  If_L+=_IQ18mpyIQX(LPFb_DC,28, If_L0,18);
  If0=If;
 /*Electrical torque of DC motor*/
torque_motor=_IQ18mpy(Iarm, _IQ18(Kf));

} /*End of Get_adc_V*/



void InitGpio(void)
{
    // sets GPIO Muxs as I/Os
    EALLOW;

   GpioMuxRegs.GPAMUX.all= 0x077F;
   GpioMuxRegs.GPBMUX.all= 0x077F;
   GpioMuxRegs.GPDMUX.all=0x0000;
   GpioMuxRegs.GPEMUX.all=0x0000;
   GpioMuxRegs.GPFMUX.all=0x0030;
   GpioMuxRegs.GPGMUX.all=0x0030;

   GpioMuxRegs.GPADIR.all=0xF8FF;
   GpioMuxRegs.GPBDIR.all=0xF8FF;
   GpioMuxRegs.GPDDIR.all=0x0000;
   GpioMuxRegs.GPEDIR.all=0x0000;
   GpioMuxRegs.GPFDIR.all=0x3FDF;
   GpioMuxRegs.GPGDIR.all= 0x0010;

   GpioMuxRegs.GPAQUAL.all=0x0000;
   GpioMuxRegs.GPBQUAL.all=0x0000;
   GpioMuxRegs.GPDQUAL.all=0x000F;
   GpioMuxRegs.GPEQUAL.all=0x000F;

   EDIS;
} /*End of Gpio_select*/
```

```
void Close_Relay(void)
{
  Uint16 i;
GpioDataRegs.GPBCLEAR.bit.GPIOB12=1;
GpioDataRegs.GPACLEAR.bit.GPIOA7= 1;
  Delay_mili_second(200);
  GpioDataRegs.GPBDAT.bit.GPIOB7 = 1;
    for (i=0; i<10; i++)
    {
    Delay_mili_second(100);
    LED_display();
    }
  GpioDataRegs.GPBDAT.bit.GPIOB12 = 1;
  GpioDataRegs.GPADAT.bit.GPIOA7 = 1;
  CONTACTOR = 1;
}

void Open_Relay(void)
{
  GpioDataRegs.GPBCLEAR.bit.GPIOB7 = 1;
  CONTACTOR = 0;
}

void Enable_Inv(void)
 {
   EvaRegs.CMPR1 = 0x0000;
   EvaRegs.CMPR2 = 0x0000;
   EvaRegs.CMPR3 = 0x0000;
   EvaRegs.COMCONA.bit.FCOMPOE=1;
 }

void Disable_Inv(void)
 {
   EvaRegs.COMCONA.bit.FCOMPOE=0;
 }
```

REFERENCES

[1] T. Orlowska-Kowalska, K. Szabat, "Control of the Drive System With Stiff and Elastic Couplings Using Adaptive Neuro-Fuzzy Approach", IEEE Transactions on Industrial Electronics, vol. 54, no. 1, February 2007, pp. 228-240.

[2] M. A. Valenzuela, J. M. Bentley, R. D. Lorenz, "Evaluation of Torsional Oscillations in Paper Machine Sections", IEEE Transactions on Industrial Applications, vol. 41, no.2, March/April 2005, pp. 493-501.

[3] Y. Hori, H. Sawada, Y. Chun, "Slow Resonance Ratio Control for Vibration Suppression and Disturbance Rejection in Torsional System", IEEE Transaction on Industrial Electronics, vol. 46, no.1, February 1999, pp.162-168.

[4] P. Hu, K. F. Ehmann, " Fifth Octave Mode Chatter in Rolling", Proceeding of the Instatution of Mechanical Engineer, Part B: Journal of Engineering Maufacture, vol.215, no.6, 2001, pp.797-809.

[5] H. Hakata, S. Tatara, R. Kurosawa, C.P. Lemone, H. Hosoda, "Application Strategies for Rolling Mill Drives", Industry Application Society Annual Meeting, vol.2, September/October 1991, pp. 1141-1147.

[6] J. C. Wachel, F. R. Szenasi, " Analysis of Torsional Vibrations in Rotating Machinery", Proceedings of 22nd Turbomachinary Symposium 1993, pp. 126-151.

[7] ABB Review, "Medium Voltage Drive Technology For metal Application", 2004.

[8] J. K. Ji, S. Sul, "Kalman Filter and LQ Based Speed Controller for Torsional Vibration Suppression in a 2-Mass Drive System", IEEE Transactions on Industrial Electronics, vol. 42, no.6, December 1995, pp. 564-571.

[9] R. Zhang, C. Tong, "Torsional Vibration Control of the Main Drive System of a Rolling Mill Based on an Extended State Observer and Linear Quadratic Control", Journal of Vibration and Control, vol.12, no.3, 2006, pp. 313-327.

[10] K. Doi, K. Ishikawa, H. Tsukuda, K. Yamamoto, N. Suganuma, T. Naito, "Analysis and Control System for Shaft Vibration in Steel Rolling Processes", Kawasaki Steel Technical Report, no. 17, October 1987, pp. 73-80.

[11] H. Naitoh, K. Suzuki, "Compensation of a GTO-NPC Inverter for the Damping of Rolling Mill Torsional Vibration by ETC (Estimated Torque feedback Control)", Power Electronics Specialist Conference (PESC), vol.1, June 1996, pp. 925-930.

[12] H. Nagase, T. Okuyama, J. Takahashi, K. Saitoh, "A Mothod for Suppressing Torque Ripple of an ac Motor by Current Amplitude Control", IEEE Transactions on Industrial Electronics, vol.36, no. 4, November 1989, pp. 504-510.

[13] T. Ohmae, T. Matsuda, M. Kanno, K. Saito, T. Sukegawa, "A microprocessor-Based Motor Speed Regulator Using Fast-Response State Observer for Reduction of Torsional Vibration", IEEE Transaction on Industrial Applications, vol. 23, no. 5, September/October 1987, pp.863-871.

[14] R. Dhaouadi, K. Kubo, "Robust Speed Control of Rolling Mill Drive Systems Using the Loop Transfer Recovery Design Methodology" International Conference on Industrial Electronics, Control and Instrumentation (IECON), vol.1, October /November 1991, pp. 555-560.

[15] D. H. Butler, M. A. Churches, Y. Anbe, H. Naitoh, "Compensation of a Digitally Controlled Static Power Converter for the Damping of Rolling Mill Torsional Vibration", IEEE Transactions on Industrial Applications, vol.28, no.2, March/April 1992, pp. 427-433.

[16] M. Nordin, "Nonlinear Backlash Compensation for Speed Controlled Elastic Systems", Doctoral Thesis 2000.

[17] Y. Hori, H. Iseki, K. Sugiura, "Basic Consideration of Vibration Suppression and Disturbance Rejection Control of Multi-inertia System using SFLAC (State Feedback and Load Acceleration Control)", IEEE Transaction on Industry Applications, vol.30, no.4, July/August 1994, pp.889-896.

[18] P. Schmidt, T. Rehm, "Notch Filter for Resonant Frequency Reduction in Dual Inertia System", Industry Application Conference, vol. 3, October 1999, pp. 1730-1734.

[19] M. A. Valenzuela, J. M. Bentley, A. Villablanca, R. D. Lorenz, "Dynamic Compensation of Torsional Oscillation in Paper Machine Sections", IEEE Transactions on Industrial Applications, vol. 41, no. 6, November/December 2005, pp.1458-1466.

[20] Y. Wu, K. Fujikawa, H. Kobayashi, "Atorque Control Method of Two-Mass Resonant System with PID-P Controller", International Workshop on Advanced Motion Control, July 1998, pp. 240-245.

[21] K. Sugiura, Y. Hori, "Nibration Suppression in 2- and 3-Mass System Based on the Feedback of Imperfect Derivative of the Estimated Torsional Torque", IEEE Transaction on Industrial Electronics, vol.43, no.1, February 1996, pp. 56-64.

[22] K. Hong, K. Nam, "A Disturbance Torque Compensation Scheme Considering the Speed Measurement Delay", Industry Application Conference, vol.1, October 1996, pp. 403-409

[23] H. Kawaharada, Ivan Godler, T. Ninomiya, H. Honda, "Vibration Suppression Control in 2-inertia System by Using Estimated Torsion Torque",Industry Application Conference, vol.3, October 2000, pp. 2219-2224.

[24] Ioannou P., J. sun, " Robust Adaptive Control", Prentice Hall, Inc., 1996.

[25] R. S. Burns, " Advanced Control Engineering", Butterworth Heinemann, 2001.

[26] P. Dorato, C. Abdalla, "Linear-Quadratic Control: An Introduction", Prentice-Hall, Inc., 1995.

[27] B. D. Anderson, J. B. Moore, "Linear Optimal Control", Prentice Hall, Inc., 1971.

[28] J. C. Doyle, G. Stein, "Robustness with Observers", IEEE Transactions on Automatic Control, vol. 24, no. 4, August 1979, pp.607-611.